Functional Neuroimaging of Electrophysiological Rhythms in Pathological and Normal Brains

A DISSERTATION
SUBMITTED TO THE FACULTY OF THE GRADUATE SCHOOL
OF THE UNIVERSITY OF MINNESOTA
BY

LIN YANG

IN PARTIAL FULFILLMENT OF THE REQUIREMENTS
FOR THE DEGREE OF
DOCTOR OF PHILOSOPHY

Dr. BIN HE, advisor

July 2012

Acknowledgements

I would like to express my most sincere gratitude to my advisor and mentor, Dr. Bin He, for his enormous support and guidance throughout my doctoral training. I would also like to acknowledge the members of my dissertation committee: Dr. Wei Chen, Dr. Matthew Johnson, and Dr. Hubert Lim for their time, support, and inspiring discussions.

I am also eager to thank our collaborators, Dr. Gregory Worrell, Dr. Benjamin Brinkmann, Ms. Cindy Nelson, and Ms. Karla Crockett at the Mayo Clinic (Rochester, MN) for supporting clinical studies and providing epilepsy data used in this work. In addition, I wish to thank Dr. Zhongming Liu, Dr. Christopher Wilke and Mr. Yunfengt Lu for their valuable contributions to the research presented in this dissertation, Dr. Gang Wang and Mr. Marc Pisansky for their assistance in data analysis, and Dr. Lei Ding, Dr. Xiaoxiao Bai, Dr. Han Yuan, Dr. Yakang Dai, Mr. Keith Jamison, Ms. Huishi Zhang, Ms. Nessa Johnson and Mr. Abhrajeet Roy for technical discussions.

Furthermore, I would like to express my appreciation to Dr. Stephen Engel, Dr. Min Bao, Dr. Thomas Henry and Dr. Zhiyi Sha for fruitful collaborations in clinical and psychology researches. I am also grateful to all the other lab members I have worked with: Dr. Audrey Royer, Dr. Xu Li, Mr. Alexander Doud, Dr. Yingchun Zhang, Dr. Xiaotong Zhang, Dr. Chengguang Liu, Dr. Dakun Lai, Mr. Jiaen Liu, Mr. Chengzong Han, Mr. Leo Mariappan, Ms. Zhaoye Zhou, and Mr. Long Yu.

Dedication

This dissertation is dedicated to my parents, for their love, support and encouragement throughout my life.

Abstract

Imaging of electrophysiological activity in the brain plays a critical role in neuroscience research. Shown by emerging neuroimaging studies, rhythmic oscillations in electrophysiology reflect important functional changes in the brain. More importantly, the mapping of electrophysiological neural signals can serve as a diagnostic tool for neurological diseases. One typical example is the electroencephalography (EEG) technique, which has been established as a core component of pre-surgical evaluation in epilepsy treatment. However, despite the recent advances of functional neuroimaging techniques, a non-invasive, high resolution, electrophysiological imaging approach still remains challenging. In the clinical application of epilepsy, there is not an established protocol that can image, non-invasively, the electrophysiological signals during the most important epileptic event – epileptic seizures. The present dissertation research aims at developing electrophysiological imaging approaches with focus on the rhythmic activity in pathological and normal brains. Towards this goal, we have developed a spatiotemporal EEG imaging method, which is suited to image dynamic changes of ictal discharges during epileptic seizures. As evaluated in a group of epilepsy patients in clinical environment, such a non-invasive seizure imaging approach could potentially translate into a more precise and less risky pre-surgical imaging tool for epilepsy diagnosis. In addition to the direct impact of seizures, we have studied the electrophysiological changes in the widespread brain networks. The spatial and spectral features of EEG rhythms can reflect important correlation with the impact of seizures and the change of cognitive functions. The electrophysiological imaging in epilepsy,

therefore, can serve as a useful tool in a pathological model to study cognition and consciousness in human brains. In order to achieve higher spatial resolution, we also improved the EEG source imaging by adding a multimodal component of functional MRI. From all the results we have obtained so far in these studies, it is suggested that the spatiotemporal EEG source imaging has the potential to improve clinical diagnosis and treatment of neurological disorders. It can also advance our understanding of basic neuroscience questions.

Table of Contents

Acknowledgements i
Dedication ii
Abstract iii
Table of Contents v
List of Tables vii
List of Figures viii
Chapter 1 Introduction 1
1.1 Overview 1
1.2 Motivation 4
1.3 Scope of the dissertation 7
Chapter 2 Background 9
2.1 Origin of EEG/MEG 9
2.2 EEG/MEG source imaging 11
2.2.1 Forward problem 11
2.2.2 Inverse problem 15
2.2.3 Dipole localization, sub-space, and beamforming methods 17
2.2.4 Localization of evoked and continuous activity 18
2.3 Integration of EEG and fMRI 20
2.4 EEG and epilepsy 22
2.4.1 Epilepsy and symptoms 23
2.4.2 Epilepsy and electrophysiology 25
2.4.3 Epilepsy and pre-surgical evaluation 28
Chapter 3 EEG monitoring and Dynamic Seizure Imaging 31
3.1 Introduction 31
3.2 Development of dynamic seizure imaging approach 33
3.2.1 Source separation 34
3.2.2 Component selection 35
3.2.3 Source re-combination 38
3.3 Clinical evaluation in operated or invasively-monitored patients 42
3.3.1 Patients 42
3.3.2 High-resolution EEG and data acquisition 44
3.3.3 Evaluation in epilepsy patients 45
3.4 Discussion 54
Chapter 4 Epilepsy and consciousness 62
4.1 Introduction 62
4.2 Methods and materials 65
4.2.1 Patients and data acquisition 65
4.2.2 Behavioral analysis 66
4.2.3 Data analysis 67
4.3 Results – spectral and spatial shifts of postictal EEG 74
4.3.1 Global spectral shift of postictal EEG 74
4.3.2 Regional spatial shift of slow waves 76

4.4 Discussion 84
Chapter 5 Multimodal spatiotemporal neuroimaging 93
5.1 Introduction 93
5.2 Methods and materials 94
5.2.1 EEG-fMRI reciprocal neuroimaging algorithm 95
5.2.2 Computer simulations 98
5.2.3 Eyes-open-eyes-closed experiment 100
5.3 Simulation and experimental results 103
5.3.1 Continuously oscillatory activity 103
5.3.2 Event-related neural responses 108
5.3.3 Experimental results 110
5.4 Discussion 112
Chapter 6 Conclusions and perspectives 119
6.1 Conclusions 119
6.2. Perspectives 122
References 126

List of Tables

Table 3.1 Surgery sites and intracranial EEG monitoring…….44

Table 4.1 Patients and their surgical outcome / intracranial EEG/ EEG indicating temporal lobe seizures……..……...66

List of Figures

Figure 2.1 The overview of a source imaging problem……..……...10
Figure 2.2 The volume conductor models and source models……...13
Figure 3.1 Schematic flow chart of the Dynamic Seizure Imaging (DSI) approach…….34
Figure 3.2 Source separation of seizure EEG……37
Figure 3.3 Source imaging at seizure onset……...39
Figure 3.4 Dynamic seizure imaging over time……41
Figure 3.5 Clinical evaluation in epilepsy patients……43
Figure 3.6 DSI in comparison with resective surgery and intracranial EEG (iEEG)……46
Figure 3.7 Localization error (LE) in comparison with iEEG……..…….49
Figure 3.8 Comparison of DSI and another frequency-domain method……....50
Figure 3.9 Comparison between 76-, 32-, and 19- electrodes……...53
Figure 4.1 Overview of the analysis of postictal EEG……...……69
Figure 4.2 An example of EEG wave forms in a complex partial seizure…….73
Figure 4.3 Relative spectral delta power change in postictal EEG……75
Figure 4.4 IL-CL (IpsiLateral-ContraLateral) analysis in the sensor space……..78
Figure 4.5 IL-CL (IpsiLateral-ContraLateral) source analysis……..79
Figure 4.6 IL-CL (IpsiLatral-ContraLateral) source analysis of the difference between complex and simple partial seizures……..81
Figure 4.7 The relative spatial delta power of postictal EEG……82
Figure 4.8 L-R (Left-Right) analysis in the sensor space……..83
Figure 5.1 Diagram of the EEG-fMRI reciprocal neuroimaging approach…….95
Figure 5.2 Illustration of the simulation settings…….101
Figure 5.3 Intermediate results of simulation...……...105
Figure 5.4 Spatiotemporal imaging and estimation of phase relations……107
Figure 5.5 Event-related spatiotemporal source estimates……..109
Figure 5.6 Experimental results in a human subject…….111

Chapter 1 Introduction

1.1 Overview

During the past several decades, the emerging neuroimaging techniques have significantly improved our ability to observe and understand the most complicated organ in human – brain. Techniques have been developed to measure neural activity in different scales, from a single-cell level to a system or network level. One of the most important advancements should be attributed to our improved capability of non-invasive neuroimaging. By accessing the anatomical and functional information of the brain without the need to open the skull, the study subjects of neuroimaging research have been broadened from invasive models (animals or patients with brain surgery or injury) to normal healthy individuals.

Human electroencephalography (EEG), since firstly measured by Hans Berger in 1929 (Berger, 1929), was soon established as one of the major non-invasive electrophysiological mapping tools. EEG measures electrical signals originating from synchronized activity of cortical neurons by non-invasive scalp electrodes. A similar electromagnetic mapping tool magnetoencephalography (MEG) measures the magnetic signals generated by synchronized neurons. EEG and MEG have high temporal resolution to track the instantaneous dynamics of underlying neural activity and a full coverage of the brain to locate the position of the sources. However, because of the many tissues between the sources and sensors, the EEG/MEG signal is blurred in space. Their application is limited by the fact that EEG and MEG cannot directly measure signals

from the source space in the brain but rather from sensors residing far-field. One type of model-based imaging technique, known as electromagnetic source imaging (Baillet et al., 2001; He and Liu, 2008; Michel et al., 2004), has been pursued to reconstruct brain activity in the source space from the scalp measurement. Such a source imaging technique improves the spatial aspects of EEG and MEG by the ability to localize the brain sources non-invasively. The spatial resolution of EEG and MEG source imaging has been further improved by integrating multimodal information from other imaging modalities with high spatial resolution, for example, the functional magnetic resonance imaging (fMRI). However, the pursuit of a noninvasive functional neuroimaging technique has never been ended, because of the fact that there is not a single imaging modality that can achieve high spatial resolution and high temporal resolution at the same time.

In addition to its role in neuroscience research, EEG is a very important clinical tool, especially in the diagnosis and treatment of epilepsy (Engel et al., 2008; Plummer et al., 2008; Rosenow and Luders, 2001). Instead of a single cause or pathology, epilepsy is in fact a syndrome that can be induced by various reasons and can have a broad impact on different areas and functions of the brain. Manifestations in behaviors can be excessive uncontrolled movements, loss or decreased consciousness and responsiveness to external stimulations, and other impaired cognitive functions, such as deficits in memory, receptive and expressive speeches, and orientation (Arthuis et al., 2009; Englot et al., 2010; Guye et al., 2006; Lee et al., 2002; Lux et al., 2002). Despite the fact that epilepsy is one of the oldest diseases recognized in human history (Littre, 1849), the

cause of epilepsy and the neural mechanisms for different behavioral changes have never been well understood. As a result, an optimal treatment to cure epilepsy has never been well established. The current treatments of epileptic seizures include anti-epileptic drugs, surgical resection, or interventional neural modulation.

In order to conduct a surgery to cure epilepsy, the most important diagnostic preparation is a pre-surgical evaluation (Rosenow and Luders, 2001) to delineate the epileptogenic zone, which is the brain region indispensable for the generation of epileptic seizures. Before the discovery of human EEG, the localization of epileptic activity depended almost solely on patients' symptoms. The discovery of human EEG in the late 1920s (Berger, 1929) opened an era of neurophysiological imaging in the treatment and diagnosis of epilepsy (Gibbs et al., 1936; Goldensohn, 1966; Hunter and Jasper, 1949). Today, neuroimaging techniques, either anatomical imaging or functional imaging, have become the dominant diagnostic tools in routine clinical practice. Several imaging protocols have been established in the past several decades. The anatomical imaging is mostly conducted by the magnetic resonance imaging (MRI), which noninvasively localizes the structural abnormalities (Henry et al., 2011; Rosenow and Luders, 2001). The structural abnormalities, if confirmed by functional imaging or neurological tests, have a high chance to be the pathological origin of epilepsy. Functional neuroimaging techniques such as single photon emission computerized tomography (SPECT), positron emission tomography (PET) and functional MRI (fMRI) measure signals carried in blood flow and indirectly reflect the neuronal activity in epilepsy patients (Blumenfeld et al., 2009; Gotman et al., 2005; Grouiller et al., 2011; Grouiller et al., 2011; Laufs et al., 2007;

Spencer, 1994; Tyvaert et al., 2008). Intracranial EEG (iEEG) measures cortical electrical activity by invasive electrodes chronically implanted in the brain. Although these imaging methods have been revolutionarily improved in the past a hundred years, our ability to detect the epileptogenic zone as the surgery target is still limited. The existing neuroimaging techniques are more or less restricted by their inherent limitations: the lack of functional information of MRI and the low spatial resolution of SPECT and PET. Neuroimaging of the epileptic brain still remains a critical challenge that limits the success rate of the epilepsy surgery.

1.2 Motivation

As discussed above, the scalp EEG provides a non-invasive approach to measure the neural electrophysiological activity with a high temporal resolution. Although many other neuroimaging techniques have emerged, the advantages of EEG, including non-invasiveness, direct measurement of electrophysiology, and high temporal resolution, make EEG an important neuroimaging tool for neuroscience research and clinical diagnosis. The application of EEG, however, is highly restricted by its relatively far distance from the underlying brain sources. Therefore, a source imaging technique, which bridges the gap between the far-filed sensors and the sources, can significantly improve our ability to noninvasively image and understand the functions of the brain.

Neural activity that is evoked by a well-designed stimulation or other tasks has been extensively studied using noninvasive imaging approaches including EEG and MEG. However, recently, increasing studies and findings have suggested the importance

of continuous rhythmic activities in the brain. The continuous rhythmic activity in the brain can represent fundamental activity and communication to maintain baseline brain functions (Laufs et al., 2003; Mantini et al., 2007; Raichle et al., 2001). It can be associated with behavioral or cognitive changes in different tasks (Feige et al., 2005; Klimesch, 1999), and can also be correlated with unpredicted neurophysiological changes in neurological diseases (Engel et al., 2008). The importance of spatiotemporal imaging of continuous rhythmic activity using EEG and MEG (Gross et al., 2001; Van Veen et al., 1997) is increasingly recognized, but the methods and algorithms are less established than the imaging of evoked activity.

The history of the application of EEG in epilepsy is almost as long as the history of EEG itself (Berger, 1933; Gibbs et al., 1936; Goldensohn, 1966; Hunter and Jasper, 1949). In the clinical setting, the EEG waveforms, especially those during seizures, are visually inspected or analyzed in the sensor space by experienced neurologists. Such a process uses a very limited amount of information from EEG, and can only approximately locate the epileptic activity. Source imaging techniques have been introduced for the localization of epileptic activity (Brodbeck et al., 2011; Knowlton et al., 2008; Knowlton et al., 2009). However, as discussed in the last paragraph, the modeling and spatiotemporal imaging of continuous ictal discharges during seizures (Assaf and Ebersole, 1997; Boon et al., 2002) remains challenging. Ictal discharges are spatiotemporal signals that can change in the time domain, frequency domain and spatial domain. The complexity of the spatiotemporal process represents the difficulty for seizure imaging.

To fulfill the needs to model and image continuous electrical activity in the normal, and more importantly in the diseased brains, the present dissertation research investigated spatiotemporal source imaging approaches to improve the localization ability of noninvasive EEG. To address the most critical challenges for such an imaging approach and its clinical and neuroscience applications, this dissertation research particularly focuses on the following questions. The first is how to model and image the spatiotemporal process of electrophysiology during a continuous period of time in the normal brain, or more importantly in the epileptic brain during seizures. As a potential diagnostic tool, what is the clinical applicability of such a non-invasive spatiotemporal seizure imaging method? Or in order words, how is the performance of such a method in comparison with other established clinical routines? Epileptic seizures are known to impact widespread brain areas, and as a result, can cause various behavioral and cognitive manifestations. In this context, can we use noninvasive imaging approaches to study the broad and continuous impact of seizure activity over the brain? Is there a certain electrophysiological feature correlated with the behavioral and cognitive changes in epileptic patients? And lastly, source imaging approaches can improve the spatial resolution of EEG and MEG to a centimeter or even smaller scale. Can we further improve the resolution of the spatiotemporal imaging by adding a multimodal component from other neuroimaging tools?

1.3 Scope of the dissertation

This dissertation addresses these questions and describes the research outcomes that we have obtained through method development, and clinical and neuroscience investigations. Experiments were conducted in epilepsy patients suffering from medically-intractable epilepsy as well as normal healthy subjects.

In chapter 2, we present a background review of the fundamentals of EEG, source imaging and other non-invasive neuroimaging techniques. After that, we briefly review the historic and current roles of EEG and other neuroimaging techniques in the diagnosis and treatment of epilepsy.

In chapter 3, we report a high-resolution EEG recording technique and a spatiotemporal imaging algorithm, particularly for the dynamic imaging of ictal discharges during seizures. The applicability of such a monitoring and imaging protocol was tested in patients suffering from medically intractable epilepsy. The performance of the non-invasive imaging was evaluated against the most invasive procedures: resective surgery and intracranial EEG.

In chapter 4, we present the electrophysiological changes in epilepsy patients with different levels of cognitive deficits. We observed the phenomenon in which after epileptic seizures, EEG rhythms in the low-frequency band changed in widespread brain networks beyond the extent of the epileptogenic zone. This phenomenon accompanied the different levels of cognitive dysfunctions in epilepsy patients, which may be an electrophysiological representation of the broad impact of epileptic seizures.

In chapter 5, we describe a novel EEG-fMRI integrated imaging algorithm for the imaging of continuous rhythmic activity. This algorithm utilizes the strategies of EEG-informed fMRI analysis and fMRI-weighted source imaging to achieve high resolution in both temporal and spatial domains, which could potentially benefit clinical application of neuroimaging. The method was evaluated through a series of computer simulations and preliminary experimental studies in normal healthy subjects.

Chapter 2 Background

2.1 Origin of EEG/MEG

EEG/MEG signals are mainly generated from net synaptic activity of cortical pyramidal cells (Baillet et al., 2001; Engel et al., 2008; He and Liu, 2008; Hämäläinen et al., 1993). These types of neurons are organized in columns, with their cell bodies residing in deep layers and their dendrites reaching out to surrounding neurons in superficial layers of cortex. Because of this organization, the pyramidal cells are aligned in parallel to each other and perpendicular to the local cortical surface. The human brain has about 10^{11} neurons. A 6 cm^2 of human cortical tissue could have 60,000,000 neurons and 600 macrocolumns (~100,000 pyramidal cells) (Engel et al., 2008; Szentagothai, 1979). EEG and MEG sensors measure far-field signals from the scalp, which is not the behavior of an individual neuron or even of an individual column, but the synchronized activation of columns of many thousands of pyramidal cells.

There are two types of synapses (Engel et al., 2008; Hämäläinen et al., 1993), excitatory synapses mostly on the dendrites and inhibitory synapses on cell bodies. When a neuron is excited by other neurons, the excitatory post-synaptic potential (EPSP) produces a primary current from the cell body to the dendritic trees, in addition to a secondary current distributed in the extracellular tissue to form a closed loop of current (Baillet et al., 2001; Engel et al., 2008; Hämäläinen et al., 1993). Input from the inhibitory synapses, on the other hand generates an inhibitory post-synaptic potential (IPSP) at the local cell body. The currents and post-synaptic potentials, driven by large number of synchronized neurons, are believed to be the main origin of EEG/MEG

signals. Sensitivity to this relatively large-scale brain activity makes EEG/MEG suitable to investigate system-level neural behaviors and the interactions between different cortical networks. The understanding of the behavior of a single or multiple neurons, such as the neuronal firing requires single-unit recording or multi-unit recording.

The net synaptic activity of synchronized pyramidal cells, when viewed from a distance (e.g., from scalp sensors), approximates a dipole (Fig. 2.1), which is a mathematical model with a current flow between a sink and a source. The dipole is located within local cortical gray matter. The direction of the dipole is perpendicular to the local cortical surface, consistent with the organization of cortical pyramidal cells. This produces an approximation of a "dipole layer" which mathematically models the distribution of cortical currents generated by columns of pyramidal cells.

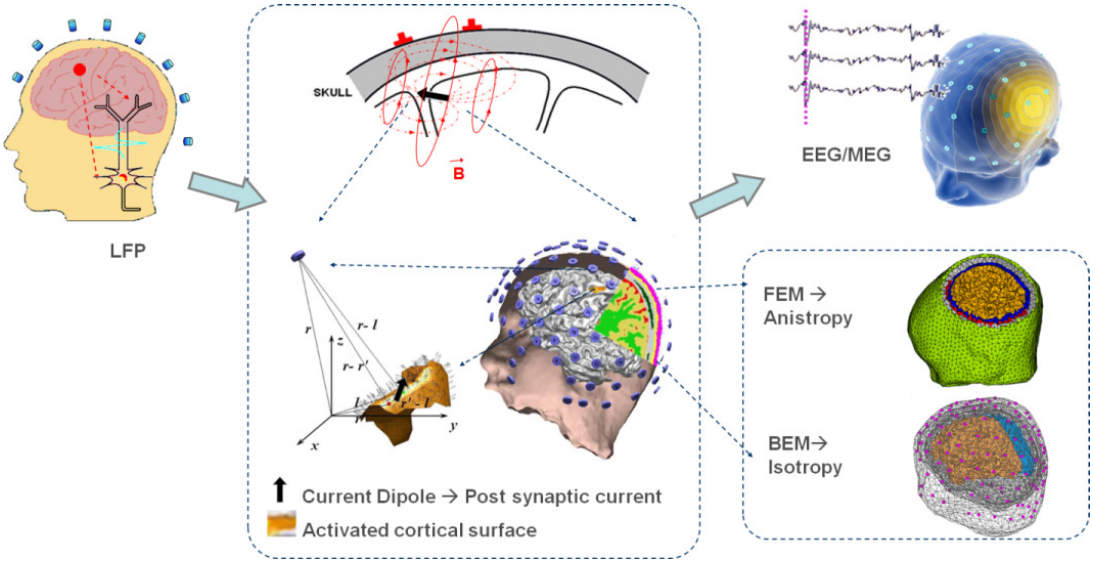

Figure 2.1 The overview of a source imaging problem (He et al., 2011 © 2011 IEEE)

2.2 EEG/MEG source imaging

The dipole, as a mathematical model of synchronized pyramidal cells, is a basic as well as the most popular source model used in EEG/MEG source imaging. The "source" here can be a single dipole, multiple dipoles, or a dipole layer with dipoles uniformly distributed within the source space. The purpose of EEG/MEG source imaging, from a mathematical perspective, is to estimate the location, magnitude and distribution of the dipoles from noninvasive scalp EEG/MEG measurements. The EEG/MEG source imaging, as a model-based approach, consists of a forward problem (from sources to sensors) and an inverse problem (from sensors to sources).

2.2.1 Forward problem

The forward problem creates a model that links a known underlying brain source with the scalp measurement. When a unit dipole at a certain location with a certain orientation is activated, the electromagnetic signals will propagate through the head volume conductor before reaching the scalp sensors. To accurately build the forward model of such a process, it is important to understand how dipoles distribute within the brain (source model) and how the conductive property changes over the pathway of electromagnetic signals (volume conductor model).

Although the dipole model is the most commonly used source model in EEG source imaging, different assumptions about the source space and orientation of dipoles can be made. The discrete dipole model (Fig2.2 D) assumes a single dipole or a known number of dipoles representing the whole brain's activity (Cuffin, 1995; He et al., 1987;

Kavanagk et al., 1978; Scherg and Von Cramon, 1985). Under the discrete dipole model, each dipole can have 6 parameters: 3 location parameters and 3 moment parameters. The discrete dipole model is used for dipole fitting, a popular EEG source imaging approach. However, the number of dipoles should be known or pre-defined before solving the dipole fitting problems. The distributed source model, on the other hand, assumes thousands of dipoles that are uniformly distributed within the source space, each of which represents a unit of source (i.e., columns of pyramidal cells). The first type of distributed source model assumes dipoles that are uniformly distributed within the 3-dimensional (3D) brain volume (Hamalainen and Sarvas, 1989) and therefore is called the 3D distributed source model (Fig. 2.2F). Under the 3D source model, the brain volume is parcellated into thousands of small cubes, each of which is a unit containing a dipole source. The orientation of a dipole is unconstrained. Another widely used type of distributed source model is called the cortical current density (CCD) model (Dale and Sereno, 1993) because of the utilization of the concept of "dipole layer" as described in Section 2.1 (Fig. 2.2E). The CCD model assumes that dipoles are uniformly distributed within the cortical gray matter, aligned parallel to surrounding dipoles, and oriented perpendicular to the local cortical surface. Under the CCD model, the cortical surface is parcellated into thousands of small triangles, each of which is a unit containing a dipole source. The orientation of each dipole can be constrained to be perpendicular to the local cortical surface.

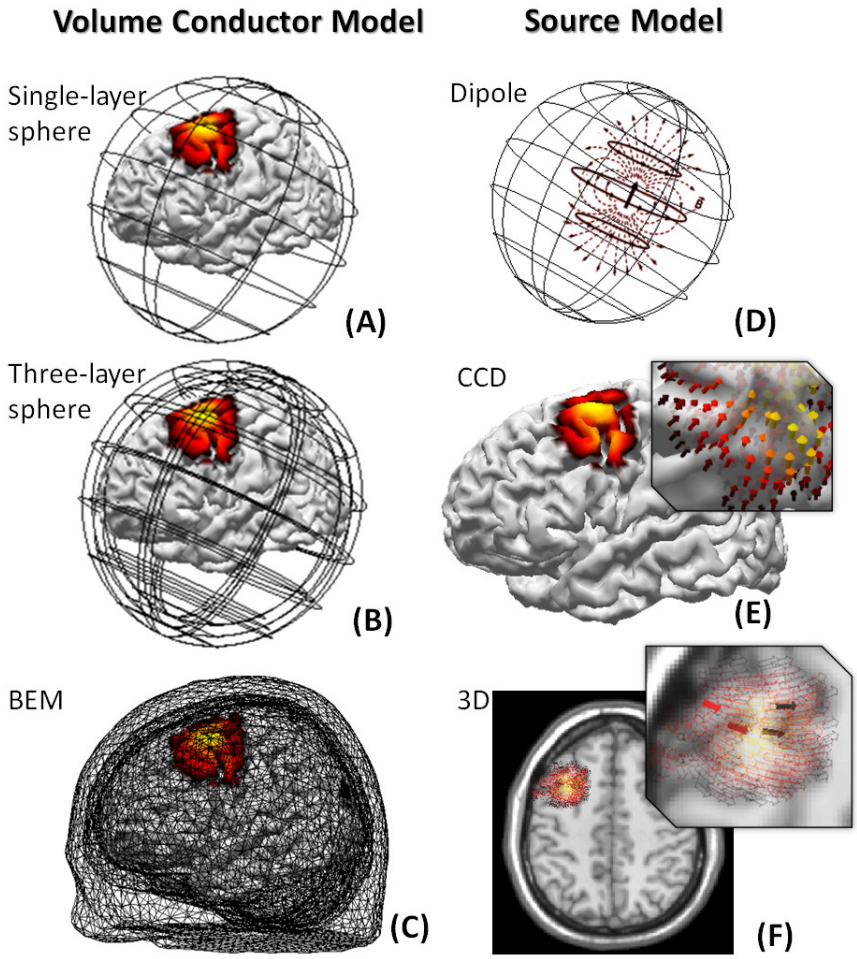

Figure 2.2 The volume conductor models and source models used for EEG or MEG source imaging problems. (A) single sphere model, (B) three-layer spherical model, (C) Boundary Element Model (BEM). (D) discrete dipole model, (E) Cortical Current Density model (CCD), and (F) 3D volume distributed source model.

The head volume conductor model can be as simple as a single spherical model (Fig. 2.2A), which uses a sphere to represent the shape of the head and assumes uniform conductivity within the sphere. Later during the development of source imaging techniques, the complexity of the structures and the variation of conductivity of different

tissues have been increasingly considered. A three-layer spherical model (Fig. 2.2B) uses three spheres to represent the layers of the skin, skull and brain and assumes homogeneous conductivity within each layer. The spherical model can be improved by fitting the spheres to each individual's structures. The spherical model has still been widely used, especially for MEG applications (Baillet et al., 2001). Taking advantage of the modern MRI techniques, more detailed volume conductor models have been developed based on the Boundary Element Method (BEM) and Finite Element Method (FEM). The BEM model (Fig. 2.2C) uses realistically shaped surfaces (e.g. reconstructed from MRI) to separate the head into three compartments of skin, skull and brain, and assumes homogeneous conductivity within each layer (Fuchs et al., 1998; Hamalainen and Sarvas, 1989; He et al., 1987). According to previous human studies, the conductivity of the three layers of the skin, the skull and the brain can be approximated by 0.032, 0.0165 and 0.032 S/M, respectively (Lai et al., 2005; Zhang et al., 2006). The BEM model incorporates model accuracy and reasonably computational efficiency, and it has been widely used for EEG source imaging. The FEM model allows the best approximation to the realistic geometry and conductivity of different tissues (Wolters et al., 2006; Yan et al., 1991). The inhomogeneity of conductivity and the anisotropy of tissues can be considered in the model. The FEM model, however, is the most computationally demanding model.

2.2.2 Inverse problem

Based on the forward modeling of distributed source models, the scalp recording and underlying dipole sources can be linked through a linear system:

$$\mathbf{Y} = \mathbf{LX} \qquad 2.1$$

where Y is a vector of scalp measurements from M sensors $\mathbf{Y} = [y_1, y_2, \dots y_M]^T$. X is a source vector of N sources $\mathbf{X} = [x_1, x_2, \dots x_N]^T$. An element x_i is the magnitude of the ith dipole at a known location r_i' in the source model. L is a pre-modeled leadfield matrix created in the step of forward modeling. Column i of the leadfield matrix $\mathbf{L}_i$ is the scalp potential pattern generated by a unit dipole at location r_i'. The solution of an inverse problem is the estimation of source vector $\hat{\mathbf{X}} = [\hat{x}_1, \hat{x}_2, \dots \hat{x}_N]^T$. The scalp potentials $\hat{x}_i L_i$ generated by activated dipoles $\hat{x}_i$, when summed over the scalp, $\hat{\mathbf{Y}} = \sum_{i=1}^{N} \hat{x}_i L_i$ best approximates the real measurement Y.

In a distributed source model, thousands of dipoles can be used to represent the distribution of pyramidal cells. However, the number of scalp measurements is limited by the possible physical recording sites. Modern EEG/MEG systems can have 32, 64, 128, 256 or even more channels, which are still significantly smaller than the number of unknown sources. Because of the imbalance between the unknown sources and the known measurements, the EEG/MEG inverse problem is highly ill-posed and lacks a unique solution (Baillet et al., 2001; He and Liu, 2008; Michel et al., 2004).

EEG/MEG inverse solutions or inverse operators $\mathbf{L}^{-1}$, however, have been developed in an attempt to obtain an "optimal" solution instead of a unique solution (Baillet et al., 2001; He and Liu, 2008; Michel et al., 2004). Hamalainen et al. (1984)

proposed the Minimum Norm (MNE) solution for the estimation of 3D distributed sources. The MNE solves an inverse problem with a least energy assumption. It estimates the approximation of source $\hat{X}$ with a minimum L2 norm ($\min||X||^2$) constraint. The minimum norm estimate therefore is also known as the L2 norm solution. Different inverse solutions have been developed by modifying the constraint term to incorporate various biophysical assumptions. Some of the popular methods are the low resolution electromagnetic tomography (LORETA) algorithm (Pascual-Marqui et al., 1994), the local autoregressive average (LAURA) algorithm (Menendez et al., 2001), the FOcal Underdetermined System Solver (FOCUSS) (Gorodnitsky and Rao, 1997), and other sparse source imaging methods (Matsuura and Okabe, 1995; Ou et al., 2009), or statistical variations of these methods (Pascual-Marqui, 2002). One category of widely used methods - weighted minimum norm (WMN) allows for the integration of physiological priors derived from other independent information source. With the strategy of weighting, the WMN solution can favor certain spatial locations. For example, the depth-weighted minimum norm compensates for the deep sources (Wang et al., 1992), which otherwise can be disfavored by MNE. The fMRI-weighted minimum norm integrates spatial information obtained from fMRI, and therefore can gain the high spatial resolution from fMRI (Liu et al., 1998).

The EEG/MEG source imaging problem can thus be summarized into two steps, one step of estimating the leadfield matrix L, and the other step of estimating the source distribution $\hat{X}$ from the scalp measurement Y. The source imaging problem with forward modeling and inverse solution can be illustrated by the flow chart in Fig. 2.1

2.2.3 Dipole localization, sub-space, and beamforming methods

Dipole localization is a solution to inverse problems based on the discrete dipole model. In the model, a single or multiple dipoles equivalently represent the synchronized activity in the whole brain. In a dipole fitting problem, the location and momentum of a single dipole or a pre-defined number of dipoles can be estimated by solving optimization problems. Because there are no more than 6 unknown parameters associated with one dipole, in most cases the dipole fitting problem is an over-determined problem. Equivalent dipole localization has been widely used for the reconstruction of spatiotemporal brain activity (Cuffin, 1995; He et al., 1987; Kavanagk et al., 1978; Scherg and Von Cramon, 1985). However, a single or a few equivalent dipoles might be oversimplified for the representation of distributed cortical pyramidal cells, which as discussed above are organized in a way that could change with the local structures of the cortex. The location of the dipole source might be estimated, whereas the distribution of the activity cannot be simply interpreted from dipole localization results. In addition, in a dipole fitting problem, a prior knowledge of dipole number is necessary but in fact cannot be easily obtained.

Other source imaging methods that are based on dipole models include the multiple signal classification (MUSIC) (Mosher et al., 1992), the recursively applied and projected MUSIC (RAP-MUSIC) (Mosher and Leahy, 1999) and the first principal vectors (FINES) approach (Ding et al., 2007). These subspace-based methods scan the dipoles in the entire source space in order to find the ones best explain the scalp measurements.

Another popular source imaging method known as beamforming is adapted from radar signal processing techniques. A beamformer is a spatial filter constructed as a weighted linear combination of sensors. The spatial filter selectively filters signals from one region of interest in the source space while suppress interference originated elsewhere (Gross et al., 2001; Sekihara et al., 2001; Van Veen et al., 1997). Spatiotemporal imaging can be achieved by scanning the entire source space and performing a beamformer filter on each location at a time. The spatial filter is region-customized, and therefore each region of interest has a different beamformer spatial filter.

2.2.4 Localization of evoked and continuous activity

Evoked activity such as event-related potential (ERP) has been extensively studied using EEG or MEG source imaging techniques. Because of the low signal to noise ratio of EEG, ERP is commonly calculated as the average of EEG signals recorded during hundreds of identical events, such as repeated visual stimulations or somatosensory stimulations. The average across repeated events can preserve the brain activity evoked by the external stimulations, while cancel noises that are independent to the events. From the ERP at a certain time instant $\mathbf{Y}(t)$, the source distribution $\hat{\mathbf{X}}(t)$ can be estimated by solving an inverse problem of $\hat{\mathbf{X}}(t) = \mathbf{L}^{-1}\mathbf{Y}(t)$ or by dipole fitting.

The spatiotemporal imaging of rhythmic activity in a relatively long period of time, however, is not as well studied as ERP in EEG. Recently, the importance of continuous activity has been more widely recognized. The resting state or background activity, which was more or less ignored before, has been demonstrated to show

spontaneous fluctuations in hemodynamics as well as in electrophysiology (Raichle et al., 2001; Laufs et al., 2003; Mantini et al., 2007). During tasks, different rhythms in EEG can carry important information about attention, memory, somatosensory, and other cognitive processes (Klimesch, 1999; Yuan et al., 2008; Yuan et al., 2010). In the diseased brain, spontaneous and unpredicted rhythmic activity can reflect the brain structures that are affected progressively by neurological diseases (Engel et al., 2008; Englot et al., 2010). In order to image continuous neural activity, a strategy of instant-by-instant source imaging, as used in ERP data, is less attractive. Because of the low signal to noise ratio of EEG, without averaging, the source estimation at each time point can be highly affected by noises. In a relatively long period of time, the calculation of inverse problems of all the time points can be computationally inefficient. Spatiotemporal imaging methods, such as dipole localization (Cuffin, 1995; He et al., 1987; Kavanagk et al., 1978; Scherg and Von Cramon, 1985) and beamforming (Gross et al., 2001; Sekihara et al., 2001; Van Veen et al., 1997) have been used to image the electrophysiological changes over time. Recently, methods have been developed to focus on certain frequency bands or spectral features of interest, because of the fact that frequencies in EEG can be associated with important brain functions (Klimesch, 1999; Yuan et al., 2008; Yuan et al., 2010). A simple example is a short-time-window based method (Worrell et al., 2000; Yuan et al., 2008), which transforms the windowed time course into Fourier space and uses the frequencies of interest to estimate the source distribution. Such a time-window-based method, however, loses temporal resolution. Compared to well-studied source imaging approaches for event-related EEG/MEG, nowadays, a spatiotemporal imaging of

continuous rhythmic activity, with high resolution and reasonable computation efficiency, still remains challenging.

2.3 Integration of EEG and fMRI

Functional MRI is a MRI-based neuroimaging technique that detects hemodynamic signals associated with brain activity. The most common form of fMRI measures the change of the blood oxygen level dependent (BOLD) contrast MRI signals, which is contributed by the variation of cerebral blood flow (CBF), cerebral blood volume (CBV) and the cerebral metabolic rate of oxygen ($CMRO_2$). Although these vascular signals are tightly correlated with the neural activity, these signals reflect neural activity in an indirect manner. Understanding the neurovascular coupling relationship that underlies the generation of fMRI signals, therefore, is crucial for the interpretation of fMRI data. Recent studies have investigated the relationship between BOLD signals and electrophysiological signals through invasive methods (in animals or in epileptic patients). The BOLD signal change is better explained by the local field potential (LFP) of many synchronized neurons rather than the neuronal firing by individual or multiple neurons (Logothetis et al., 2001; Mukamel et al., 2005). In line with the invasive investigations, non-invasive EEG-fMRI studies have also revealed a tight correlation between BOLD and EEG/MEG signals (Debener et al., 2005; Feige et al., 2005; Goldman et al., 2002; Liu et al., 2010; Oakes et al., 2004).

Based on the modern MRI technique, fMRI is a non-invasive procedure, which requires no surgical intervention or injection of agents. Since the early effort in 1990s

(Bandettini et al., 1992; Kwong et al., 1992; Ogawa et al., 1992), this relatively young imaging technique has become one of the major functional neuroimaging tools, especially in neuroscience research. Similar to other MRI techniques, the fMRI measure of neural activity is characterized by high spatial resolution, which can distinguish functional changes on a millimeter scale. Recent development of high-field MRI has further improved our ability to visualize functional changes in deep and fine structures. However, in opposed to the high resolution in the spatial domain, the fMRI signal has temporal resolution much lower than the time scale of neuronal activity. The nature of the blood flow signals highly restricts the BOLD-fMRI's capability to track the rapid changes of neurons

It has been widely recognized that EEG and fMRI are featured with complementary advantages and limitations: high temporal resolution but low spatial resolution of EEG, in contrast to high spatial resolution but low temporal resolution of fMRI. The complementary features of the two imaging methods have motivated the development of multimodal integration of EEG and fMRI, in a hope to obtain a neuroimaging approach with high resolution in both the spatial and temporal domains. Most commonly, EEG and fMRI signals are combined through an EEG-informed fMRI analysis or an fMRI-weighted EEG source imaging. The first strategy of EEG-informed fMRI analysis (Debener et al., 2005; Feige et al., 2005; Goldman et al., 2002; Gotman et al., 2005) uses EEG signals to form a temporal regressor, and then scans the brain to find activated/deactivated fMRI signals that can be explained by the electrophysiological signatures. This strategy is based on the assumption that neuronal signals measured by

EEG and the vascular signals measured by fMRI are correlated in the time domain. The second strategy of the fMRI-weighted EEG source imaging (Liu et al., 1998; Liu and He, 2008) uses fMRI map as a spatial weighting or mask for solving EEG source imaging problems. This strategy is based on the assumption that the neuronal signals measured by EEG and the vascular signals measured by fMRI are overlapped in the spatial domain. The integrated EEG-fMRI imaging incorporates the information from both EEG and fMRI, and is designed to provide high resolution in time and space simultaneously.

2.4 EEG and epilepsy

Epilepsy is a common chronic neurological disorder that affects about 50 million people worldwide. According to a report by the World Health Organization (WHO) in 2009 (http://www.who.int/mediacentre/factsheets/fs999), about 0.4 – 1% of the general population are affected by epilepsy and the number can increase to 0.6 – 1% in developing countries. An annual increase of new cases is around 40 – 70 per 100,000 people in developed countries and twice as high in developing countries. Epilepsy causes disease burden not only because of early death but also because of life-long disability and illness. The burden of epilepsy accounts for around 0.5% of the burden of all the diseases in the world, and contributes even more significantly to the burden caused by disability (Leonardi and Ustun, 2002). In addition to the measurable burdens, epileptic patients suffer more social and economic impacts. The discrimination, misunderstanding and social stigma can be worse than the disease itself.

The record of epilepsy in human history can be traced back for 3000 years. It is one of the oldest recognized diseases in human history, during which epilepsy has long been considered as a "Sacred Disease" (Eadie and Bladin, 2001). A less spiritualized understanding of epilepsy also began early. The first formal record to describe the pathological origin of epilepsy can be traced back to 400 B.C., when the Greek physician Hippocrates attributed the symptoms of epilepsy to pathological causes in his book of *On the Sacred Disease*:

"The disease is in my opinion no more divine than any other; it has the same nature as other diseases, and the cause that gives rise to individual diseases. It is also curable, no less than other illnesses, unless by long lapse of time it be so ingrained as to be more powerful than the remedies that are applied

The brain is the cause of this affliction..." (Foyaca-Sibat, 2011; Littre, 1849)

2.4.1 Epilepsy and symptoms

Despite the early efforts of scientific investigations, the supernatural perspectives of epilepsy dominated people's understanding for thousands of years. The modern medical era of epilepsy did not begin until the 19th century, when epilepsy was studied on a pathological and anatomical basis. Pioneered by the work of John Hughlings Jackson, the origins of epilepsy have been attributed to the *"occasional, sudden, excessive, rapid and local discharges of gray matter"* (Jackson, 1873). Such a definition holds true and is widely used nowadays. An important contribution of the 19th century is the discovery of the connection between seizure semiology and cortical localizations,

which led to the beginning of the *"era of the symptomatogenic zone"* (Rosenow and Luders, 2001). Early epilepsy surgeries were conducted and cured patients using the seizure semiology to determine the brain tissues to be resected in the surgery. After more than 200 years, today, a systematic semiology-to-localization connection has been established and the seizure semiology is considered as an indispensable component for the diagnosis in epilepsy treatment (see (Blair, 2012; Rosenow and Luders, 2001) for review).

One special type of seizure symptoms is the loss of consciousness and responsiveness during and after seizures. Whether consciousness is impaired or not has been widely used for the classification of seizures. As proposed by the International League Against Epilepsy (ILAE) (Commission of ILAE 1981), partial seizures can be categorized to simple partial seizures and complex partial seizures, with the former preserving and the latter impairing normal consciousness. The mechanisms underlying the loss of consciousness in epileptic seizures, however, have never been well understood. Back to the 19th century, Jackson attributed the cognitive deficits to *"the very highest nervous centers of the cerebral hemisphere"* (Jackson et al., 1931). Today, anatomical and functional dysfunctions in brain regions directly or indirectly impacted by epileptic seizure are believed to be the neural origin of the altered consciousness in seizures. For example, in temporal lobe seizures, the verbal-memory functions of the temporal lobe (Kelley et al., 1998) have been used to explain the memory deficits and impairments of expressive and receptive speeches (Lux et al., 2002). Other hypotheses of seizure-induced loss of consciousness include but are not limited to the disruption of

subcortical arousal systems (Blumenfeld et al., 2009), dysfunction of neocortical networks that are crucial for higher-order information processing (Blumenfeld et al., 2004; Englot et al., 2010; Lee et al., 2002; Lux et al., 2002), and abnormal communication between brain regions (Arthuis et al., 2009; Guye et al., 2006).

2.4.2 Epilepsy and electrophysiology

Soon after human EEG was discovered by Hans Berger in 1929 (Berger, 1929), a series of studies measured epileptic activity in the scalp EEG (Berger, 1933; Gibbs et al., 1936). The scalp EEG distinguished differences between locations and time periods. Such a finding of the location-correlated EEG features raised the interest to delineate electrophysiologically *"Where do epileptic seizures start"* (Gibbs et al., 1936). In fact, the position of EEG as an important monitoring and localization tool in epilepsy diagnosis has been established since then and has not been changed fundamentally over the decades. The prototype of modern video EEG monitoring was also developed during this era, when simultaneous EEG and video recording of behaviors was proposed (Goldensohn, 1966; Hunter and Jasper, 1949). Through decades of clinical practice, the noninvasiveness of the scalp EEG allows its application to every patient without concerns of risks. Using scalp electrodes, we can obtain a full coverage of the brain and therefore gain a whole picture of the electrical activity in different locations. However, scalp EEG has relatively low resolution and sensitivity to the underlying brain activity because of the barriers (e.g., skull, skin) and distance between the sources and the sensors.

In an attempt to achieve more precise electrophysiological mapping, the invasive form of EEG – intracranial EEG (iEEG) has been applied to the epilepsy treatment since the 1950s (Ajmone-Marsan and Van Buren, 1958; Rosenow and Luders, 2001). The iEEG measures brain activity through electrodes implanted over the cortical surface (e.g., electrocorticography - ECoG) or inserted into the deep structures (e.g., depth electrodes), and therefore allows the recording without the barriers of the skull and skin. However, because of the risks and expenses associated with invasive procedures, iEEG is always considered as the last choice if all the other non-invasive measurements or tests cannot converge to a conclusive diagnosis.

The recording of EEG, either non-invasively or invasively, has been commonly used to localize or lateralize critical brain regions involved in epilepsy. The epileptic activity of the most importance is the ictal discharges during seizures, because the ultimate goal of any epilepsy treatment is to stop or significantly reduce the frequency of seizures. Nowadays, scalp and intracranial EEG are the only clinical tools that have fine temporal resolution to track the fast dynamics of ictal discharges. The EEG measurement is capable of distinguishing the seizure onset zone, where a clinical seizure is generated, from the widespread epileptic network. The recording and localization of interictal spikes has also been widely studied in epilepsy patients. An interictal spike is a transient discharge with pointed peak clearly distinguishable from background activity. Interictal spikes are generated from the irritative zones and will not develop any clinical symptoms. In many cases, the location and extent of the irritative zones provide important information about the location of the seizure onset zone. However, a precise correlation

between the interictal events and the clinical seizure onset zone remains unclear (Marsh et al., 2010).

In addition to the ictal discharges and interictal spikes that have been studied since the 1930s, various biomarkers in the epileptic brain have been explored extensively using new recording and analysis techniques. One important finding recently is the abnormal rate of the high-frequency EEG oscillations in the epileptogenic zone versus other regions. Studies found that transient high-frequency events, such as ripple (100-250 Hz) and fast ripple (250-500 Hz) oscillations, tended to increase in the seizure onset zone of epileptic patients (Blanco et al., 2011; Zijlmans et al., 2012). Removing the regions of high frequency oscillations may lead to better surgical outcome (Blanco et al., 2011; Zijlmans et al., 2012). As opposed to the localization value of the high-frequency components, the low-frequency EEG oscillations have been more related with the behavioral and cognitive changes in epileptic patients. Slow waves during postical period or resting state in the temporal lobe of seizure onset (Hufnagel et al., 1995; Jan et al., 2001; Panet-Raymond and Gotman, 1990; Tao et al., 2011) have long been reported. In addition to the epileptogenic zone, recent iEEG studies have found abnormal slow oscillations in the fronto-parietal regions in seizure types that impair consciousness but not seizure types that preserve consciousness (Blumenfeld et al., 2004; Englot et al., 2010). A possible connection between the neocortical fronto-parietal slow waves and the altered consciousness level may explain the behavioral changes in epilepsy patients. Another important biomarker is the functional connectivity change in the epileptic brain, which represents the excessive or insufficient communications between different parts of

the brain. Abnormal connectivity in the epileptogenic zone versus other regions was found during seizures and even during resting state (Wilke et al., 2011). Such a correlation with the surgery target (e.g., epileptogenic zone), suggests the localization value of the connectivity measure. Outside the epileptogenic zone, over-synchronized connectivity between subcortical arousal systems and neocortical fronto-parietal networks has also been found. Because of the importance of the two structures in maintaining normal consciousness, the excessive synchronization has been hypothesized as an explanation for altered consciousness in epileptic patients (Arthuis et al., 2009; Guye et al., 2006).

2.4.3 Epilepsy and pre-surgical evaluation

In the clinical practice, antiepileptic drugs are usually the first choice of treatment for patients suffering from epileptic seizures. In a majority of the treated patients, their seizures can be cured or significantly reduced. However, about 30% of the patients will continue to have uncontrolled seizures despite optimal medication therapy. For this subset of patients with medically-intractable epilepsy, resective surgery becomes one of the remaining curative options. In order to achieve optimal surgical outcome in surgery in which patients become seizure free post-operatively, the epileptogenic zone has to be completely removed or disconnected.

The pre-surgical evaluation includes a series of neurological tests and neuroimaging protocols performed prior to the surgery. The purpose is firstly to evaluate patients' candidacy that whether a patient is a good surgical candidate, and then to

determine the brain tissues to be resected in the surgery. Seizure semiology, long-term video EEG and iEEG monitoring described earlier in this chapter are three important components of the routine pre-surgical evaluation. Seizures are infrequent, sudden and spontaneous activity, which usually happen without clear predictive signs. The capability of long-term recording thus is extremely important to reliably capture the infrequent ictal events. Nowadays, the EEG and iEEG are the only two electrophysiological monitoring tools that allow for continuous monitoring for more than 24 hours. Another electromagnetic imaging technique similar with EEG is the Magnetoencephalography (MEG) (Hämäläinen et al., 1993). Its applicability to localize the epileptic activity has been extensively studied and demonstrated in large patient groups (Knowlton et al., 2008; Knowlton et al., 2009; Stefan et al., 2003). However, the hardware of MEG requires patients to maintain still during the recording. Such an inflexible recording environment restricts the recording time and therefore makes it impossible to reliably capture seizure activity. For this reason, MEG has been used most commonly for the localization of the interictal spikes and functional eloquent brain instead of ictal discharges.

The development of MRI techniques is a breakthrough in the neuroimaging field. In the diagnosis of epilepsy, the MRI provides a way to non-invasively access the anatomical changes and abnormalities in the brain. The fast-developing high-field MRI technique has further improved the resolution to image subtle and deep structural changes in epileptic brains (Henry et al., 2011). If the MRI, scalp EEG and other neurological tests can converge to a conclusive surgical plan, the invasive EEG monitoring can be avoided. Recently, functional neuroimaging techniques with minimum invasiveness such

as SPECT, PET and fMRI have been explored in a hope that the hemodynamic signal change can reflect the neural activity in the epileptogenic zone. These techniques identified epileptic networks showing positive and negative responses to the epileptic activity (Blumenfeld et al., 2009; Grouiller et al., 2011; Laufs et al., 2007; Spencer, 1994; Tyvaert et al., 2008), however the low temporal resolution of the hemodynamic signals limits their ability to distinguish the seizure onset zone from the widespread epileptic network involved in the propagation of seizures.

Chapter 3 EEG monitoring and dynamic seizure imaging

3.1 Introduction

For patients suffering from medically intractable epilepsy, surgical treatment provides a curative solution that may stop or significantly reduce the frequency of seizures. To achieve optimal surgical outcome, in which a patient become seizure free, the epileptogenic zone has to be completely removed or disconnected (Rosenow et al., 2001). Therefore, a pre-surgical evaluation, which aims to delineate the epileptogenic zone, is crucial for achieving a successful surgical outcome.

Scalp EEG, as discussed in the last two sections, has been established as one of the important diagnostic tools for the pre-surgical evaluation of epilepsy. It has the advantages of non-invasiveness, low risk and low cost compared to iEEG. At the same time, scalp EEG shares the excellent temporal resolution of iEEG. It is the only non-invasive pre-surgical mapping tool that measures the electrophysiological onset and the rapid development of seizures. Other functional neuroimaging techniques (Blumenfeld et al., 2009; Grouiller et al., 2011; Knowlton et al., 2008; Tyvaert et al., 2008; Vitikainen et al., 2009) such as SPECT, PET and fMRI have been useful to identify the epileptic networks, but their lack of temporal resolution restricts their ability to separate the primary seizure focus from propagated areas.

Nevertheless, scalp EEG has not been considered an imaging tool but rather a scalp mapping tool. Its intrinsic limitations include low spatial resolution (typically 19-32 electrodes for clinical EEG) and indirect correlation with underlying neural generators due to volume conduction effect. Simple visual inspection of EEG waveforms, which is

commonly conducted in clinical practice, remains inadequate for the precise delineation of the seizure onset zone (SOZ). Having been studied intensively in the past decades, non-invasive source imaging (Baumgartner and Pataraia, 2006; Plummer et al., 2008) techniques have gradually been considered as a possible tool for surgery guidance, particularly with the recent development of high-resolution recording techniques, such as dense-array EEG (Brodbeck et al., 2011; Holmes et al., 2010; Koessler et al., 2010; Lantz et al., 2003) and MEG (Knowlton et al., 2008; Knowlton et al., 2009; Stefan et al., 2003). Most of the studies or applications have utilized signals recoded during interictal period (Brodbeck et al., 2011; Knowlton et al., 2008; Knowlton et al., 2009; Plummer et al., 2008; Stefan et al., 2003) as opposed to ictal period (Assaf and Ebersole, 1997; Assaf et al., 2003; Boon et al., 2002; Ding et al., 2007), because of the fact that the recording of seizures by some modern techniques (e.g. MEG) and the source imaging of dynamic ictal discharges have remained challenging. However, although the localization of interictal events is helpful, the precise correlation of neural sources of these events with the clinical SOZ remains unclear (Marsh et al., 2010). Non-invasive recording and imaging of electric sources during seizures is therefore a missing, but essential, aspect of the pre-surgical evaluation.

In this chapter, we describe a high-resolution seizure imaging protocol for potential application in pre-surgical planning of the epilepsy treatment. We developed a 76-electrode EEG system for long-term video EEG monitoring. We have also developed a novel dynamic seizure imaging algorithm that is particularly designed for spatiotemporal imaging of ictal rhythmic discharges. To evaluate the clinical

performance of such a noninvasive imaging tool, we studied a large group of patients with medically intractable epilepsy. In the group of patients, the source imaging results, derived non-invasively, were compared with iEEG recordings and/or resective surgery outcomes. Through this comparison, we sought to determine (i) the degree to which the non-invasive seizure imaging agrees with the clinical information obtained through invasive procedures; and (ii) whether the dense-array recording technique improves the performance of seizure imaging.

3.2 Development of dynamic seizure imaging approach

The dynamic seizure imaging (DSI) approach consists of steps of: (i) source separation of ictal EEG in the sensor space, (ii) localization of neural generators of seizure components, and (iii) source-recombination in the source space of the brain to form a spatiotemporal imaging. This method was designed particularly for the imaging of spatiotemporal signals, which in the context of epilepsy can be the spatiotemporal ictal discharges during epileptic seizures. The method of DSI can be illustrated as a flowchart in Fig. 3.1.

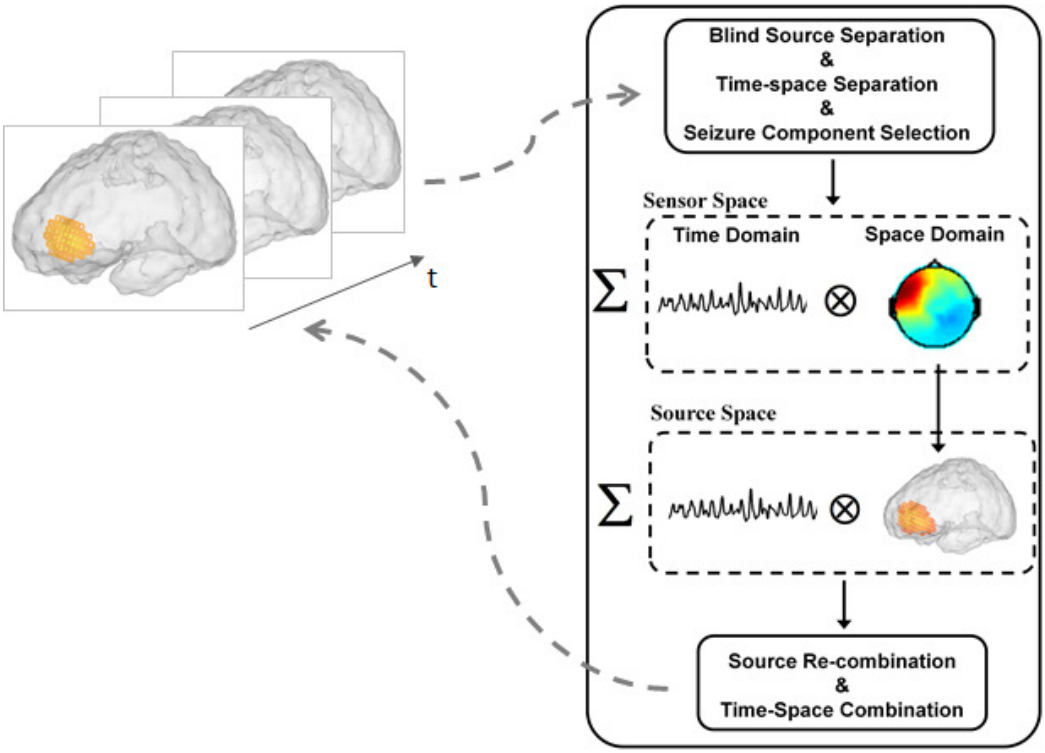

Figure 3.1 Schematic flow chart of the Dynamic Seizure Imaging (DSI) approach. It consists of steps of (i) source separation in the sensor space, (ii) localization of seizure components, and (iii) source re-combination in the source space to form a spatiotemporal imaging (Adapted from Yang et al., 2011).

3.2.1 Source separation

As discussed in chapter 2, according to EEG forward modeling, spatiotemporal EEG signal Y can be related with underlying brain activity S through a linear system:

$$\mathbf{Y} = \mathbf{LS} + \mathbf{B} \qquad 3.1$$

where Y is a $n \times t$ signal matrix (n is the number of electrodes and t is the number of time points), S is a $m \times t$ source matrix (m is the dimension of source space), B is a noise matrix, and L is a $\mathbf{n} \times \mathbf{m}$ lead field matrix. In this chapter, we calculated the lead

field matrix using the boundary element method (Fuchs et al., 1998; Hamalainen and Sarvas, 1989; He et al., 1987) and a 3D distributed source model.

Seizure EEG measures ictal discharges, which evolve through time, space and frequency (Jung et al., 2009; Nam et al., 2002; Patel et al., 2008) plus measurement noise, moving artifacts and other background brain oscillations (Jung et al., 2000; Urrestarazu et al., 2004). To analyze such complicated signals, independent component analysis (ICA) was used to decompose seizure EEG into a series of temporally independent but spatially fixed components as follows (Delorme and Makeig, 2004):

$$\mathbf{Y} = \sum_{i=1}^{Nc} \mathbf{Q}_i \mathbf{T}_i \qquad 3.2$$

where Nc is the number of independent components (ICs), and $\mathbf{Q}_i$ is the spatial map of the ith IC, and $\mathbf{T}_i$ is the time course of the ith IC. Assuming Ns out of the Nc ICs are associated with seizure activities, the scalp measurement generated by seizures becomes $\mathbf{Y} = \sum_{i=1}^{Ns} \mathbf{Q}_i \mathbf{T}_i$.

3.2.2 Component selection

Seizure activities are characterized by abnormal synchrony of discharges. The dynamic signal in the time and frequency domains can be observed in both IC time courses (Nam et al., 2002; Patel et al., 2008; Jung et al., 2009) and the scalp EEG signals. As such, the time-frequency similarity between the ICs and the original EEG signals was used for the selection of seizure components. From the ICA analysis, the ICs with artifactual origins, such as eye blinks, eye movements and muscle activity, were rejected (Jung et al., 2000; Jung et al., 2009; Urrestarazu et al., 2004). The EEG signals can be de-

noised by removing the artifactual components and back-projecting the signal components to EEG time courses. From the de-noised EEG signals, we computed the spectrogram of each channel. We picked the 15 channels with the largest spectral power in the frequency band of the ictal rhythms. We then selected a subset of these 15 channels whose spectral power after the seizure onset was statistically significantly stronger than that prior to the seizure onset. The mean spectrogram of these selected channels was considered as the spectrogram of original EEG (EEG-spectrogram). A spectrogram was then computed for each IC (IC-spectrogram). Correlations between each IC-spectrogram and the EEG-spectrogram were calculated. Statistical significance of the correlation between the EEG-spectrogram and each IC-spectrogram was calculated by a nonparametric statistical test using a surrogate method (Palus and Hoyer, 1998; Theiler et al., 1992). In the test, surrogate datasets were created from EEG signal and each IC time course so that their mutual correlations were not preserved. In each surrogate step, correlation between a new EEG-spectrogram and a new IC-spectrogram was computed. From the surrogated datasets, a distribution of correlation values can be obtained, from which components with statistically significant correlations with the EEG-spectrogram can be selected and considered as seizure components.

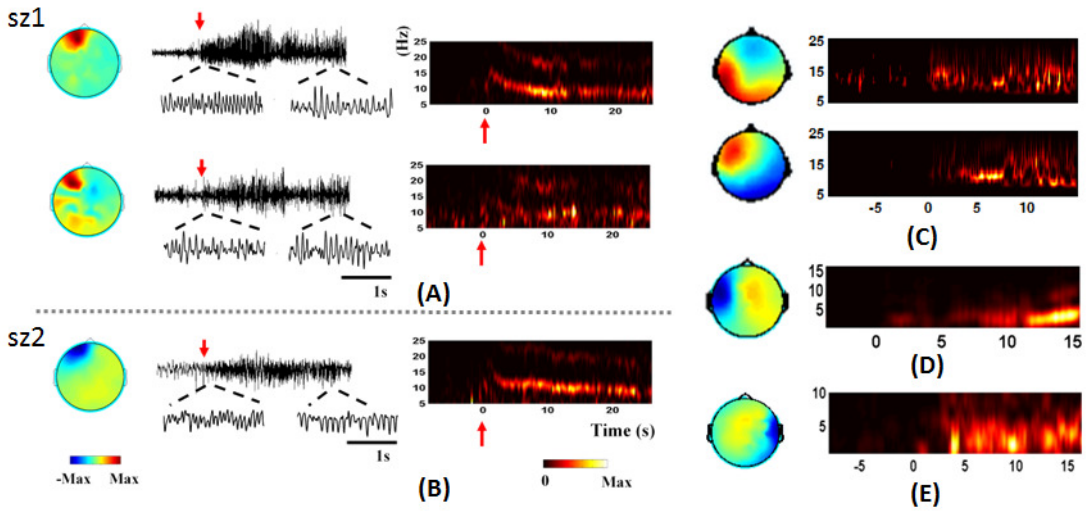

Figure 3.2 ICA separates ictal EEG into a series of independent components. (A) Spatial maps, time courses and spectrograms of two components identified from one frontal lobe seizure (sz) indicated the spatial, temporal and spectral features of the ictal discharges. (B) The maximal seizure component in another seizure of the same patient, which identified very similar spatial, temporal and spectral features (Adapted from Yang et al., 2011). (C) Two components identified from a temporal lobe seizure indicated temporal lobe focus. (D) Delta and theta band activity is most common in temporal lobe seizures.

ICA separated the seizure components from the background and noise of EEG. Fig. 3.2 shows several example ICs we identified from seizure EEG data. Fig. 3.2A-B shows a patient with frontal lobe epilepsy. Two components identified from one seizure of the patient (Fig. 3.2A) displayed increased rhythmic oscillations at about 15Hz at the seizure onset, which later progressed to an alpha-band discharge. This time-frequency evolution pattern of the ictal rhythmic discharges can be visualized in both IC time courses and their spectrograms in Fig. 3.2A, and was consistent with the independent observation reported by clinical epileptologists. The maximal seizure component

identified from another seizure of this patient (Fig. 3.2B) displays similar spatial, temporal and spectral features. Fig. 3.2C showed two components identified from a temporal lobe seizure of another patient. The spectrograms displayed alpha-band oscillation and the scalp maps indicated left temporal focus of the seizure activity. Delta-band (1-4 Hz) and theta-band (4-7 Hz) oscillations are most common in temporal lobe seizures. Fig. 3.2 D-E showed the maximal seizure components identified from two temporal lobe seizures from two different patients. Their spectrograms showed rhythmic oscillations varied over time in the delta and theta bands, and their scalp maps indicated strong electrical activity in the left and right temporal regions.

3.2.3 Source re-combination

From the selected components, an inverse solution of the de-noised EEG signal Y can be approximated as:

$$\hat{\mathbf{S}} \approx \sum_{i=1}^{N} (\mathbf{L}^{-1}\mathbf{Q}_i) \times \mathbf{T}_i \qquad 3.3$$

where

$$\hat{\mathbf{S}}_i \approx \mathbf{L}^{-1}\mathbf{Q}_i \qquad 3.4$$

is the inverse solution of each seizure component. The estimation of the spatiotemporal signal $\hat{\mathbf{S}}$ is approximated by a linear summation of the ICs in the source space, which can be seen as an inverse process of ICA. Different source imaging techniques based on distributed source model can be used to estimate the inverse operator $\mathbf{L}^{-1}$, such as the algorithms of minimum norm (Hamalainen and Sarvas, 1989), low resolution electromagnetic tomography (LORETA) (Pascual-Marqui et al., 1994), sLORETA-

weight minimum norm (SWARM) (Wagner et al., 2007), or fMRI-weighted minimum norm (Liu et al., 1998). Given the estimated spatiotemporal source signal $\hat{S}$, source distribution can be displayed at different time instant or in different time window.

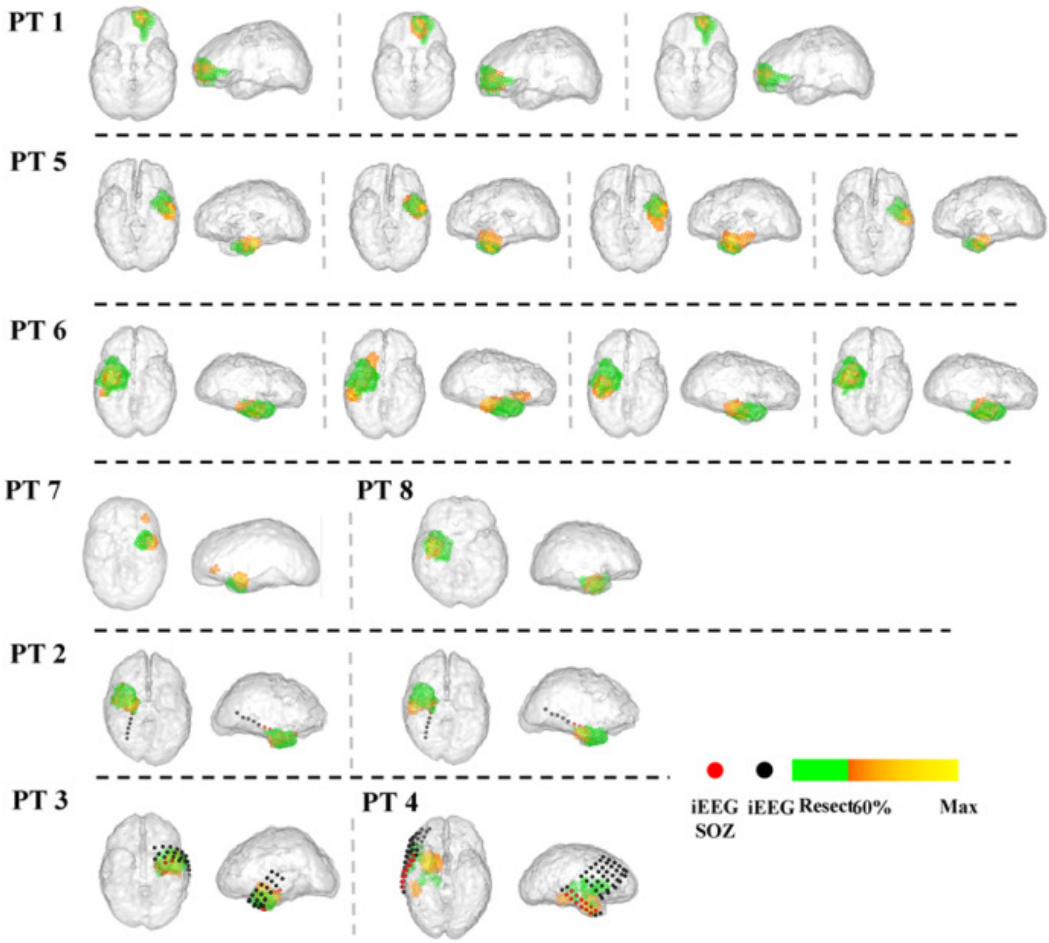

Figure 3.3 Estimated source at seizure onset (yellow to orange color bar) in comparison with surgically resected region (green) and iEEG recordings (Yang et al., 2011).

We tested the noninvasive DSI imaging approach in a small group of eight patients using surgical resection as the reference. In each patient who underwent resective surgery followed by a post-operative MRI scan, the brain tissues resected were determined from the post-operative MRI. Fig. 3.3 shows the source distribution at the seizure onset time. The estimated source of a frontal lobe seizure was reconstructed in a 3D brain model (Fig. 3.3, PT1 - yellow to orange color bar). A surgical excision was performed from the anterior left frontal lobe of this patient. A significant portion of the estimated source was localized to the epileptogenic focus resected in the left frontal lobe (Fig. 3.3, green voxels). The estimated source maximum was located within the surgically resected zone. The patient was rendered seizure free following surgery, which suggests that the estimated source was co-localized with the resected region and also the epileptogenic zone. The estimated sources of the other 7 patients (Fig. 3.3) were localized using DSI to the left or right temporal lobe. Among these patients, three (patient 2-4) were implanted with intracranial electrodes (Fig. 3.3, spherical dots). Independent visual interpretation of the iEEG reported by clinical epileptologists identified these seizures' onsets recorded by temporal lobe electrodes (Fig. 3.3, red dots). It can be observed that the DSI localization in the three patients was consistent with or in adjacent to the clinical gold standard iEEG. Among the 7 patients, six (patient 2, 3, 5-8) underwent resective surgery and were rendered seizure-free after 1 year follow-up. In each of the 13 seizures analyzed in this group, significant overlap was observed between the estimated SOZ and surgically resected region. Patient 4, who did not undergo resective surgery, had SPECT scans as part of the pre-surgical evaluation. SPECT analysis suggested several adjacent

foci of ictal hyperperfusion in the right temporal lobe (Fig. 3.3, green voxels), which may also serve as an evidence of right temporal lobe seizure.

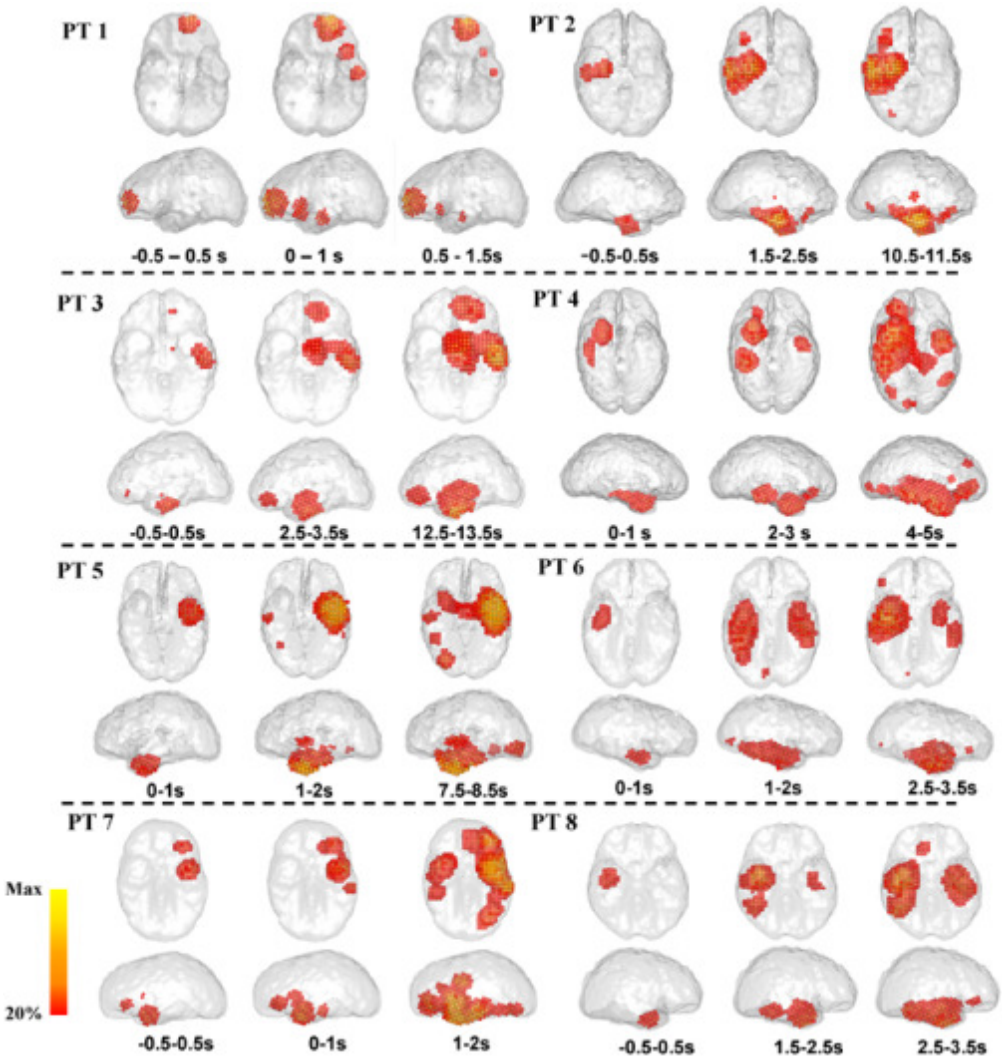

Figure 3.4 Dynamic seizure imaging over time reveals the development and propagation of seizures (Yang et al., 2011).

The DSI spatiotemporal imaging also reconstructs propagated activity after seizure onset. Shown in Fig. 3.4, from the estimated spatiotemporal source activity $\hat{s}(t)$, time-varying source power in each voxel was calculated as the spectral power of the ictal rhythms during 1-s time window. The source power distribution over the ictal period suggested the propagation of seizure activity from a focal location to extended regions ipsi-laterally or contra-laterally.

3.3 Clinical evaluation in operated or invasively-monitored patients

The ultimate goal of developing a noninvasive seizure imaging protocol is to improve the clinical diagnosis and treatment of epilepsy. In this chapter, we developed a high-resolution EEG monitoring protocol, in combination with the dynamic seizure imaging approach. In order to test the clinical applicability and performance of such a non-invasive seizure imaging protocol, we systematically evaluated the protocol in a large group of epilepsy patients who underwent at least one invasive procedure: resecitve surgery or iEEG chronic monitoring as illustrated in Fig. 3.5.

3.3.1 Patients

We studied 30 adult patients who underwent pre-surgical evaluation at Mayo Clinic, Rochester, MN. The study was approved by the Institutional Review Board (IRB) of the University of Minnesota (Minneapolis, MN) and the IRB of Mayo Clinic (Rochester, MN). All patients gave written informed consent before entering the study.

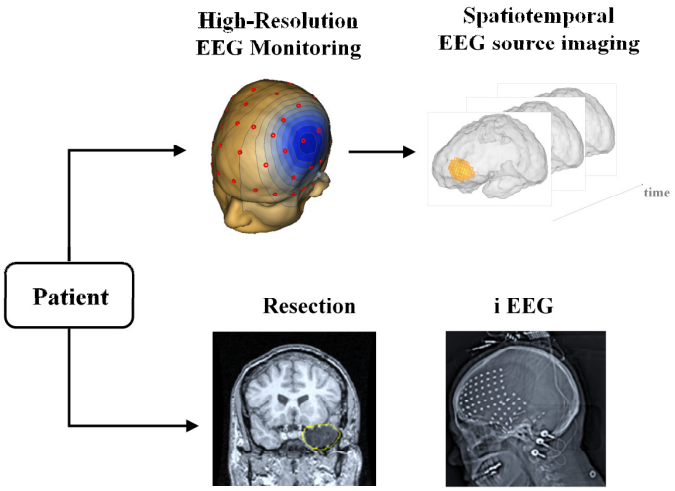

Figure 3.5 The patients were studied using a protocol consisting of a long-term high-resolution EEG monitoring and a spatiotemporal seizure imaging. The results were evaluated by comparing the results with invasive procedures, such as the outcome of resective surgery or intracranial EEG (Adapted from Yang et al., 2011).

Patients were selected to the study if they ultimately underwent at least one invasive procedure: (i) resective surgery and a post-operative follow-up of at least 12 months; (ii) a long-term invasive iEEG monitoring. Among the 30 patients, 15 of them had iEEG and 24 of them underwent resective surgery. After the surgery, 15 patients became seizure free (ILAE 1-2 outcome according to the International League Against Epilepsy - ILAE) and 9 patients had recurrent seizures (ILAE 3-5 outcome) according to their most recent follow-up. Patients, if not seizure free, may undergo other surgical procedures such as Vagus Nerve Stimulation (VNS). For these patients, although the outcome can be followed up several years ago, they were still considered as non-seizure-free cases. The surgery site, outcomes and iEEG monitoring results are shown in Table 3.1.

Surgery Site	n = 24
Temporal lobe	18
Extra-temporal lobe	3
TL with spread to E-TL	3

Surgery Outcome*	n = 24
ILAE 1-2	15
ILAE 3-5	9

Intracranial EEG	n = 15
Temporal lobe	10
Extratemporal lobe	4
TL with spread to E-TL	1

Table 3.1 30 adult patients were studied in order to test the clinical applicability of a non-invasive seizure imaging protocol. The patients were selected if they at least underwent one invasive procedure.

* Follow up of the resective surgery was conducted in 2011 or 2012 according to ILAE system. The ILAE outcome score is collected annually and can change every year.

3.3.2 High-resolution EEG and data acquisition

We used a 76-channel EEG system (XLTEK, Natus Medical Incorporated, CA, USA) for patient monitoring as an alternative to traditional 19- or 32-channel EEG. A total number of 76 individual electrodes were attached to the patient's scalp according to a 10-10 montage. The 76-channel dense-array EEG was continuously recorded as conventional long-term EEG for two days or even longer. The EEG signals were recorded with a 1-70 Hz band pass filter and a 500-Hz sampling rate. The EEG was carefully reviewed by experienced clinical epileptologists and clinical seizures were

identified. For each seizure, we segmented the ictal epoch with a short preictal period. Ictal EEG segments of different seizures of a same patient were concatenated if their electrophysiological features during seizures were similar.

In addition to the dense-array EEG, a MRI scan was conducted as part of the pre-surgical evaluation on each patient who participated in the study. If a patient had resective surgery, another anatomical MRI scan may be taken 3-4 months post-operatively. If a patient had chronic iEEG monitoring, a CT scan was taken in order to determine the location of the implanted electrodes.

3.3.3 Evaluation in epilepsy patients

Evaluation by invasive iEEG

In the 15 patients who underwent iEEG monitoring, the iEEG waveforms were carefully reviewed by experienced epileptologists. The iEEG electrodes involved in the seizure onset were determined by visual inspection. Each patient underwent a CT scan while the electrodes were implanted. The locations of the iEEG electrodes were segmented from CT images and co-registered with the pre-operative MRI images. We then compared the dynamic seizure imaging results with the seizure onset zone delineated by iEEG (iEEG-SOZ) in order to determine how the non-invasive seizure imaging deviates from the invasive recording.

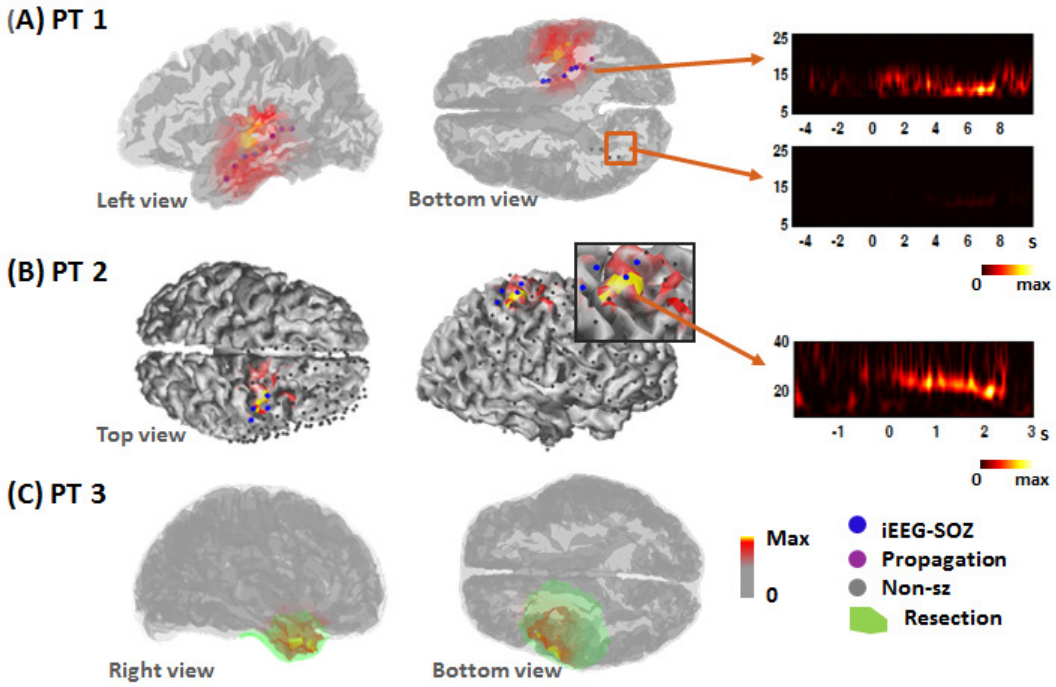

Figure 3.6 (A) DSI source estimation at seizure onset period in comparison with iEEG and resection in three example patients. Spectrograms are shown from regions of interest (ROIs). (A) One patient with left temporal lobe seizure without propagation to the right temporal lobe. (B) One patient with extra-temporal lobe seizure. And (C) another patient with temporal lobe seizure in consistent with resection.

Fig. 3.6A shows a patient with temporal lobe seizures. We plotted the spectral power distribution of the ictal rhythms in one-second time window at the seizure onset in the source space (Fig. 3.6A, red to yellow color bar). The DSI localized the seizure onset to the left temporal lobe, which agreed with the iEEG-SOZ (Fig. 3.6A depth electrodes marked by blue). We then computed the spectrograms of source waveforms in two regions of interests (ROIs), one in the left temporal lobe and the other near a depth electrode in the right temporal lobe. The spectrograms (Fig. 3.6A) of the two ROIs

indicated that the left temporal lobe was activated after the seizure onset and it showed alpha-band (8-12 Hz) ictal discharges, whereas the right temporal lobe was not activated throughout the ictal period. According to the visual inspection of iEEG, the ictal discharges started in the left temporal lobe (Fig. 3.6A, blue electrodes as iEEG-SOZ) and remained in the left hemisphere (Fig. 3.6A purple electrodes as propagation) without propagating to the contralateral temporal lobe (Fig. 3.6A, gray electrodes as inactive throughout the seizure). The spatiotemporal imaging of DSI indicated a similar propagation pattern as revealed by iEEG. Fig. 3.6B shows a patient with extra-temporal lobe seizure in which the patient's seizure showed short-term fast oscillations before the behavioral onset. The DSI localized the fast oscillations to a focal region in the right hemisphere (Fig. 3.6B) without propagation to other areas, which agreed with iEEG measurements (Fig. 3.6B, blue electrodes). The spectrogram from an ROI including this focal region (Fig. 3.6B) showed a fast oscillation in the beta frequency band.

We computed the localization error as the minimal distance between the estimated source maximum to all the electrodes involved in the iEEG-SOZ. The localization error for all 15 patients that underwent iEEG recording was around 2cm. However, there were two cases in which the DSI identified sources at regions without iEEG coverage. The patient was not seizure free at the most recent follow-up. The DSI results suggest more iEEG coverage of the brain which may be beneficial for pre-surgical planning. By removing these two cases, the mean localization error was about 1.4 times of the spatial resolution of iEEG (Fig. 3.7), as the inter-electrode distance of iEEG electrodes is around 1cm. We then conducted source imaging from the original EEG data using a frequency-

domain method (Worrell et al., 2000; Yuan et al., 2008; Yuan et al., 2010), which transforms the windowed time course of original EEG into Fourier space and uses the dominant ictal frequency to estimate the source distribution. Using the original EEG data, confounding components such as background brain signals were included for the source analysis. Therefore, the localization error using this method (Fig. 3.8A) in comparison with iEEG is significantly larger than the DSI method ($p<0.01$).

The location of the epileptogenic zone (e.g., mesial temporal, neocortical temporal, extra-temporal region) represents different level of difficulty for surgery treatment or for neuroimaging. In the studied patients, we categorized the patients into groups of neocortical temporal lobe seizure onset (neo-TL), medial temporal lobe seizure onset (med-TL) and extra-temporal lobe seizures (extra-TL), if their seizure onset was recorded respectively by surface temporal electrodes (grids and strips), depth electrodes, or surface extra-temporal electrodes. The resultant localization error was smaller (Fig. 3.7) in cases where seizures started from the superficial portion of the cortex (neo-TL and extra-TL) but relatively larger in seizure recorded by depth electrodes. However, because the number of patients in each group is small, the statistical difference between different groups cannot be reliably tested.

Evaluation by resective surgery

Fig. 3.6C shows a patient with temporal lobe seizures. The DSI localized the seizure onset to the right temporal lobe. The patient underwent a right temporal lobectomy (Fig. 3.6C, green volume) and became seizure free after the surgery. The

estimated source overlaps with the resected region (Fig. 3.6C, green volume) and the DSI maximum was localized within the boundary of the resection. The seizure free outcome indicates the co-localization of the epileptogenic zone with the surgically-removed region, and therefore the DSI source.

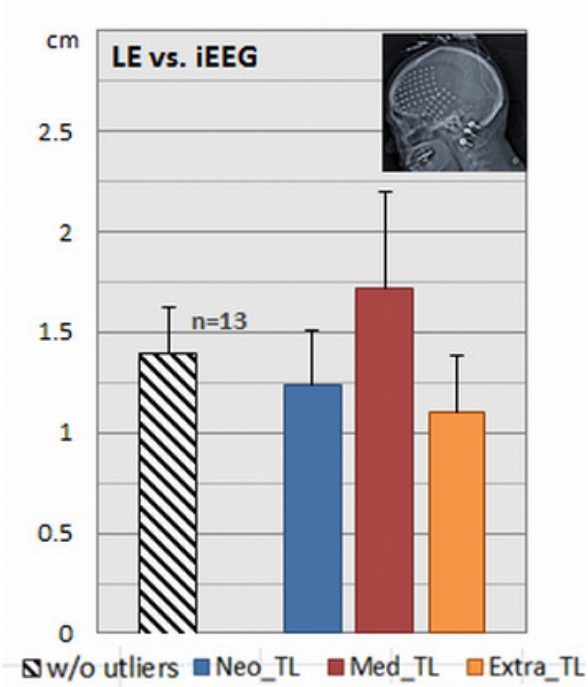

Figure 3.7 The localization error (LE) of the source imaging results in comparison with the seizure onset zone delineated by iEEG in all the patients without two outliers (estimated source localized in the region without iEEG coverage), patients with seizure onset in the neocortical-temporal (blue), medial-temporal (red), and extra-temporal (orange) regions. The error bar in this chapter represents the standard deviation of the mean of each group.

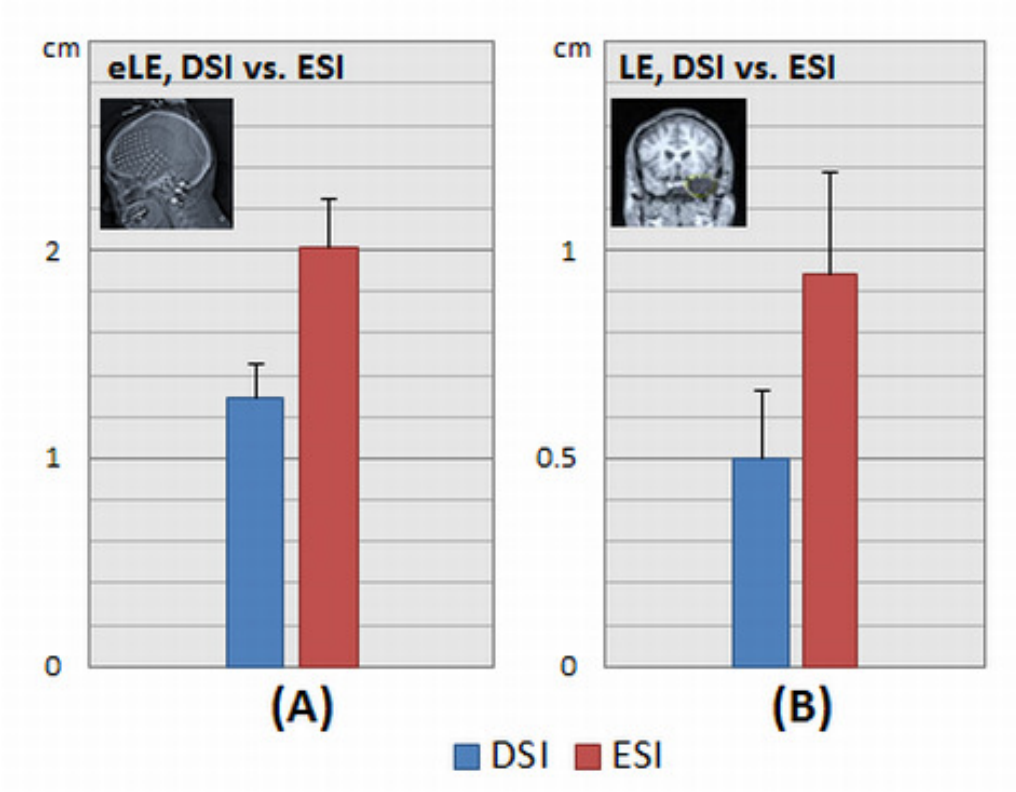

Figure 3.8 Comparison of dynamic seizure imaging (DSI) results with the frequency-domain method applied on original EEG (indicated as EEG source imaging – ESI here). (A) Localization error in comparison with iEEG (eLE) in all the patients with iEEG recordings excluding two outliers. (B) Localization error (LE) in comparison with resection in the group of patients with seizure free outcome.

There were 24 patients who underwent resective surgery and had at least one-year follow up (Table 3.1). The ILAE score is taken annually and therefore can track the change of surgery outcomes over time. But here we used the ILAE score obtained most recently to determine their surgery outcomes and to group patients. In most cases, patients underwent a post-operative MRI scan 3-4 months after the surgery, allowing for the segmentation of the resected regions from the post-operative MRI. Some patients who

underwent a standard temporal lobectomy did not undergo a post-operative MRI. In these patients, the surgically removed regions were determined according to the description in the surgery notes. We computed a localization error as the distance from the estimated source maximum to the boundary of the resected volume, in order to quantify how the DSI source deviates from the surgically removed regions.

In the group of 24 patients, the mean localization error using non-invasive seizure imaging was around 1cm. However in the subset of patients who became seizure free, the localization error was less than 0.6cm, which is much smaller. A patient becoming seizure free or not is an indication of whether the patient's epileptogenic zone was completely removed. Among the 24 patients, 15 of them had ILAE 1-2 outcome at the most recent follow-up, which means they became seizure free for at least one year. The other group of patients had ILAE 3-5 outcome at the most recent follow-up. The reduction of seizure frequency indicated that a significant part of the critical epileptic network may be removed or disconnected. However, the occurrence of seizures after the surgery indicated that the epileptogenic zone was not removed completely. In the group of patients who became seizure free, the localization error was significantly smaller than that in the group of patients who obtained suboptimal surgical outcomes ($p<0.05$). When the frequency-domain method (Worrell et al., 2000; Yuan et al., 2008; Yuan et al., 2010) was applied to the original EEG data in the seizure free group (Fig. 3.8B), the resultant localization error was larger than that of the DSI method ($p<0.05$).

High-resolution vs. low-resolution EEG

We used 76-channel EEG in the studied cohort, as opposed to the 32-channel or 19-channel EEG commonly used in clinical settings for the monitoring of epilepsy patients. To compare the imaging capability of different electrode densities, we down sampled the scalp electrodes from 76 to 32 and 19. We then solved the inverse problems using the each electrodes configuration. Note here, the down-sampling of the electrodes was conducted during the step of inverse problems. The 76-channel information was still used for ICA and component selection. So the imaging accuracy of 32- and 19-channel systems was partly contributed by the increased spatial sampling of the dense-array 76-channel system.

In the patients who underwent iEEG monitoring or resective surgery, the localization error increased as the number of electrode decreased. In the patients who underwent iEEG monitoring (Fig. 3.9A), without the two outliers, the difference was statistically significant between the 76-channel, 32-channel and 19-channel. In the subset of patients who underwent surgery and became seizure free (Fig. 3.9B), the difference was also statistically significant between the 76-channel, 32-channel and 19-channel. In the subset of patients with recurrent seizures (not shown here), the difference between the 76-channel and 32-channel however was not as significant as that in the seizure-free cases. This may be caused by the fact that the resected region is not a good approximation of the epileptogenic zone if the patients were not seizure free. Therefore, the reference (e.g., resection) itself may introduce localization error, making the effect of channel numbers less significant.

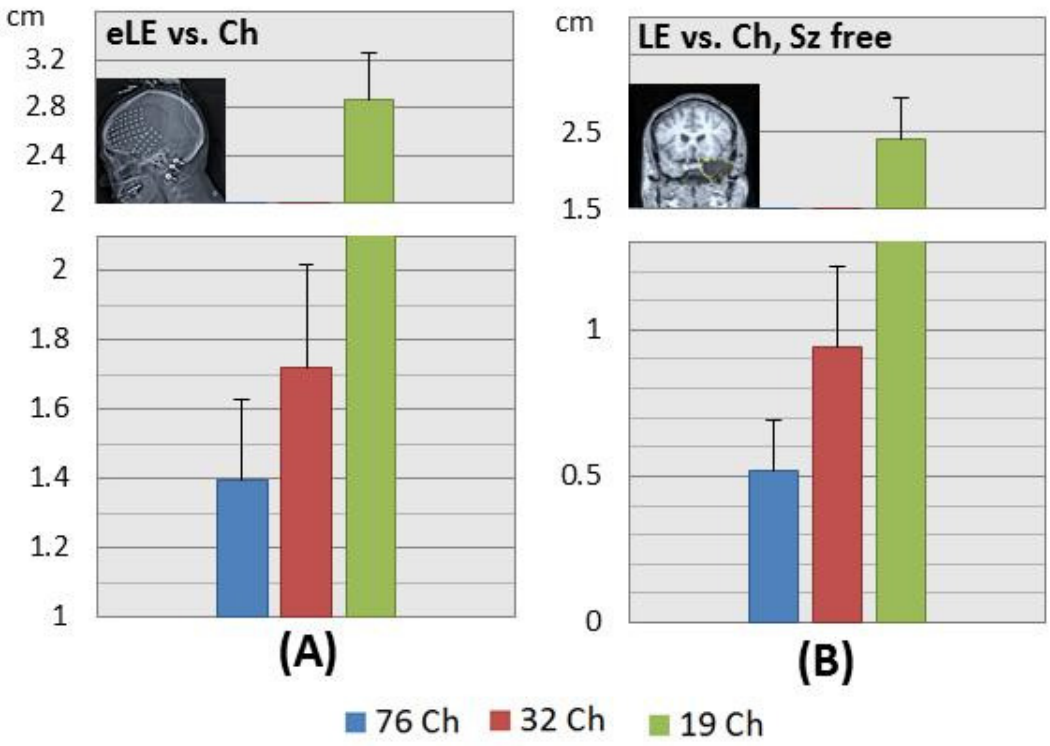

Figure 3.9 The performance of source imaging using 76- (blue), 32- (red), and 19- (green) electrodes, in patients who had (A) intracranial EEG monitoring and (B) resective surgery and became seizure free.

To quantify the difference between two distributions, we then defined a volume localization error (vLE), which is the mean distance between each pair of voxels in two volumes: one in the DSI delineated source volume $\mathbf{V}$ and the other in the resected volume $\mathbf{V_0}$, as:

$$\mathbf{vLE} = mean_{r\in \mathbf{V}, r'\in \mathbf{V_0}}|r - r'| \qquad 3.5$$

Note that, a volume can have a volume distance to itself, because each pair of voxels within the volume has distance between them. For the resected volume, the value is:

$$\mathbf{vLE_0} = mean_{r,r'\in \mathbf{V_0}}|r - r'| \qquad 3.6$$

The percentage of change of volume localization error is:

$$vLE\% = (vLE - vLE_0)/vLE_0 \qquad 3.7$$

The volume of the estimated source V changes when different thresholds are applied. We used a threshold that gave a same size volume as the resected region V_0. Therefore, the vLE quantifies the distance between the estimated source volume and the resected volume when the two volumes are equalized. This distance measurement is an indication of the performance if the same volume is resected based on the source imaging results. This volume localization error therefore quantifies how the two volumes or distributions deviate from each other. In the seizure-free group, the volume localization error increased as the number of channels decreased. The differences of the localization accuracy between 76 channel, 32 channel and 19 channel systems also demonstrated that increasing the number of scalp sensors would benefit the estimation of the distribution of seizure sources.

3.4 Discussion

In this chapter, we developed and evaluated the clinical applicability of a high-resolution EEG monitoring and a non-invasive seizure imaging protocol. In the studied cohort, the 76-channel dense-array EEG successfully replaced the conventional 19- or 32-channel systems for routine long-term EEG video monitoring. In addition to seizure recording, the dynamic seizure imaging algorithm achieves the localization of ictal discharges in concordance with the most invasive procedures: invasive recording of iEEG and/or the brain tissues removed in the surgery. In general, the degree to which the source imaging results agreed with the resection was associated with an increased likelihood of a

seizure free post-operative outcome. Increase the number of scalp electrodes from 19 and 32 to 76 also significantly improved the performance of the source imaging.

In the past a few decades, the development of non-invasive neuroimaging techniques has significantly improved our ability to localize epileptic sources for pre-surgical evaluation (Brodbeck et al., 2011; Rosenow and Luders, 2001; Spencer, 1994). MRI provides a way to non-invasively access anatomical abnormalities. High-field MRI further improves the resolution to delineate subtle and deep structural changes (Henry et al., 2011). Functional neuroimaging techniques (e.g., SPECT, PET and fMRI) have also been utilized to image the slow hemodynamic signal change in the epileptic network (Blumenfeld et al., 2009; Grouiller et al., 2011; Spencer, 1994; Tyvaert et al., 2008). However, despite the rapid development of neuroimaging techniques, there lacks a functional imaging protocol that is non-invasive and fast enough to track the neural activity in a millisecond time scale.

EEG and MEG source imaging techniques represent the recent advancement to image electrophysiological brain activity through non-invasive approaches (Plummer et al., 2008). With the recent development of high-resolution recording techniques, such as MEG and dense-array EEG, the localization of interictal activities has been more frequently considered as a potential clinical tool to assist the pre-surgical evaluation (Brodbeck et al., 2011; Knowlton et al., 2008; Knowlton et al., 2009; Stefan et al., 2003). However, it is also well known that the irritative zone defined by inter-ictal spikes do not reliably determine the minimum region of brain tissue that must be resected in order to render the patient seizure free (Marsh et al., 2010). Fewer studies have investigated the

source imaging of seizures (Assaf and Ebersole, 1997; Boon et al., 2002; Ding et al., 2007), and only recently has seizure source imaging from high-resolution EEG/MEG recording been investigated (Assaf et al., 2003; Holmes et al., 2010; Koessler et al., 2010). This is partially due to the fact that the recording of seizures requires long-term monitoring (e.g., 2-3 days) in a relatively flexible recording environment. The MEG techniques, however, cannot be easily adapted to such a long-term application. For patients with less frequent seizures, the monitoring time can be even longer, which can be also challenging for some dense-array EEG systems (Holmes et al., 2010). In this chapter, we described an EEG system which increased the scalp sampling sites by increasing the number of scalp electrodes. However, instead of using a cap or a net with integrated electrodes, we used individual electrodes that have been commonly used for clinical EEG monitoring. The 76-channel system, therefore, closely resembles the clinical EEG that has been tested through decades of practice. In the studied cohort, the 76-channel EEG successfully captured seizures in all patients.

In addition to the recording, the mathematical modeling and imaging of dynamic seizure activity represents another difficulty of seizure imaging. Source imaging techniques, such as dipole localization (Assaf and Ebersole, 1997), sub-space scanning methods (Ding et al., 2007), time-instant- or short-window- or microstate-based source imaging techniques (Holmes et al., 2010; Lantz et al., 2001; Worrell et al., 2000) have been developed in order to track the dynamics of seizure activity. In this chapter, we used a dynamic seizure imaging algorithm to image the spatiotemporal features of the seizure activity. The change of ictal discharges in the spatial, temporal and frequency domain

were all considered. The non-invasive imaging from the dense-array EEG recording is capable of reconstructing the pattern of the way in which a seizure starts and develops, in concordance with the measurement or evaluation obtained through the most invasive procedures - resective surgery and iEEG. The source imaging results in the seizure-free group agreed with the surgical resection significantly more than that of patients who continued to have uncontrolled seizures. The statistical difference between the two groups suggests that patients have a higher chance to achieve optimal surgical outcome if the brain tissue near the estimated source is removed.

The invasive monitoring of iEEG is the current clinical golden standard. However, its invasiveness restricts the number of patients who can receive such an electrophysiological brain imaging. In this chapter, however, we suggests a non-invasive approach which provides spatiotemporal imaging in a spatial domain similar with iEEG but with increased spatial coverage. In the studied cohort, this non-invasive approach localizes the seizure onset zone in concordance with iEEG. Considering the iEEG has relatively low spatial resolution (inter-electrode distance is about 1cm), the brain region between electrodes can be poorly sampled. The localization error (Fig. 3.7) was therefore contributed not only by the errors of source imaging but also by the low spatial resolution of iEEG. The close approximation of the source imaging results to iEEG invasive measurement suggests the localization value of this non-invasive seizure imaging approach. Its non-invasive nature allows for the application of such an electrophysiological seizure imaging approach to every patient for pre-surgical evaluation. If an agreement was achieved between this non-invasive electrophysiological

imaging, MRI and other neuroimaging or neurological tests, the proportion of patients who must go to invasive recording can be significantly decreased. In two cases, our source imaging results were localized to the brain regions without iEEG coverage, and the patients were not seizure free after the resection of the iEEG-SOZ. The discrepancy may be caused by the fact that scalp EEG can miss small activity recorded by iEEG. However, it may also suggest that there were critical regions of the brain not well covered by iEEG. In fact, the performance of iEEG significantly relies on how well the extent of electrode sampling could cover the seizure onset zone or epileptogenic zone. Priori information from non-invasive measurement or neurological tests is extraordinarily important for the guidance of the electrodes' placement (Knowlton et al., 2009). The present non-invasive seizure imaging protocol provides full coverage of the brain. With this priori information obtained by this noninvasive protocol, there is a higher chance to obtain complete coverage of the epileptogenic network, and as a result improve the diagnostic yield of iEEG.

The localization accuracy in the studied cohort differs in patients with superficial or deep seizure onset zones. The source imaging deviates less from the iEEG if the activity was recorded by surface temporal or extratemporal electrodes (grids or strips), but relatively more from the iEEG if the activity was recorded by depth electrodes. This may be caused by the fact that EEG source imaging, as a non-invasive modeling method, is more sensitive to superficial activity, and therefore would favor the estimation of sources close to the surface of the brain. It may also be caused by the poor spatial coverage of depth electrodes. The depth electrodes usually cover 1-D space in the deep

temporal lobe structures, and the chance of incomplete coverage and sampling of the real seizure source is prevalent. Activity in a depth electrode likely represents strong activity in surrounding tissues rather than activity at the electrode itself. However, because the number of patients in each group is small, the observation of the difference may not have enough statistical power.

Over the past thirty years, numerous studies have been conducted to support an advanced high-resolution form of non-invasive electromagnetic recording (e.g. dense-array EEG (Gevins, 1993) and MEG (Hämäläinen et al., 1993). Theoretical and experimental studies suggested recordings from approximately 100 scalp sites for a good spatial sampling rate and a stable spatial representation (Spitzer et al., 1989; Srinivasan et al., 1996). In the clinical realm, while standard EEG monitoring still uses conventional 19-to-32-electrode montages, recent adoption of high-resolution EEG/MEG for the pre-surgical localization of partial epilepsy has increased in popularity. One EEG study (Lantz et al., 2003) revealed in a group of interictal discharges that the localization accuracy can be significantly improved by increasing the number of EEG electrodes from 31 to 63, yet only slightly improved by increasing the number from 63 to 123. According to these previous studies, increasing the channel number to 76, as in our system, provides significantly more spatial detail for the localization of epileptic sources. We evaluated the seizure imaging results using 76, 32 and 19 electrodes in a relatively large group of patients. We found that increasing the number of scalp electrodes significantly improve the localization accuracy in comparison with invasive procedures. The 76-channel EEG performed the best in terms of the localization of the onset of ictal discharges. The

increased implementation time could be a potential disadvantage of high-density EEG. However, it only required an average of 60 minutes to mount the 76 electrodes by two experienced medical staff, compared to 30 minutes using a 32-channel clinical EEG. Recent studies have reported a fast-capping EEG technique for which the preparation time can be as short as 15 minutes (Holmes et al., 2010). Such a technique however is limited by relatively shorter recording time due to the fact that patient usually cannot comfortably wearing the device for more than 2 to 3 days (Holmes et al., 2010). The 76-channle recording protocol, on the other hand, used similar electrodes with the conventional clinical EEG whose feasibility of long-term monitoring has been demonstrated over several decades' worth of clinical practice. Considering the benefits of having such a non-invasive high-resolution electrophysiological imaging approach, and the fact that the clinical long-term monitoring usually lasts for at least two days, the increased 30 minutes preparation time is minimal.

In conclusion, this chapter describes a non-invasive seizure imaging protocol consists of the high-resolution EEG monitoring and the dynamic seizure imaging approach. This protocol provides a way to non-invasively access electrophysiological abnormalities during seizures. The concordance of this non-invasive imaging approach with iEEG and surgical outcome suggests a potential position for such an approach in routine pre-surgical evaluation, from mainly two aspects: (i) aiding the implant of iEEG electrodes to improve the localization yield and accuracy of iEEG, and in some cases (ii)

assisting the non-invasive localization of the epileptogenic region as a potential alternative for the invasive long-term iEEG monitoring.

Chapter 4 Epilepsy and consciousness

4.1 Introduction

Loss of normal brain functions is one of the most common symptoms accompanying epileptic seizures. Partial seizures can be divided into simple partial seizures and complex partial seizures, with the former preserving and the latter impairing normal responsiveness or consciousness (Commission of ILAE 1981). Partial seizures can occasionally develop into secondarily generalized seizures, which recruit widespread brain regions (Blumenfeld et al., 2009; Engel, 1989) and can induce deep unconsciousness. In temporal lobe seizures, the most common form of epilepsy, patients have a significant chance of experiencing loss of responsiveness and consciousness (Arthuis et al., 2009; Engel, 1989; Englot et al., 2010; Lee et al., 2002). After the termination of seizures, there can be a postictal period (Fisher and Schachter, 2000; Hammers et al., 2007), during which patients may experience confusion, decreased responsiveness, memory deficits, disorientation, and other cognitive deficits (Fisher and Schachter, 2000). The postictal state is the time in which the brain recovers from the trauma caused by seizures before regaining normal functions. This abnormal state can last anywhere from minutes to hours, and is generally longer in the case of more severe seizures, such as generalized seizures.

The phenomenon of loss of consciousness and responsiveness has been investigated in several different models, such as coma (Bickford and Butt, 1955), anesthesia (Alkire et al., 2008), and slow-wave sleep(Alkire et al., 2008; Hofle et al., 1997; Massimini et al., 2005). Studies have suggested that loss of consciousness can be

associated with abnormal subcortical/cortical activity, the breakdown of subcortical-to-cortical and cortical-to-cortical integration, or the loss of discriminable firing patterns that code higher-order information processing (Alkire et al., 2008; Hofle et al., 1997; Massimini et al., 2005). In temporal lobe epilepsy, anatomical and functional abnormalities have been found, either permanently or temporarily. In patients with epilepsy-induced cognitive dysfunctions, studies have found altered functions of temporal cortex, subcortical structures, and corticothalamic connectivity (Arthuis et al., 2009; Blumenfeld et al., 2009; Guye et al., 2006; Lux et al., 2002). In addition to the dysfunctions of the epileptogenic network, recent neuroimaging studies have discovered decreased activity in neocortical fronto-parietal regions in epileptic brains. SPECT and fMRI measured decreased cerebral blood flow (CBF) and blood-oxygen-level dependence (BOLD) signals, respectively, in the fronto-parietal cortex, overlapping with the default mode network, during different types of epileptic activities (Bai et al., 2010; Gotman et al., 2005; Grouiller et al., 2011; Laufs et al., 2006; Siniatchkin et al., 2010). This deactivation occurs during seizures and persists into the postictal period (Blumenfeld et al., 2009).

EEG and intracranial EEG studies have recorded abnormal slow-wave activity in patients with seizure-induced dysfunctions. Postictal (Hufnagel et al., 1995; Jan et al., 2001) or background (Panet-Raymond and Gotman, 1990; Tao et al., 2011) slow waves in the temporal lobe have commonly been measured in epileptic patients. The postictal slowing has a significant chance of lateralizing to the temporal lobe of seizure onset (Hufnagel et al., 1995; Jan et al., 2001). Not until recently has the presence of neocortical

slow-wave activity in the fronto-parietal lobe been implicated to seizure induced behavioral changes. Recent iEEG studies have recorded increased slow waves in lateral fronto-parietal electrodes during ictal and postictal periods. The elevation of slow-wave activity, especially delta-band activity (<4Hz), was correlated with behavioral changes in simple partial and complex partial seizures (Blumenfeld et al., 2004; Englot et al., 2010). However, iEEG lacks the spatial coverage that is necessary to investigate slow-wave activity in the whole brain. The cortical coverage from iEEG depends on the placement of the electrode array, which can vary significantly between patients. The implanted electrodes usually cover the epileptogenic zone (e.g., bi-lateral temporal lobes in temporal lobe epilepsy) to a suitable extent, as the delineation of the epileptogenic is of most clinical importance. However, other cortical areas, such as the medial and lateral fronto-parietal cortex, may be poorly sampled by the iEEG array.

In this chapter, we used dense-array scalp EEG to study postictal slow-wave activity in a group of 28 patients with temporal lobe seizures. The seizures were categorized to simple partial, complex partial and secondarily generalized seizures according to behavioral changes during and after seizures. Previous studies have demonstrated that the behavioral and cognitive changes, deactivation of metabolic signals, and elevation of slow-wave activity can persist into the postictal states (Blumenfeld et al., 2004; Blumenfeld et al., 2009; Englot et al., 2010; Fisher and Schachter, 2000). We studied the postictal period in order to focus the analysis on slow waves, while excluding the active portion of ictal rhythmic discharges. We used dense-array EEG and the EEG source imaging technique to reconstruct the common spatial

distribution of slow waves across the group of patients, despite the difference between individuals. We further investigated the variation of spectral and spatial features of postictal EEG signals in simple partial, complex partial and secondarily generalized seizures.

4.2 Methods and materials

4.2.1 Patients and data acquisition

We studied 28 adult patients who underwent a pre-surgical evaluation for medically intractable temporal lobe epilepsy at the Mayo Clinic in Rochester, MN. The study was approved by the IRB of the University of Minnesota (Minneapolis, MN) and the Mayo Clinic (Rochester, MN). All patients gave written informed consent before entering the study.

Each patient underwent long-term dense-array EEG monitoring using a 76-channel system (XLTEK, Natus Medical Incorporated, CA, USA). A total number of 76 individual electrodes were attached to the scalp according to a 10-10 montage. The EEG signals were recorded with a 1-70 Hz band pass filter and a 500-Hz sampling rate. Patients were selected for the analysis if the epileptogenic zone involved the left or right temporal lobe, as determined by successful resective surgery, iEEG measurement, and/or ictal scalp EEG. Detailed information of patients studied, including their surgical outcome, iEEG and EEG measurements can be found in Table 4.1.

<table>
<tr><th colspan="3">Seizure free / Intracranial EEG (n =23)</th><th>Surgery</th><th>EEG</th></tr>
<tr><td>15</td><td>11</td><td>1</td><td>3</td><td>2</td></tr>
<tr><td rowspan="2">Sz free
(> 1 yr)</td><td rowspan="2">Ictal iEEG</td><td>Interictal
iEEG</td><td>> 50% reduction
(> 1 yr)</td><td rowspan="2">Ictal
EEG</td></tr>
<tr><td>Ictal EEG</td><td>Ictal EEG</td></tr>
</table>

Sz free: seizure free after the resection of part of the temporal lobe; **>50% reduction**: ILAE 3-4 outcome; **Ictal iEEG**: intracranial EEG measured seizure onset in temporal lobe; **Interictal iEEG**: intracranial EEG measured interictal events in temporal lobe; **Ictal EEG**: scalp EEG measured seizure onset in temporal lobe

Table 4.1 Patients and their surgical outcome / iEEG / EEG indicating temporal lobe seizures

4.2.2 Behavioral analysis

In order to determine whether patients experienced any impairment in responsiveness or consciousness, they were presented with questions, simple commands, and a memory phrase, such as "remember purple banana". After the seizure they were asked to recall the memory phrase. If patients did not respond to questions or commands, or were unable to recall a memory phrase, they were classified as having complex partial seizures. If patients were fully alert and appropriately responsive throughout the event and recalled the memory phrase, they were classified as having simple partial seizures. Seizures that had developed to secondary generalization were also identified if ictal discharges propagated to a wide-spread portion of the brain after a short period of focal activation. The identification of the secondarily generalized seizures agreed with the symptoms recorded by videos or clinical notes.

4.2.3 Data analysis

The continuous EEG was reviewed by experienced epileptologists and EEG technicians. For each patient, seizures were identified and the end of each seizure was considered as the EEG offset of ictal rhythmic discharges. In some seizures, the offsets were difficult to decipher because of pronounced artifacts before and after the seizures terminated. In these cases, the seizure offset was determined as the time when the artifacts or noise subsided. Seizure duration, defined as the time from seizure onset to offset, varied significantly between patients. In studied cohort, the mean seizure duration was 75±37 s for simple partial, 90±41 s for complex partial, and 210±165 s for secondarily generalized seizures. Approximately one minute of post-ictal EEG was segmented following the seizure offset. Electrodes and periods of EEG signals with significant artifacts and noise were removed from the analysis. In patients with fewer seizures, relatively longer postictal EEG periods were segmented. In the postictal period of secondarily generalized seizures, there can be a period of suppression of widespread brain areas, during which the EEG signal is "quiet" and "smooth" with a substantial decrease of voltage (Blumenfeld et al., 2004). Following this suppression can be a "burst-and-suppression" pattern, in which bursts of slow wave activity are seen once every several seconds. In these cases, we analyzed the postictal EEG on average 75 seconds after the seizure offset (can be shorter or longer because of the variation of the suppression period between patients) with slow waves or the burst-and-suppression pattern, because this pattern contains large amplitude slow waves and resembles slow-

wave bursts that have been observed in other states of altered consciousness, such as anesthesia (Alkire et al., 2008; Liu et al., 2011).

The analysis of the postictal EEG is summarized by the schematic flow chart displayed in Fig. 4.1. The postictal EEG of each seizure was first filtered using a 1-30 Hz band-pass filter. For each patient, postictal EEG segments of the same seizure types (simple partial, complex partial or secondarily generalized) were concatenated and submitted to extended infomax ICA (Delorme and Makeig, 2004). Each independent component (IC) can be represented by a spatial map that indicates the source location, as well as a time course that represents the source temporal dynamics. The ICs with extra-cerebral origins such as eye blinks, eye movements and muscle activity were rejected (Jung et al., 2000). Dipolar sources were fitted to the spatial map of each of the remaining ICs (Delorme and Makeig, 2004). Components that could not be explained by dipolar sources (with a residual variance of more than 25%) were rejected (Delorme and Makeig, 2004; Jung et al., 2009). The remaining ICs were considered physiologically plausible signal ICs (Debener et al., 2006; Makeig et al., 2002; Nam et al., 2002; Yang et al., 2010), representing rhythmic activities of the functional networks in the postictal brain. The EEG signals can be de-noised by removing the artifactual ICs and regenerating EEG time courses.

Two indices - relative spatial delta power $rRel\delta$ (with r indicating 'spatial') and relative spectral delta power $fRel\delta$ (with f indicating 'spectral') were used to measure the spatial and spectral features of the delta-band activity in the different seizure types. A Fast Fourier transform (FFT) was used to calculate the spectral properties of each time

courses. The spectral power of a frequency band was determined by integrating the spectral power within the frequency band. The power of delta band activity was calculated by integrating spectral power from 1-4 Hz.

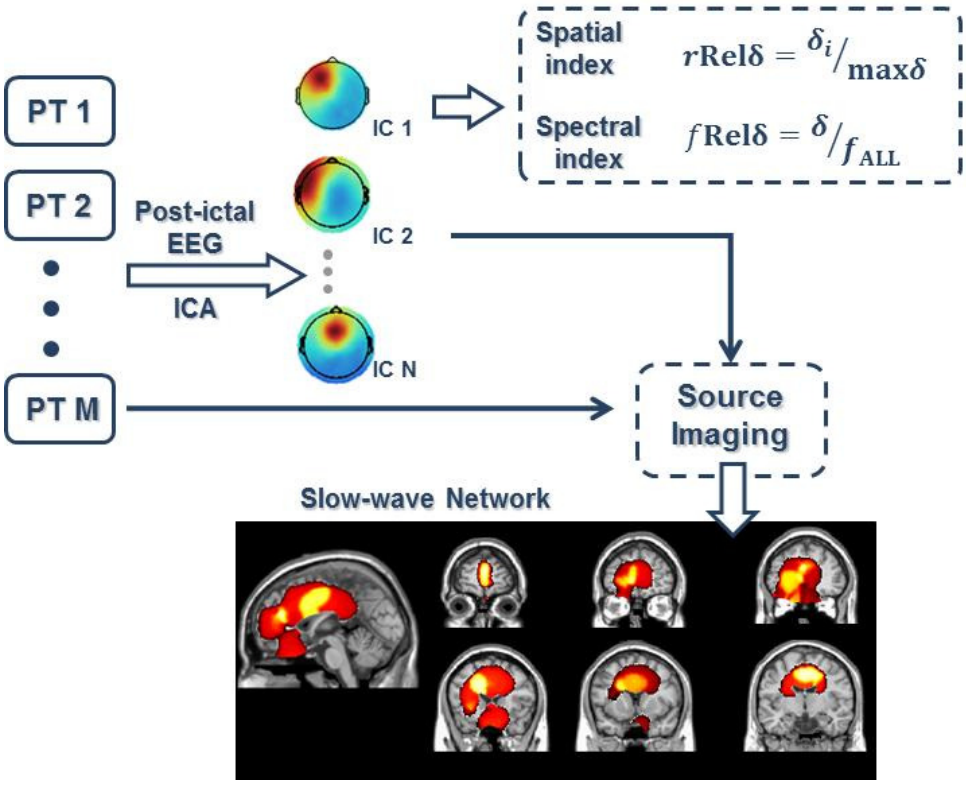

Figure 4.1 Schematic flow chart of the data analysis protocol. Two indices, relative spatial delta power $r\text{Rel}\delta$ and relative spectral delta power $f\text{Rel}\delta$, were used to quantify the spatial and spectral features of postictal EEG. ICA and EEG source imaging were used to find the spatial distribution of postictal slow waves. IC = Independent Component; PT = Patient.

The first index of delta power, $r\text{Rel}\delta$, measures the delta power in one region normalized by the maximum across regions. From the de-noised EEG, the EEG sensors can be grouped by their scalp locations into N regions (e.g., frontal region vs. temporal

region). The relative spatial delta power of one region is $r\mathrm{Rel}\delta = \delta_i / max\delta$, where δ_i is the mean delta power of a region and $max\delta$ is the maximum mean delta power amongst all regions. The $r\mathrm{Rel}\delta$ is a ratio in the range of [0, 1] which reflects the spatial delta distribution. The $rRel\delta$ can be also calculated for ICs, as the scalp maps of ICs indicate different cortical distributions. When N ICs are derived for a seizure, the $rRel\delta$ for each IC is calculated as $r\mathrm{Rel}\delta = \mathrm{IC}\_\delta_i / \mathrm{maxIC}\_\delta$, where IC_δ_i is the delta power of an IC and maxIC_δ is the maximum delta power of all ICs. The index of relative spatial delta power could also be affected by an increase or decrease of total EEG power, which would affect all frequency bands including 1-4Hz.

The second index of delta power, $fRel\delta$, measures the delta power relative to the total spectral power from 1-30Hz. For a time course $x(t)$, the relative spectral delta power can be calculated as $f\mathrm{Rel}\delta = \delta / f_{\mathrm{ALL}}$, where δ is spectral power of the time course in the delta band (1-4 Hz) and f_{ALL} is the spectral power in the band of 1-30 Hz. In this way, the relative spectral delta power can be calculated for the time course of an EEG channel or for the time course of an independent component. The relative spectral delta power, $fRel\delta$, and relative spatial delta power, $rRel\delta$, thus measure different aspects of EEG signals, as the former measures how the EEG power shifts in the frequency domain and the latter measures how the EEG power shifts in the spatial domain.

We studied the postictal EEG of three types of seizures: simple partial, complex partial and secondarily generalized seizures. From de-noised EEG, the $rRel\delta$ and $fRel\delta$ were calculated for electrodes covering different regions. The group means of the two indices in each region were calculated for each seizure type. Derived from ICA analysis,

the ICs of all seizures were then clustered using the k-means clustering technique (Seber, 1984; Spath, 1985). The scalp map and dipole location for each IC were inputs for the k-means clustering, and the squared Euclidean distance was used as the distance function of the k-mean cluster (Delorme and Makeig, 2004; Seber, 1984; Spath, 1985). We first separated the signal components into 20 clusters using the k-means clustering technique, then combined components with similar scalp potential distributions into left/right temporal, left/right frontal, orbito-frontal, dorsal medial frontal, central-parietal, left/right parietal, and occipital clusters. The $rRel\delta$ and $fRel\delta$ were also calculated for each IC. The group means of the two indices were calculated for each seizure type within each cluster.

The cortical source distribution of a cluster was computed by solving the EEG inverse problem to estimate a source distribution from the cluster's centroid. Each cluster's centroid map was the averaged scalp map of all components in a cluster. We used a standard head model provided by the Montreal Neurological Institute (MNI) (Collins et al., 1998), a realistic boundary element model consisting of three conductive layers of skin, skull and brain (Fuchs et al., 1998; Hamalainen and Sarvas, 1989; He et al., 1987), and a cortical current density source model (Dale and Sereno, 1993). A sLORETA-weighted minimum norm (SWARM) source imaging algorithm (Wagner et al., 2007) was utilized to estimate a cortical source distribution for each cluster. The cortical distributions of different clusters were displayed and overlapped on a MNI cortex model to visualize the slow-wave network.

The patients included in this chapter had left temporal, right temporal or bi-lateral temporal lobe seizure onset. In the previously mentioned analysis, the difference between seizures with left temporal lobe onset and right temporal lobe onset was not considered. Therefore the difference caused by the effect of seizure onset is not accounted for in the group analysis. We therefore specify this analysis and the associated results as L-R (Left-Right-not-specified) analysis. In order to divide the EEG responses into the ipsilateral hemisphere and contralateral hemisphere of the seizure onset zones, we also performed an IL-CL (IpsiLateral-ContraLateral-specified) analysis. In patients with right temporal lobe seizure onset, the EEG signals were changed so the ipsilateral activity was displayed on the left side and the contralateral activity was displayed on the right side. The group-level relative spatial delta power and relative spectral delta power, and slow-wave source distribution were also computed for the IL-CL analysis.

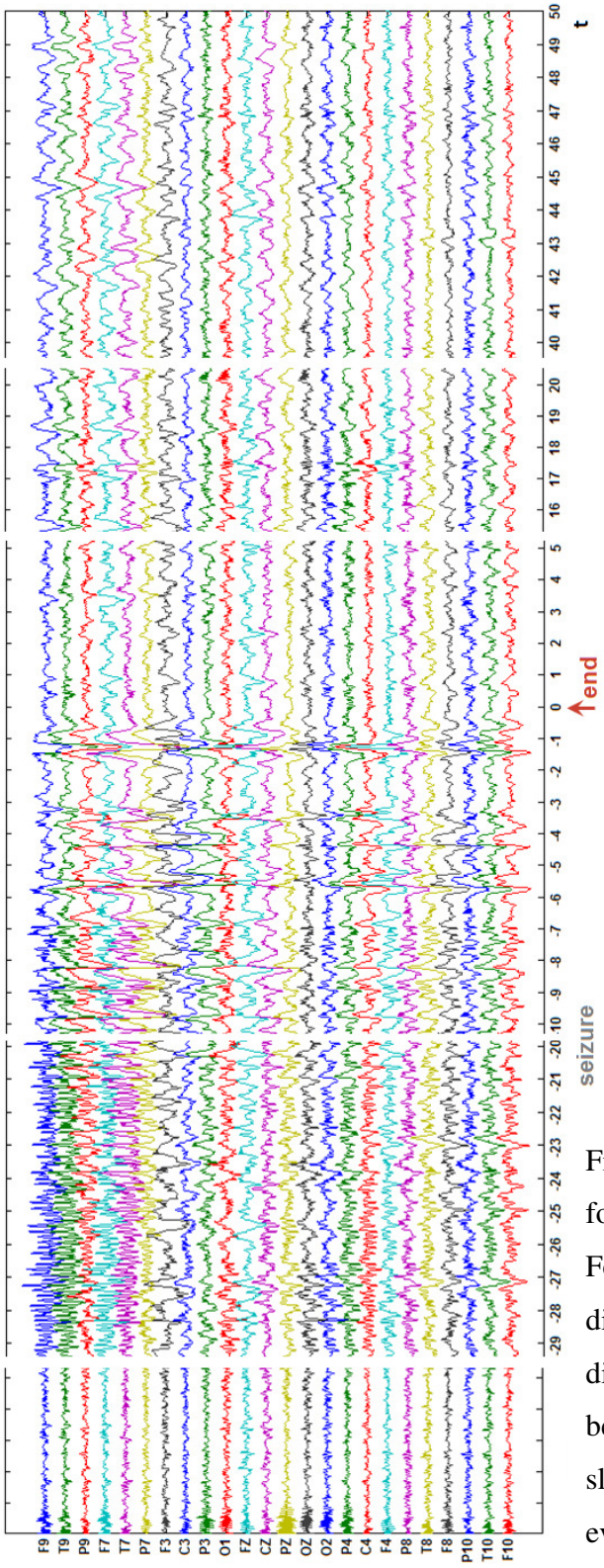

Figure 4.2 An example of EEG wave forms in a complex partial seizure. Following the termination of the ictal discharges (0-s), a postictal period differed with the preictal period because of the appearance of increased slow waves. The slow waves persist even after 50-s of the seizure offset.

4.3 Results – spectral and spatial shifts of postictal EEG

We studied the post-ictal EEG recordings of 22 simple partial, 60 complex partial, and 18 secondarily generalized seizures. Fig. 4.2 shows an example EEG in a complex partial seizure. Following the termination of the ictal discharges (Fig. 4.2, 0-s), the EEG signal differed from the preictal state. The postictal EEG included increased low-frequency activity lateralized to the ipsilateral hemisphere of seizure onset.

4.3.1 Global spectral shift of postictal EEG

We first examined the $fRel\delta$ in EEG during four different behavioral conditions (the postictal periods of simple partial, complex partial, and secondarily generalized seizures, and baseline). The relative spectral delta power, as defined in the methods section, measures the percentage of the delta-band power relative to the 1-30 Hz total spectral power in a time course. From the de-noised EEG signals, the mean $fRel\delta$ was calculated for electrodes covering the left/right temporal, frontal, central, parietal and occipital regions, respectively. The relative spectral delta power (Fig. 4.3) showed increased activity in the delta band accompanying the increased severity of seizures. Secondarily generalized seizures showed the highest relative spectral delta power, followed by complex partial seizures and simple partial seizures. The statistical significance of the difference between seizure types was tested using an unpaired t-test. The difference of $fRel\delta$ was statistically significant between simple partial and complex partial seizures ($p<0.005$), simple partial and generalized seizures ($p<0.0005$), and complex partial and generalized seizures ($p<0.05$). The relative spectral delta power was

also computed in a one minute uninterrupted background EEG of each patient (Fig. 4.3, Gray shaded area shows the $mean \pm std$ of baseline). The value of $fRel\delta$ in simple partial seizures was no much greater than that of the baseline state, whereas complex partial and secondarily generalized seizures both showed greater $fRel\delta$ than the baseline EEG.

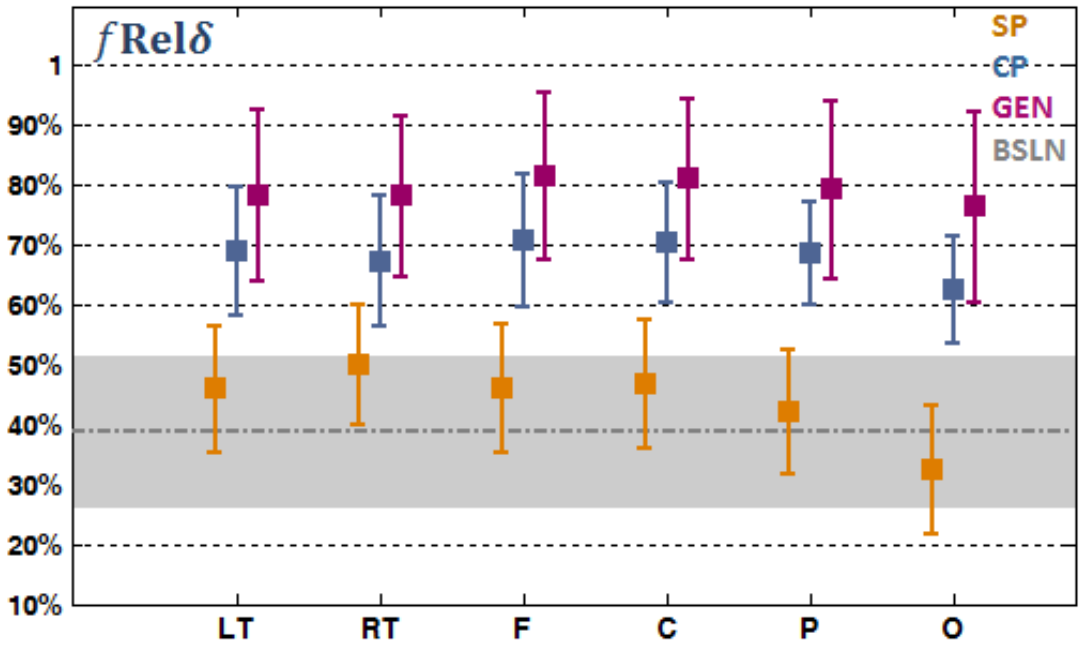

Figure 4.3 Relative spectral delta power, fRelδ, of the left temporal (LT), right temporal (RT), frontal (F), central (C), parietal (P) and occipital (O) electrodes in the postictal EEG of simple partial seizures (SP), complex partial seizures (CP) and secondarily generalized seizures (GEN). The average baseline relative spectral delta power of all regions is indicated by a gray dotted line and the standard deviation is indicated by a gray-shaded area.

Although the relative spectral delta power changed substantially across different conditions, the variation among temporal, frontal, central, parietal, and occipital regions within each condition was relatively small (Fig.4.3). The spectral shift to lower frequencies in different seizure types appears to be a global effect including widespread regions of the brain.

4.3.2 Regional spatial shift of slow waves

We then examined the regional variation and spatial distribution of postictal slow waves for the three seizure types. Fig. 4.4 A shows the clustered components with group-level relative spatial delta power for the IL-CL (IpsiLateral-ContraLateral-specified) analysis. The relative spatial delta power, as defined in the methods section, is a spatial index quantifying the delta power of a region/IC normalized by the maximum across regions/ICs. The clusters in Fig. 4.4 A are ordered by the mean value of $rRel\delta$ of complex partial seizures in each cluster.

For postictal EEG of simple partial seizures, the ipsilateral temporal region displayed the highest $rRel\delta$ (Fig. 4.4A, 9th cluster). However, for complex partial and secondarily generalized seizures, the postictal EEG $rRel\delta$ decreased in the ipsilateral temporal region but increased in other regions, especially frontal regions (Fig. 4.4A, 1st, 2nd, 4th and 7th clusters). We presented the clusters in two different categories. The first category included clusters (Fig. 4.4A, 1st-8th clusters) that showed higher mean $rRel\delta$ in complex partial seizures than in simple partial seizures. In these clusters, the most prominent slow waves were seen in the frontal regions. The frontal slow waves were

lateralized to the ipsilateral hemisphere in complex partial seizures (Fig. 4.4A, 1st cluster vs. 7th cluster), but were stronger in medial-frontal region in secondarily generalized seizures (Fig. 4.4A, 2nd cluster). The contralateral temporal region (Fig. 4.4A, 3rd cluster) displayed a larger $rRel\delta$ in complex partial than in simple partial seizures, which is consistent with the previous observation that complex partial seizures have a higher chance of affecting both temporal lobes (Englot et al., 2010; Lux et al., 2002). The cluster with medial centro-parietal focus (Fig. 4.4A, 5th cluster) also showed slow waves, but the difference between the three types of seizures was minimal. Other clusters, such as parietal clusters (Fig. 4.4A, 6th and 8th clusters), appeared in a small number of patients.

The second category of clusters (Fig. 4.4A, 9th-10th clusters) showed higher $\mathrm{rRel}\delta$ for simple partial seizures than for complex partial seizures. The ipsilateral temporal cluster (Fig. 4.4A, 9th cluster) displayed the largest $rRel\delta$ than any other clusters for simple or complex partial seizures. However, the value of $rRel\delta$ in this cluster was much smaller in complex partial than in simple partial seizures. The occipital cluster (Fig. 4.4A, 10^{th} cluster) also appeared most frequently in simple partial seizures. This cluster displayed the highest relative spectral alpha power than all other clusters (the alpha power was not shown here). The occipital cluster was not involved in further source analysis, as it is likely associated with the occipital alpha rhythm, which is common in resting state EEG.

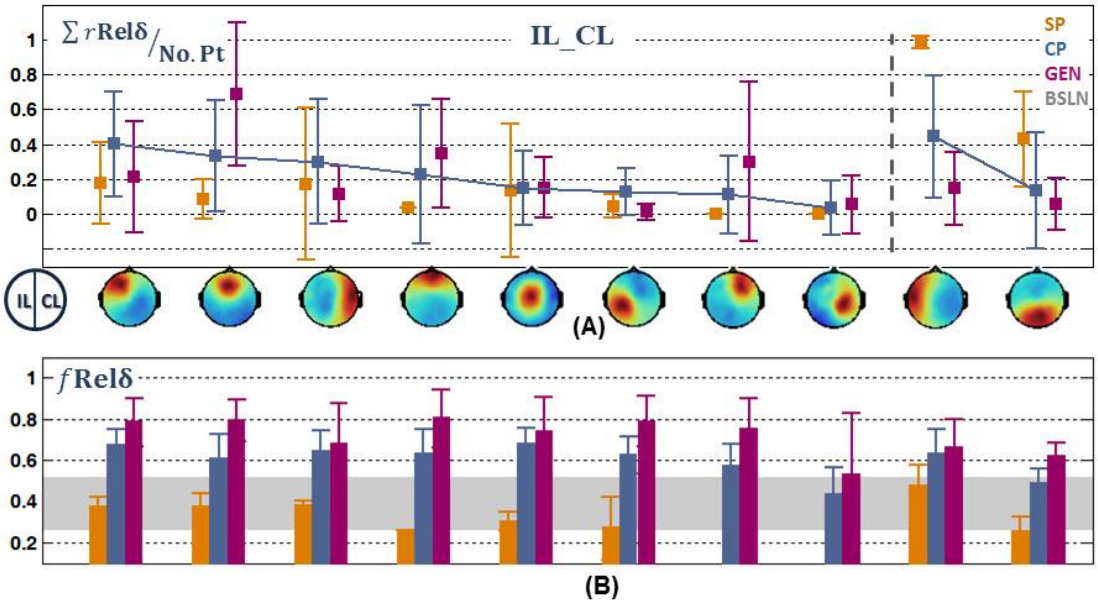

Figure 4.4 IL-CL (IpsiLateral-ContraLateral) analysis. (A) Clustered components ordered by the mean rRelδ of complex partial seizures in each cluster. The first category of the 1st to 8th clusters showed relatively higher rRelδ in complex partial than in simple partial seizures. Whereas the second category of the 9th -10th showed higher rRelδ in simple partial than in complex partial seizures. Clusters with left-, medial-, and right-orbitofrontal foci were combined into an orbito-frontal cluster, and clusters with temporal and posterior temporal foci were combined into a temporal cluster for presentation purposes. However, these clusters were analyzed separately for subsequent source analysis. If a patient did not display an IC in a certain cluster, the value of rRelδ for this patient in the cluster was defined as 0. The group mean of rRelδ, thus represents both the magnitude rRelδ and the frequency of occurrence of a certain cluster in the patient group. (B) The mean relative spectral delta power fRelδ in each cluster. Note that we did not assign a 0 value for fRelδ of patients not present within a certain cluster. The group level mean thus only represents the magnitude of fRelδ but not the frequency of occurrence a cluster within patients.

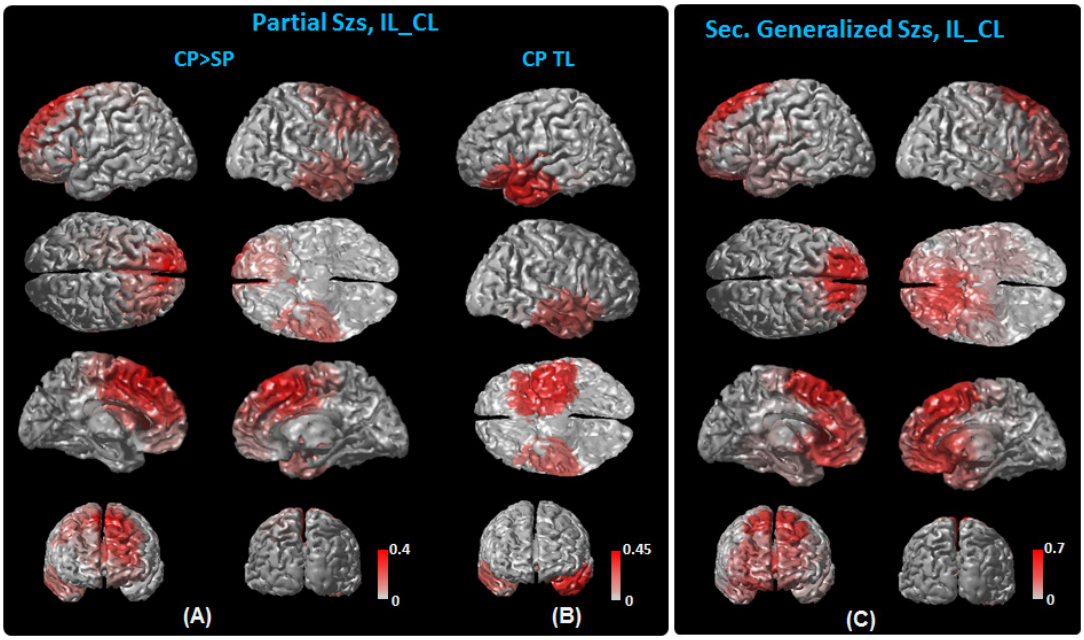

Figure 4.5 IL-CL (IpsiLateral-ContraLateral) source analysis. (A) Cortical slow-wave distribution of the 1st-8th clusters as shown Fig. 3, which had higher rRelδ in complex partial than in simple partial seizures (CP>SP), and (B) the ipsilateral and contralateral temporal (CP_TL) slow-wave distribution. The source maps of clusters are weighted by their relative rRelδ of complex partial seizures, summed and displayed on the cortex model. In secondarily generalized seizures (Sec. Generalized Szs), the slow-wave distribution (C) showed similar spatial coverage. Note that for this analysis the left side denotes the ipsilateral side to seizure onset while the right denotes the contralateral side. The color bar is scaled to the maximal value of each category as shown in Fig. 4.4.

The source imaging results (Fig. 4.5) further localized the clusters of postictal slow waves to anatomical structures. The source distribution (Fig. 4.5A) of the first category of clusters displayed higher $rRel\delta$ in complex partial and generalized seizures than in simple partial seizures. The source distribution of each cluster was weighted by the mean $rRel\delta$ of complex partial seizures and superposed on the cortical surface of a MNI cortex model (Fig. 4.5A). These clusters recruit the lateral frontal, prefrontal, and dorsal medial frontal cortex, with spread to the contralateral temporal and parietal cortex. In Fig. 4.5B, we displayed the source maps of the ipsilateral temporal cluster of the second category, for which $rRel\delta$ was higher for simple partial seizures (Fig. 4.4A), along with that of the contralateral temporal cluster. Consistent with Fig. 4.4A, the slow waves in the ipsilateral hemisphere (Fig. 4.5 A-B) were higher than those in the contralateral hemisphere. Secondarily generalized seizures showed a similar location of slow-wave activity (Fig. 4.5C). However, the regional $r\mathrm{Rel}\delta$ differed in magnitude between complex partial and secondarily generalized seizures, as the $rRel\delta$ in the frontal region was higher for generalized seizures than for complex partial seizures (Fig. 4.4A).

To visualize the difference of the $rRel\delta$ between the two types of partial seizures, the source map of each cluster was weighted by the difference of the $rRel\delta$ between complex and simple partial seizures. The weighted source maps of each cluster were then summed in the source space and plotted on the cortical surface (Fig. 4.6). Only positive values (complex partial seizures larger than simple partial seizures) are displayed in Fig. 4.6. Consistent with the scalp maps (Fig. 4.4A), the most prominent differences were

seen in the lateral frontal, prefrontal, and medial frontal cortex, with spread to the contralateral temporal and parietal cortex.

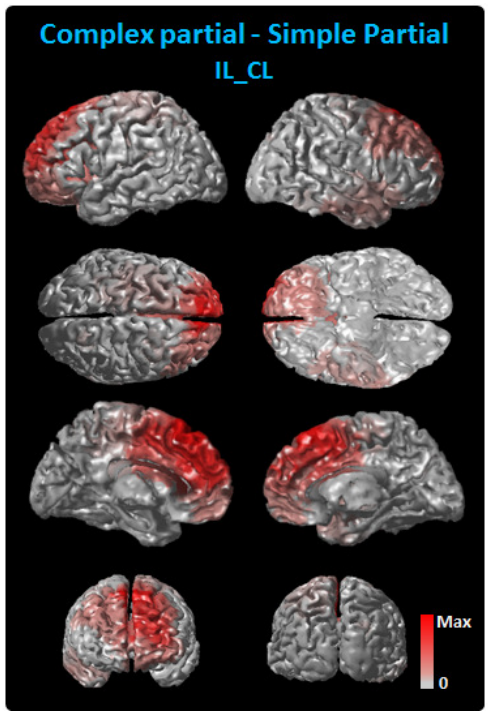

Figure 4.6 IL-CL (IpsiLatral-ContraLateral) source analysis. (A) Cortical source distribution of the difference between complex partial seizures and simple partial seizures. Each cluster's map was weighted by the rRelδ of complex partial seizures subtracted by simple partial seizures. Only positive source distribution (complex partial seizures larger than simple partial seizures) was displayed. Note that for this analysis the left side denotes the ipsilateral side to seizure onset while the right denotes the contralateral side.

Fig. 4.8 shows the results of the L-R (Left-Right-not-specified) analysis. For the postictal EEG of simple partial seizures, the left/right temporal region displayed the highest $rRel\delta$ (Fig. 4.8A, 8th and 9th cluster). However, for complex partial and

secondarily generalized seizures, the $rRel\delta$ decreased in temporal regions but increased most prominently in clusters with frontal focuses (Fig. 4.8A).

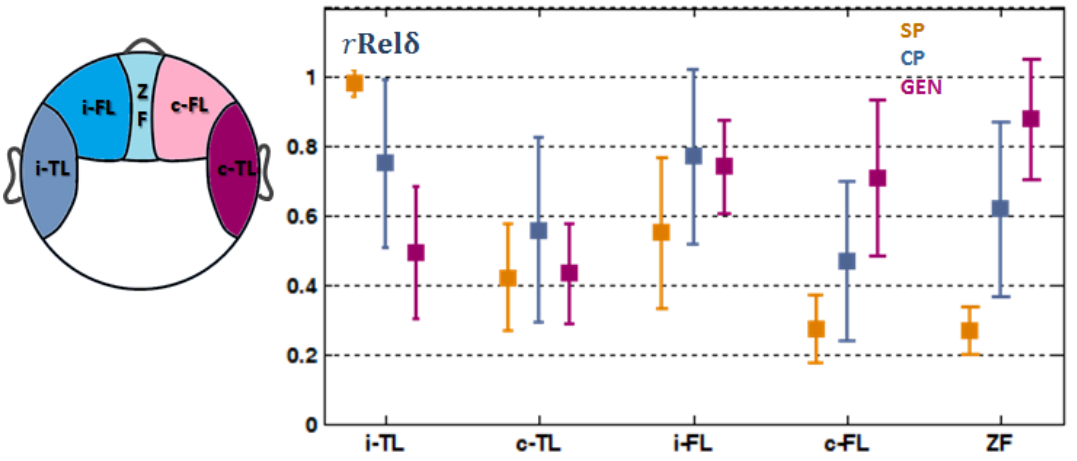

i-TL	SP>CP	SP>GEN	CP>GEN	c-FL	SP<CP	SP<GEN	CP<GEN
	p<0.05	p<0.0001	p<0.01		p<0.05	p<0.0005	p<0.01
i-FL	SP<CP	SP<GEN	CP<GEN	zF	SP<CP	SP<GEN	CP<GEN
	p<0.05	p<0.05	-		p<0.005	P<0.0001	P<0.005

Figure 4.7 The rRelδ of electrodes covering ipsilateral temporal (i-TL), contralateral temporal (c-TL), ipsiltaterl frontal (i-FL), contralateral frontal (c-FL), and midline frontal (zF) regions. The difference between simple partial (SP), complex partial (CP) and secondary generalized seizures (GEN) and different regions were statistically tested. The p-value of each individual test is shown in the table.

The most prominent differences in the regional distribution of postictal slow waves for the different types of seizures were in temporal and frontal regions. From the de-noised EEG, we further calculated the $rRel\delta$ for electrodes covering the temporal and frontal regions. An unpaired t-test was conducted to test the statistical significance of the difference between seizure types. Fig. 4.7 shows that the $rRel\delta$ in the ipsilateral temporal

region decreased from simple partial to complex partial to secondarily generalized seizures. However, the $rRel\delta$ in frontal regions increased from simple partial to complex partial and generalized seizures. These differences were statistically significant and the p-value of each individual test can be found in Fig. 4.7. A paired t-test was also conducted to test the statistical significance of the difference between ipsilateral and contralateral temporal regions and between ipsilateral and contralateral frontal regions. The ipsilateral temporal and frontal regions displayed higher $rRel\delta$ than the contralateral temporal and frontal regions, respectively, in partial seizures ($p<0.05$). The differences between the two hemispheres, however, were not significant in secondarily generalized seizures.

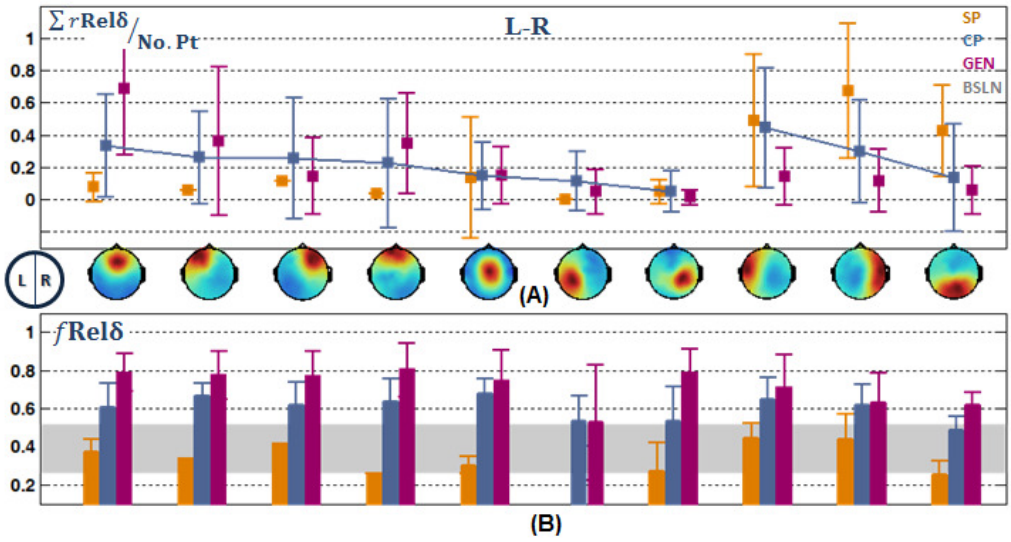

Figure 4.8 L-R (Left-Right) analysis. (A) Clustered components ordered by the mean relative spatial delta power rRelδ of complex partial seizures in each cluster. (B) The mean relative spectral delta power fRelδ in each cluster. Note that in this figure, the left side of a scalp map denotes the left and the right side of a scalp map denotes the right.

4.4 Discussion

This chapter investigated the spectral and spatial differences of the postictal EEG in simple partial, complex partial and secondarily generalized seizures. Associated with the increased severity of seizures, we found a 'global' elevation of the relative spectral delta power (delta-band power relative to 1-30 Hz total power) over widespread brain regions. In addition to the 'global' spectral shift, we found a 'regional' difference, in which the relative spatial delta power (delta-band power in one region normalized by the maximum across regions) decreased in the ipsilateral temporal region but increased in other regions, especially the frontal region, in complex partial and secondary generalized seizures. The postictal slow-wave network recruits the temporal, lateral frontal, dorsal medial frontal and prefrontal cortex, with spread to the parietal regions. This network partially overlaps with fronto-parietal cortical regions, which have previously shown decreased CBF/BOLD during epileptic activities (Bai et al., 2010; Gotman et al., 2005; Grouiller et al., 2011; Laufs et al., 2006; Siniatchkin et al., 2010).

Spatial distribution of slow waves

Dysfunctions in the temporal lobe, as well as disruptions of sub-cortical structures, have long been associated with seizure-induced cognitive problems. The verbal-memory functions of the temporal lobe (Kelley et al., 1998) may explain the memory deficits and impairments of expressive and receptive speech that are frequently observed in temporal lobe seizures (Lux et al., 2002). However, temporal lobe dysfunctions alone cannot fully explain the loss of consciousness, which requires

interaction between the subcortical system and the neocortical fronto-parietal regions (Arthuis et al., 2009; Guye et al., 2006). Recent SPECT/fMRI studies have discovered CBF/BOLD activation in sub-cortical structures (Blumenfeld et al., 2009; Lee et al., 2002) accompanied with CBF/BOLD deactivation in the fronto-parietal cortex (Bai et al., 2010; Gotman et al., 2005; Grouiller et al., 2011; Laufs et al., 2006; Siniatchkin et al., 2010). Consistent with these neuroimaging studies, iEEG studies have recorded fronto-parietal slow waves in epileptic seizures that impair consciousness (Blumenfeld et al., 2004; Englot et al., 2010). Studies have hypothesized a "network inhibition" mechanism (Englot et al., 2010), in which sub-cortical structures send inhibitory output to neocortical neurons and induce the suppression of consciousness. A reciprocal cortico-subcortical connection is also possible, and the neocortex may have an active role in the suppression of consciousness (Alkire et al., 2008). In the chapter, we focused solely on the cortical slow waves, so the connection between the cortex and subcortical structures cannot be examined.

To improve the spatial coverage of iEEG, we used dense-array EEG and source imaging techniques to reconstruct a whole-brain distribution of the slow-wave activity. In line with previous studies, but with more spatial coverage, our results indicated that cortical slow waves were most prominent in the temporal (Blumenfeld et al., 2004; Hufnagel et al., 1995; Jan et al., 2001) and lateral frontal cortex (Englot et al., 2010). In addition to these regions, we found prominent slow waves in the medial portion of the frontal cortex (Blumenfeld et al., 2004, Englot et al., 2010), especially in generalized seizures. The frontal slow-wave pattern resembles the pattern that has been observed

during slow-wave sleep (Dang-Vu et al., 2008), which suggests that the postictal behavioral change may have some similar neural substrates to slow-wave sleep. The anatomical distribution of the slow waves (Fig. 4.5, 4.6) partially overlaps with the regions that showed a decrease in CBF during the partial activation, generalization, and postictal periods in a similar cohort of epilepsy patients (Blumenfeld et al., 2009). The slow-wave distribution also partially overlaps with the "default mode network", a network known to show decreased activity in attention-demanding or goal-directed tasks (Fox et al., 2005; Raichle et al., 2001). The default mode network is known to be associated with abnormal activity or connectivity in many other mental disorders (Broyd et al., 2009). The consistency of results between multiple imaging modalities (EEG, iEEG and SPECT) and the functional importance of these cortical regions suggests a connection between cortical slow waves and inhibited consciousness and responsiveness in epileptic seizures.

The slow waves during the ictal period, as suggested by previous iEEG studies, carry important information in correlation with consciousness. The slow waves and hemodynamic signal changes during the ictal period, however, can persist into postictal period in similar regions (Blumenfeld et al., 2004; Blumenfeld et al., 2009; Englot et al., 2010; Fisher and Schachter, 2000). It is possible that the spectral and spatial features found in postictal EEG could also reflect some of the features of ictal slow waves. We limited the study of slow waves to the postictal period, because the scalp EEG measures signals of relatively low frequency. In temporal lobe seizures, the measured ictal activity is usually in the theta or delta band, which may also contribute to the spectral power we

are interested in. We studied the postictal EEG here in order to avoid the inclusion of significant ictal rhythms. This represents a limitation of this chapter. In order to study the instantaneous impact of seizures, the spectral and spatial features of ictal slow waves must be studied separately and further pursued in future work.

Slow waves, spectral & spatial shifts

In the studied patients, we observed a trend of 'global' spectral shift ($fRel\delta$) to low frequency in seizure types that affect responsiveness and consciousness (Fig. 2). The relative spectral delta power was highest for generalized seizures, the second highest for complex partial seizures, and the lowest for simple partial seizures. The relative spectral delta power for simple partial seizures did not differ as significantly from that of the baseline EEG signal as the other two seizure types. These results suggest that the brain might be brought into a 'global' 'slower' state in the postictal period for seizures associated with loss of consciousness. This spectral power shift to the lower frequency band resembles the wide synchronization of low-frequency oscillations in the anesthetic brain (Alkire et al., 2008; Hudetz and Imas, 2007; Liu et al., 2011). The burst-and-suppression pattern observed in the postictal EEG of generalized seizures can also be found in deep anesthesia (Alkire et al., 2008; Hudetz, 2006; Liu et al., 2011). Therefore some of the neural mechanisms of altered consciousness in seizures may be similar to those of anesthesia. Previous studies of anesthesia have postulated that during period of unconsciousness, the brain was engaged in certain hyper-synchronous, but stereotypic

patterns (Alkire et al., 2008; Hudetz, 2006; Liu et al., 2011). During this time, the brain can lose the information capacity (Alkire et al., 2008) to process cognitive functions.

In addition to the global spectral shift is a 'regional' difference between various regions as quantified by the relative spatial delta power. The relative spatial delta power increased prominently in frontal regions but decreased in the ipsilateral temporal region in seizure types that affect consciousness. The complex partial and secondarily generalized seizures may share similar spatial locations underlying the slow-wave activity. This similarity, despite the differences in consciousness between the seizure types, suggests that it may not be the spatial location, but rather the spectral and regional magnitude that distinguish between complex partial and generalized seizures. Previous neuroimaging findings have suggested a similar phenomenon in which common anatomical structures were involved in the hemodynamic deactivation during seizures with partial activation, generalized activation (Blumenfeld et al., 2009) and absence seizures (Bai et al., 2010).

In the ipsilateral temporal region, the relative spatial delta power was reduced in complex partial seizures compared to simple partial seizures (Fig. 4.4A, Fig. 4.7). The postictal EEG of simple partial seizures may reflect a brain state similar to a baseline state, as the relative spectral delta power in simple partial seizures was no much greater than that of the resting state baseline (Fig. 4.4B). In such a close-to-baseline state, the epileptognic zone (ipsilateral temporal lobe) may show strong interictal activity, which could elevate the total EEG power and therefore the 1-4 Hz component of the total EEG power. This is a limitation of the relative spatial delta index, as it can be affected by the

increase or decrease of total EEG power. The occipital cluster also appeared most frequently in simple partial seizures. Because it had the highest relative spectral alpha power, it is likely associated with the occipital alpha rhythm, which is common in resting state. This also suggests that the postictal state of simple partial seizures more closely resembles the normal resting state than complex partial or generalized seizures.

Clinical implications

The differences in slow-wave activity found in simple partial, complex partial and secondarily generalized seizures may provide insights into a more quantitative evaluation of responsiveness and consciousness during and following seizures. The current practice of behavioral analysis relies significantly on the language and motor abilities of patients (Commission of ILAE 1981). It can be difficult to clearly distinguish whether unresponsiveness is caused by dysfunctions of consciousness, language, or motor processing (Lux et al., 2002). The spectral and spatial delta power change may provide quantitative information to aid behavioral testing in epilepsy treatment. This method can avoid language-motor-associated biases, as it is entirely data-driven. However, a systematic perspective study, including detailed behavioral testing, is needed in order to delineate different types of cognitive dysfunctions and their electrophysiological representations. Recent studies have used more complicated behavioral scores (Arthuis et al., 2009), which can distinguish the impairment of different functions. In addition to conducting more detailed behavioral testing, it will be important in future studies to

acquire behavior information over time to track the behavioral and associated electrophysiological changes throughout the ictal and postictal periods.

The difference in slow waves between the two hemispheres showed lateralization and localization values of postictal EEG. The ipsilateral hemisphere (e.g., ipsilateral temporal and frontal regions) displayed higher delta power than that of the contralateral hemisphere in the postictal EEG of partial seizures. Analysis of post-ictal slow wave activity could therefore supplement other noninvasive localization tools for the pre-surgical evaluation of epilepsy treatment.

Technical considerations

The elevation of temporal lobe slow waves was observed in the studied cohort. This is consistent with previous studies of temporal lobe postictal slow waves (Hufnagel et al., 1995; Jan et al., 2001). However, previous intracranial EEG studies measured less elevation of slow waves in the epileptogenic zone compared to other regions (Englot et al., 2010). It is possible that the temporal lobe tissue around the epileptogenic zone still generates synchronized slow waves. These signals can be recorded by scalp EEG because scalp sensors measure the summed activity from a large area of the brain. The signals may not be recorded by iEEG implanted in the epileptogenic zone as iEEG measures signals directly from the vicinity of the electrodes. It is also possible that there are relatively higher-frequency components in the temporal lobe, such as interictal events, superposed onto slow waves. This may explain why the ipsilateral temporal lobe

component had the highest EEG power in simple partial seizures while the relative spectral delta power was not much larger than the resting baseline.

In the postictal EEG, the orbito-frontal activity, when projected onto the scalp sensors, is mixed with the electrooculography (EOG) activity that is generated by eye blinks and movements. ICA may not be able to completely separate the two signals. In order to remove eye-blink artifacts in our analysis (Jung et al., 2000), we visually reviewed all of the IC time courses. Components with brief and large-amplitude peaks that were distinct from the background EEG were identified. They were then compared to the original EEG waveforms to determine whether the signal was consistent with the eye-blinks (brief, large monopolar potentials) observed in the EEG. Lastly, we examined the scalp maps of the selected components to see if the signal had a focus in the far frontal electrodes. We cannot exclude the possibility that some of the slow waves may have been rejected because they were superimposed in the components that represented the eye blink signals. Therefore, the orbito-frontal components studied here may be under-estimated, and the delta power in this cortical region may be even higher than that derived here.

In conclusion, in the postictal EEG of temporal lobe seizures, in this chapter we found (i) a global spectral power shift to low frequencies, and (ii) a spatial power shift to the frontal regions associated with increased severity of seizures (from simple partial to complex partial and secondarily generalized seizures). The spectral and spatial shifts of slow-waves suggest a possible connection between behavioral states and

electrophysiological changes. Epileptic seizures provide a pathological model (Blumenfeld et al., 2009; Englot et al., 2010; Lux et al., 2002) to study consciousness, responsiveness, and other cognitive functions, in addition to other more frequently used models, such as slow-wave sleep (Alkire et al., 2008; Hofle et al., 1997; Massimini et al., 2005) and anesthesia (Alkire et al., 2008; Hudetz and Imas, 2007; Liu et al., 2011).

-

Chapter 5 Multimodal spatiotemporal neuroimaging

5.1 Introduction

Numerous efforts have been made in an attempt to improve the imaging resolution of functional neuroimaging in the spatial domain and temporal domain. EEG and MEG measure the scalp electromagnetic field generated by neuronal currents. They have millisecond temporal resolution capable of capturing neuronal level activity, but relatively low spatial resolution. FMRI, on the other hand, detects hemodynamic changes accompanying neural activity, most commonly through measuring blood oxygen level dependent (BOLD) contrast MR signals (Bandettini et al., 1992; Kwong et al., 1992; Ogawa et al., 1992). The fMRI technique has high spatial resolution but low temporal resolution, as complementary to EEG and MEG (for reviews, see (Dale and Halgren, 2001; He and Lian, 2002; He and Liu, 2008)).

EEG-fMRI multimodal imaging techniques have been developed in a hope to combine the fine temporal resolution of EEG and the fine spatial resolution of fMRI. EEG and fMRI signals are most commonly integrated through fMRI-weighted source imaging or EEG-informed fMRI analysis. As an early effort of Liu et al (1998), the fMRI map in correlation with tasks was used as a spatial weighting in the EEG/MEG source analysis. It is capable of incorporating high spatial resolution of fMRI into EEG/MEG source imaging. However, the EEG/MEG and fMRI are generated and measured at significantly different temporal scales. Therefore, it remains a challenge to use sluggish fMRI signal to explain transient EEG/MEG phenomena that may not necessarily arise at the same time (Liu and He, 2008). The EEG- (or MEG-) informed fMRI analysis

(Goldman et al., 2002; Gotman et al., 2005; Laufs et al., 2003; Vulliemoz et al., 2010), on the other hand, uses EEG temporal information to delineate fMRI maps in correlation with specific electrophysiological signatures. In most of the previous studies, the temporal regressors are calculated from either a single channel or the global field power of EEG. The EEG/MEG signals, as limited by the low spatial resolution represent mass neural response not necessarily originated from a given location where the BOLD signal is being measured. An improved strategy has been developed to use independent component analysis (ICA) to separate signals in the sensor space and use an independent time series to conduct the EEG-informed fMRI analysis (Debener et al., 2006; Feige et al., 2005). However, EEG-informed fMRI analysis alone may fail to differentiate brain regions with signals similar in hemodynamics but different in electrophysiology.

In this chapter, we describe a data-driven method for the integration of EEG (or MEG) and fMRI, by combining both the EEG (or MEG)-informed fMRI analysis and the fMRI-constrained EEG (or MEG) source imaging. While this method is applicable to either EEG-fMRI or MEG-fMRI integrative analysis, we focus on EEG-fMRI analysis to illustrate the merits of the proposed method, and shall call the proposed approach the EEG-fMRI reciprocal neuroimaging.

5.2 Methods and materials

The key concept of the EEG-fMRI reciprocal neuroimaging method is illustrated in Fig. 5.1. It contains five steps: 1) ICA is applied to multi-channel EEG data to obtain a number of temporally independent components (ICs). 2) The time course of each IC is

used to derive a temporal regressor for an EEG-informed fMRI analysis, 3) The fMRI map, corresponding to each IC, is further used as a spatial prior to constrain the EEG source estimation through fMRI-weighted source imaging. 4) The estimated sources are re-combined in the source space, giving rise to a spatiotemporal source imaging.

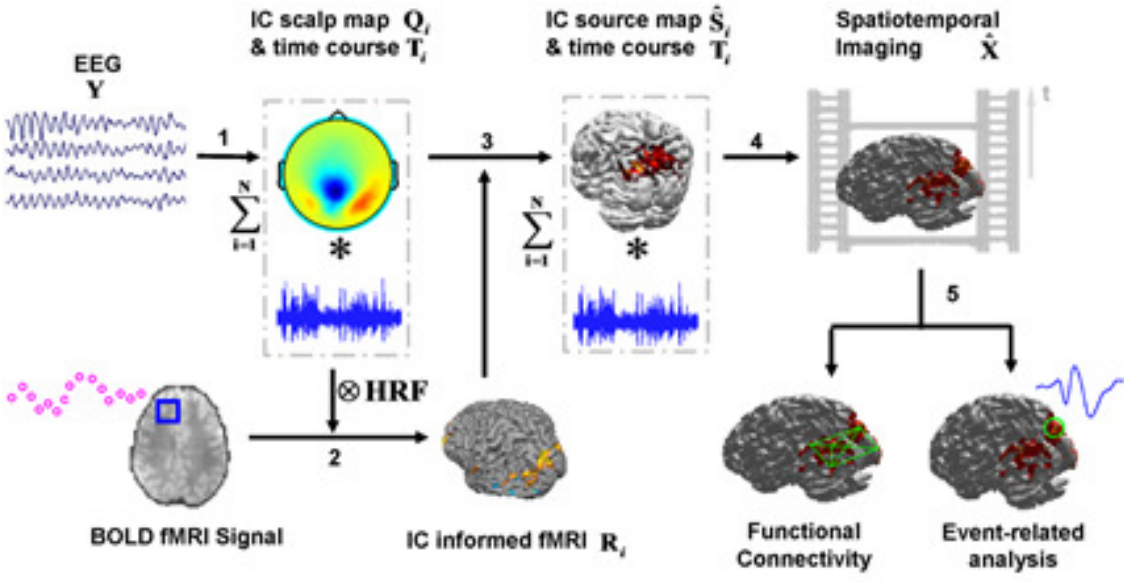

Figure 5.1 Diagram of the EEG-fMRI reciprocal neuroimaging approach. It consists of steps of (1) ICA; (2) IC-informed fMRI analysis; (3) fMRI-constrained IC source imaging; (4) Source re-combination; (5) Further analysis using the spatiotemporal imaging can be conducted.

5.2.1 EEG-fMRI reciprocal neuroimaging algorithm

As discussed in previous chapters, the EEG measurement can be separated into independent components as:

$$Y = \sum_{i=1}^{N} Q_i T_i \qquad 5.1$$

In addition of removing artifacts and noises, we can further separate brain electrophysiological sources by selecting ICs with spatial or time-frequency features

associated with certain aspects of neural activities (Debener et al., 2005; Debener et al., 2006; Makeig et al., 2002; Nam et al., 2002).

Neural activity can be associated with BOLD fMRI signal through a hemodynamic response function (HRF). In this chapter, we assume a linear neurovascular coupling relationship, where the BOLD fMRI response can be predicted by the power of local synaptic current convolved with a canonical HRF. Considering the time course $\mathbf{T}_i$ of IC as the temporal dynamics of a group of synchronized neurons, an fMRI regressor $\mathbf{F}_i$ can be derived as:

$$\mathbf{F}_i = g(\mathbf{T}_i) \otimes \mathbf{HRF} \qquad 5.2$$

where $g(\mathbf{T}_i)$ is a function of $\mathbf{T}_i$, representing the functional linkage between the neural signal and fMRI signal. Here, we use the power of neural activity ($g(\mathbf{T}_i) = \mathbf{T}_i^{\,2}$) and band-pass filtered activity ($g(\mathbf{T}_i) = \sum_{f=\min}^{\max} \mathbf{P}_i(f,t)$, where $\mathbf{P}_i(f,t)$ spectral power at frequency f and time t). Various linear or nonlinear neurovascular coupling models (Büchel et al., 1998; Kilner et al., 2005; Mukamel et al., 2005) can be easily incorporated by defining the function $g(\mathbf{T}_i)$ and by changing the HRF.

Fitting each $\mathbf{F}_i$ to fMRI time series using general linear model (GLM) analysis gives rise to a map $\mathbf{R}_i$ that highlights the regions, in which the hemodynamic response (or modulation) is temporally consistent with the electrophysiological response (or modulation) of the i-th IC of EEG (Friston et al., 1994; Friston et al., 1998). The IC-specific fMRI map $\mathbf{R}_i$ can be represented by a $N_X \times 1$ vector, and integrated with IC

scalp map $\mathbf{Q}_i$ by solving an fMRI-weighted EEG inverse problem. The absolute value of each element in $\mathbf{R}_i$ represents the fMRI weighting assigned to an equivalent dipole at the location where fMRI is measured. Knowing lead field matrix L, EEG topography $\mathbf{Q}_i$ and fMRI weighting $\mathbf{R}_i$, we can derive an IC-specific source estimation $\hat{\mathbf{S}}_i$ ($i = 1 \sim N$) by solving an optimization problem:

$$\min \quad \| \mathbf{L}\hat{\mathbf{S}}_i - \mathbf{Q}_i \|^2 + \lambda^2 \| \mathbf{C}_S{}^{-1}\hat{\mathbf{S}}_i \|^2 \qquad 5.3$$

where λ is a regularization parameter estimated using L-curve function (Hansen and O'Leary, 1993), and $\mathbf{C}_S$ is an $N_X \times N_X$ source covariance matrix, where the i-th diagonal element incorporates the fMRI weighting $\mathbf{R}_i$ (Liu et al., 1998; Liu and He, 2008). The spatio-temporal source activity $\hat{\mathbf{X}}$ can be derived as:

$$\hat{\mathbf{X}} \approx \sum_{i=1}^{N} \hat{\mathbf{S}}_i \mathbf{T}_i \qquad 5.4$$

The reconstructed spatio-temporal source activity $\hat{\mathbf{X}}$ is a $N_X \times N_T$ matrix. Further time series analysis can be conducted based on the estimation, such as connectivity analysis in the source space or single-trial analysis. One example is the phase synchronization value (PSV) to estimate brain functional connectivity between different regions (Lachaux et al., 1999; Lachaux et al., 2000; Rodriguez et al., 1999). Assuming time courses $\hat{\mathbf{X}}_a$ (row a of the matrix $\hat{\mathbf{X}}$) and $\hat{\mathbf{X}}_b$ (row b of $\hat{\mathbf{X}}$) are extracted from two cortical regions, the PSV analysis starts with filtering the time courses with Morlet wavelets (Lachaux et al., 1999; Lin et al., 2004) , the outcomes of which are time-

frequency complex $W_a(t,f)$ and $W_b(t,f)$. The phase difference $\theta_{a-b}(t,f)$ between the cortical regions a and b can be calculated by (Lachaux et al., 1999):

$$\theta_{a-b}(t,f) = \phi_a(t,f) - \phi_b(t,f) \qquad 5.5$$

$$\phi_i(t,f) = \tan^{-1}\left[\mathrm{Im}(W_i(t,f)) / \mathrm{Re}(W_i(t,f))\right]$$

where $\phi_i(t,f)$ is the estimated phase value at a cortical voxel, Im indicates the imaginary part and Re indicates the real part of a complex number. In continuous data, PSV has been proposed as a numerical indicator of functional connectivity, which calculates the variability of phase difference between two time series across successive time-window δ (Lachaux et al., 2000). PSV can be defined as a function of time t and frequency f as:

$$PSV(t,f) = \frac{1}{\delta}\int_{t-\frac{\delta}{2}}^{t+\frac{\delta}{2}} \exp(j\theta_{a-b}(\tau,f))d\tau = \frac{1}{\delta}\sum_{t-\frac{\delta}{2}}^{t+\frac{\delta}{2}} \exp(j\theta_{a-b}(\tau,f)) \qquad 5.6$$

The significance test can be conducted by a nonparametric statistical test, which randomly generates a group of new time series and calculating the PSV between the new series and the original signal (Lachaux et al., 1999; Lachaux et al., 2000). The proportion of these PSVs higher than the original PSV at time ***t*** indicates the chance of false positive for a significance level (Lachaux et al., 1999; Lachaux et al., 2000).

5.2.2 Computer simulations

A series of computer simulations were conducted to evaluate the performance of the method. In the computer simulations, we used a realistically shaped BEM created

from high resolution anatomical T1 images ($1 \times 1 \times 1 mm^3$). The head volume was separated into three compartments: the brain, the skull and the scalp. Their conductivity values were set to be 0.33 S/m, 0.0165 S/m and 0.33 S/m, respectively (Lai et al., 2005; Zhang et al., 2006). To model the neuronal distribution, a cortical current density source model was used. Several thousand equivalent current dipoles were positioned evenly on the folded cortical surface (Dale and Sereno, 1993). The orientations of the dipoles were fixed to be perpendicular to local cortical surface.

We firstly tested the capability of the method of imaging continuously oscillatory activity. We simulated nine sources belonging to three functional networks (Fig. 5.2A). These simulated source locations have been reported to be largely involved in neural oscillatory activities during resting state (Laufs et al., 2003; Mantini et al., 2007). Ninety-second waveforms with dominant alpha or beta oscillations were assigned to the nine sources (see Fig. 5.2 for details). As illustrated in Fig. 5.2B, sources had synchronized temporal oscillations within the same network, but were temporally de-synchronized across different networks. The 9th source was simulated as a confounding source. It was assigned a waveform in the same frequency band and modulation pattern with the sources in network 1. But it was de-synchronized with any other sources during the entire time period. From the simulated source locations and waveforms, scalp EEG signals were simulated and sampled every 1 millisecond. Gaussian white noise with maximum signal-to-noise-ratio (SNR) of 3 was added to the simulated EEG signals. The BOLD fMRI signal was generated at every brain voxel by convolving the simulated source power with an HRF function. Gaussian white noise with maximum SNR of 10 was added to the

simulated fMRI signal as well as other brain voxels where there are no neural activities. ICA was applied to decompose the simulated EEG data. Artifactual components were removed based on their scalp maps and time courses (Iriarte et al., 2003; Jung et al., 2000; Urrestarazu et al., 2004). The total power ($\boldsymbol{f}(\mathbf{T}_i) = \mathbf{T}_i^2$) of each source IC was fitted into a GLM fMRI analysis. A statistical threshold with $p<0.005$ was used. After the stepwise source reconstruction, the spatial locations, time-frequency features and connectivity patterns were compared with the simulation setting.

In the second simulation, three current dipoles (Fig. 5.2C) were placed at discrete cortical regions along the right hemisphere visual pathway. Typical waveforms were assigned to these dipoles to simulate event-related responses. The source waveforms were repeated twice per second during 30-second task blocks (Fig. 5.2D) interleaved with 30-second control blocks during which alpha band oscillations (8 – 12 Hz) were randomly generated. Scalp EEG was simulated based on the source configuration and Gaussian white noise was added the same way as described in the 1st simulation. Event-related source activities were estimated from the simulated fMRI and EEG data by using the proposed method, in comparison with the simulation setting.

5.2.3 Eyes-open-eyes-closed experiment

To further assess the performance of the proposed approach in imaging continuously oscillatory activity, we conducted a pilot human experiment using an eyes-open-eyes-closed paradigm. A healthy subject (male, age 27) was recruited to participate in the human experiment under the approval of the Institutional Review Board at the

University of Minnesota. Written informed consent was obtained before the experiment. During a period of 3.5 minutes, the subject laid quietly in the dark MR scanner. EEG recording and fMRI scanning started with the subject's eyes closed. Every 30 seconds, the subject was given an aural signal to open or close his eyes. In the eyes-open conditions, the subject was instructed to gaze at a central fixation point.

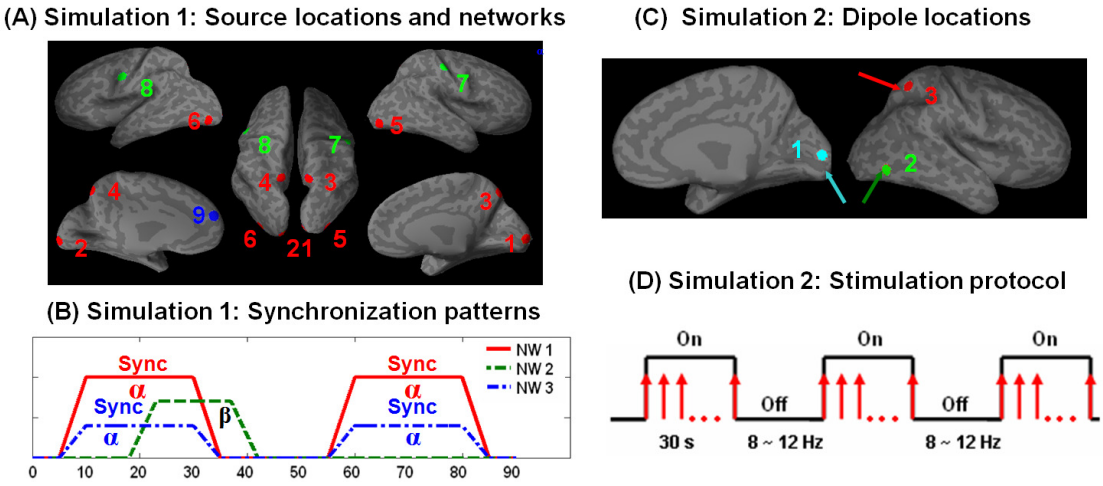

Figure 5.2 Illustration of the simulation settings. In the first simulation, (A) Nine sources within three networks (color coded) were simulated. (B) The synchronization patterns within and across of these three networks were modeled so that sources within each network were synchronized during the "Sync" blocks and de-synchronized in the control blocks. In the 1st network (red), 11-Hz EEG signal extracted from a resting eyes-closed experiment was assigned to source 1. It was further shifted for certain phase delays and assigned to the sources 2-6. Sources in network 2 (green) were synchronized at 17 Hz. The source 9 in network 3 (blue) was designed as a confounding source. It was assigned an alpha signal filtered from a Gaussian white noise. In the second simulation, (C) three current dipole sources were simulated. (D) The event-related paradigm including three 30-s task blocks interleaved by four 30-s control blocks. During an "on" block, the stimulus (red arrow) was repeated every 500 ms to induce repeated single-trial responses. During an "off" block, alpha oscillations were randomly generated.

During the experiment, EEG and fMRI data were simultaneously acquired. The MRI and fMRI data were collected on a 3-T MRI system (Siemens TrioTim, Siemens, Germany). The high resolution anatomical MRI dataset was acquired using the following parameters: TR/TE = 2530ms/4ms, voxel size $= 1 \times 1 \times 1 mm^3$. The $T2^*$-weighted functional images were acquired from 24 slices covering the whole brain using the following parameters: TR/TE = 1200ms/30ms, voxel size $= 3 \times 3 \times 4 mm^3$, flip angle = 45. The fMRI images were preprocessed by the slice scan time correction, motion correction, spatial smoothing (FWHM = 4) and high-pass temporal filtering (BrainVoyager QX, Brain Innovation, Netherlands). EEG signals were collected using a 64-channel MR-compatible system (BrainAmp MR 64 plus, BrainProducts, Germany) and referenced at FCZ. Gradient artifact and cardiac ballistic artifact were removed from the raw EEG data by means of template subtraction (Vision Analyzer, Brain Products, Germany). The EEG data were then down-sampled (250 Hz) and band-pass filtered (1 ~ 30 Hz).

It is well known that alpha-band EEG signal changes most predominantly in eyes-closed condition versus eyes-open condition. This design thereby experimentally generates a modulation of oscillatory activity. To image the spatial and temporal patterns of this rhythmic modulation, we selected ICs showing alpha-band spectral power change with significant correlation with the experimental paradigm. The power of each 8-12-Hz-band-pass filtered IC time course was used to calculate an IC-specific fMRI regressor. The regressor derived from each IC was fitted into a GLM fMRI analysis. A statistical threshold with $p<0.005$ was used. The spatial and temporal patterns of the oscillatory

activity modulated by the alternation of the eyes-open and eyes-closed conditions were reconstructed. The cortical synchrony between different voxels was estimated.

5.3 Simulation and experimental results

5.3.1 Continuously oscillatory activity

In the first simulation, five source ICs were derived after noisy components were excluded. Fig. 5.3A shows their scalp maps (right) and spectrograms (left). The spectrograms here were calculated by a wavelet-based time-frequency analysis. The spatial map of each IC was consistent with a certain combination of the scalp potential maps generated by individual sources. As such, an IC scalp potential map was a summation of a subset of the simulated sources. The oscillatory signal modulations were revealed by the spectrograms: alpha-band oscillations from posterior and medial frontal channels; beta-band oscillations from central parietal channels. These rhythmic signal modulations were in agreement with the simulation setting (illustrated in Fig. 5.2B).

The fMRI regressors (Fig. 5.3B) were derived from the IC time courses. The regressors corresponding to the first three ICs (Fig. 5.3B orange box) displayed similar patterns, regardless of their temporal independence captured by EEG in a fine time scale. Similarly, the 4th and 5th ICs (Fig. 5.3B blue box) showed similar regressors. As a result, the fMRI maps in correlation with these similar regressors derived from distinct ICs showed almost identical populations of neural sources. For instance, the fMRI map corresponding to the 1st IC (Fig. 5.3C, red-to-yellow color bar) showed a spatial pattern covering the posterior and frontal cortical regions, which was similar with the fMRI maps

obtained for the 2nd and 3rd ICs (not shown). The fMRI maps corresponding to the 5th (Fig. 5.3C dark-blue-to-light-blue color bar) and 4th (not shown) ICs identified the same central parietal cortical regions. These results indicate that the IC-related fMRI maps lack the ability to distinguish sources with independent neuronal temporal features but similar hemodynamic temporal dynamics, which is caused by the low temporal resolution of fMRI signals.

Each above mentioned fMRI map related to each IC was applied as a spatial constraint to the reconstruction of the cortical current density distribution that generated the associated IC scalp potential map. The estimated source distributions (Fig. 5.3D) inherited high spatial resolution from fMRI signal. Furthermore, it was possible to distinguish neural activity generated by distinct ICs (color coded in Fig. 5.3D), which failed to be clarified by IC-informed fMRI analysis (Fig. 5.3C).

A spatiotemporal brain imaging was achieved by the EEG-fMRI integrated imaging. A fast Fourier transformation (FFT) was used to transform the estimated time course at each cortical voxel to a frequency spectrum. The power of 8-12 Hz and 12-28 Hz were plotted on the same cortical surface, giving rise to the cortical distributions of the alpha-band (Fig. 5.4A, red-to-yellow color bar) and beta-band power (Fig. 5.4A, dark-blue-to-light-blue color bar), respectively, which is consistent with the simulation settings. Spectrograms extracted at simulated source locations (Fig. 5.4A) successfully reveal the rhythmic modulation patterns consistent with the simulation settings.

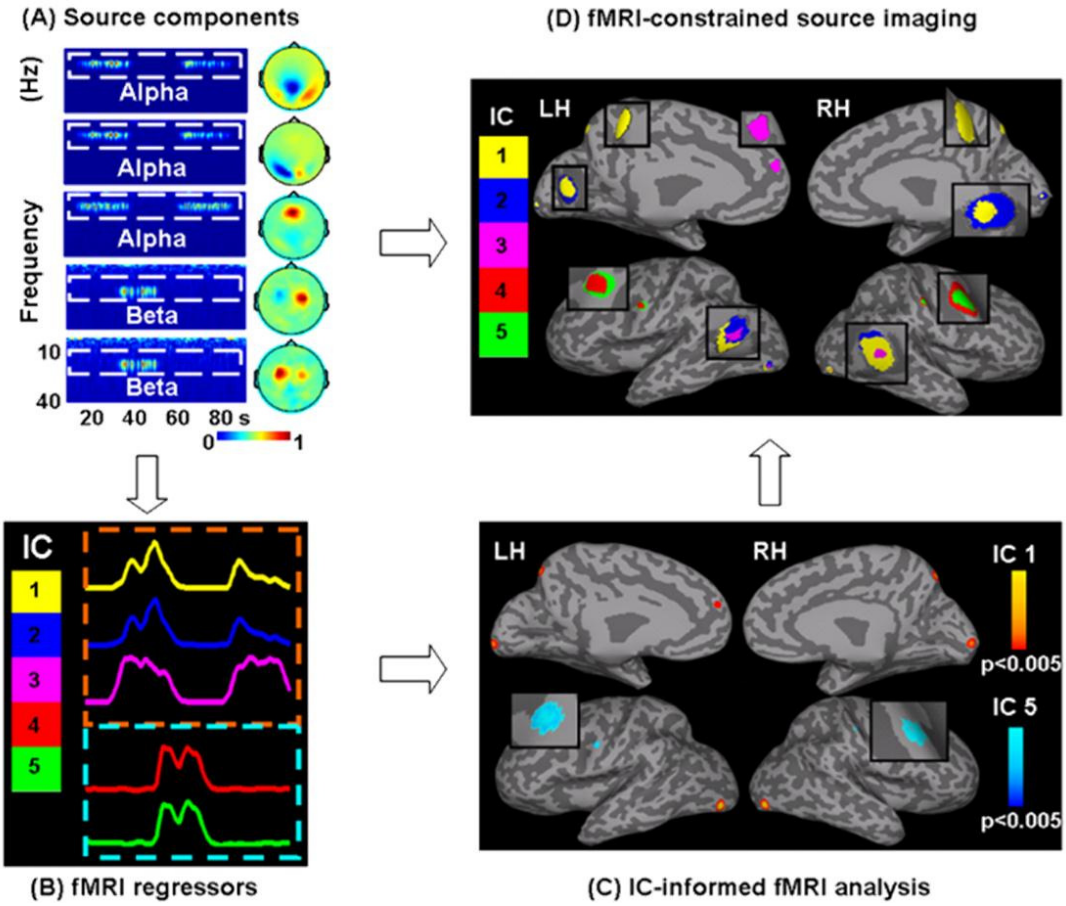

Figure 5.3 Intermediate results of simulation 1. (A) IC scalp potential maps (right column) and spectrograms of the IC time courses (left column). The first three ICs show alpha-band oscillations, and the other two ICs show beta-band oscillations. (B) fMRI regressors derived from IC time courses. The regressors in the orange box and blue box share similar temporal patterns. (C) IC-informed fMRI maps corresponding to the 1st (red color bar) and 5th ICs (blue color bar). The fMRI map in correlation with the 1st IC highlights posterior and medial frontal brain regions. The fMRI map in correlation with the 5th IC shows central parietal response. (D) fMRI-constrained EEG source imaging of the selected ICs. The source distributions corresponding to the five ICs are illustrated in different colors according to the color bar shown on the left.

We further evaluated the inter-cortical synchronization by extracting the estimated source time course from a seed region (region 1 as illustrated in Fig. 5.2A; red line circled in Fig. 5.4A) and then computing the phase relations between this time course and those from other regions of interest (ROIs) (regions 2-9 as illustrated in Fig. 5.2A). The phase plot (Fig. 5.4B, left) indicates synchronized phase difference between the seed region and the 6th ROI within the alpha band. The PSV curve at 11 Hz (Fig. 5.4B, bottom) shows a significant phase-synchronization between these two regions during periods of 5s~35s and 55s~85s. De-synchronization between the seed point and the 7th (Fig. 5.4C) and 9th ROIs (Fig. 5.4D) were also reflected in the corresponding PSV estimates, which were both under the significance level. Collectively, these results render a functional connection pattern (Fig. 5.4A, middle panel): ROIs 2-6 (Fig. 5.4A connected with the seed region by solid lines) were synchronized with the seed region during the simulated "Sync" blocks, and the ROIs 7-9 (Fig. 5.4A, connected with the seed region by dotted lines) were de-synchronized with the seed region over time. The results were in agreement with the simulation settings. The 9th ROI was simulated as a confounding source. It was designed with similar modulation pattern with the seed region and ROIs 2-6, but was de-synchronized with any other sources.

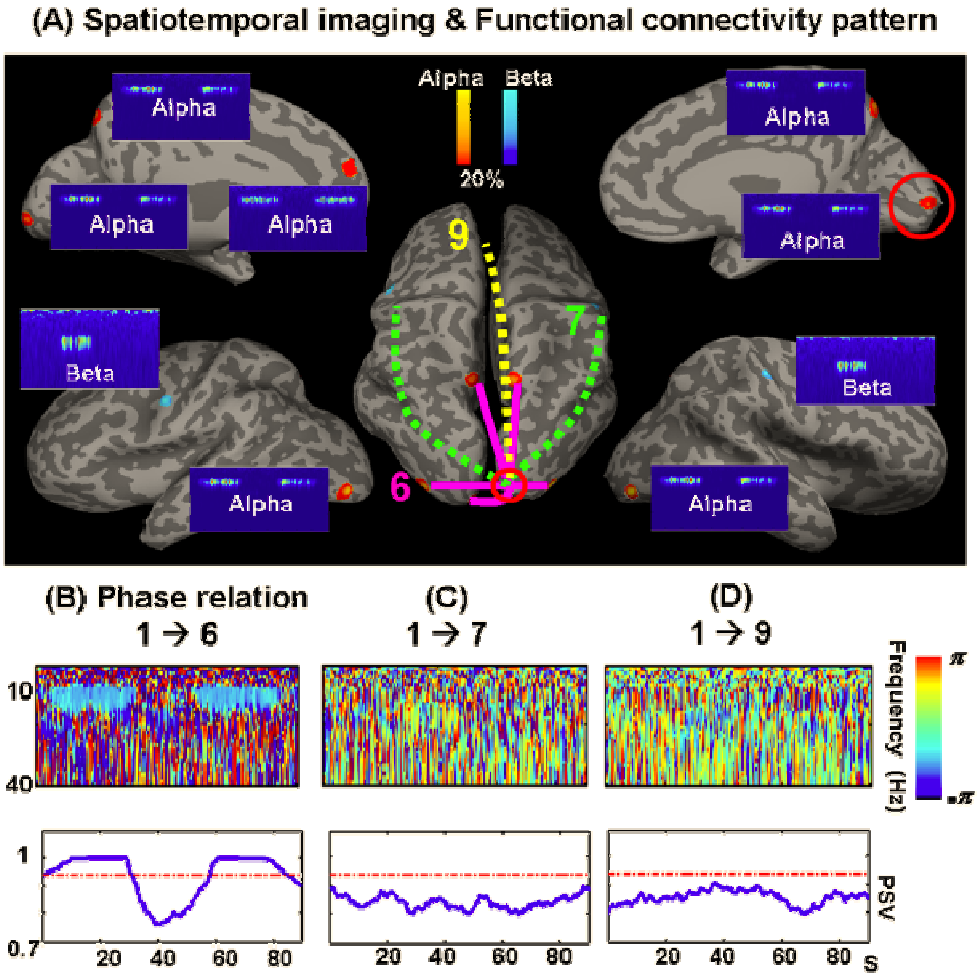

Fig 5.4 Spatiotemporal imaging and estimation of phase relations. (A) Alpha (red-to-yellow color bar) and beta (dark-blue-to-light-blue color bar) power distribution visualized on the inflated cortical surface. Estimated source spectrograms are shown close to the simulated source locations. The central panel depicts the functional networks estimated through phase synchronization analysis. ROIs 2-6 were synchronized (pink solid lines) with the seed region (red solid line circled) and ROIs 7-9 were de-synchronized (dotted lines) with the seed region. (B-D) Phase plots (upper) and PSV curves (lower) estimated between the seed region and ROIs 6, 7 and 9, respectively. Only the 6th ROI shows synchronization with the seed region at a synchronized phase delay. 1% statistical significance value was marked by the red dotted lines.

5.3.2 Event-related neural responses

In the second simulation, temporally uncorrelated source waveforms (Fig. 5.5B cross lines) were assigned to the three cortical locations as illustrated in Fig. 5.2D. Time delays between these event-related waveforms were used to model their different responding times. Event-related source waveforms and distributions were derived by averaging the estimated spatiotemporal activities with respect to the event onsets. Fig. 5.5A shows the event-related cortical source distributions at three peak latencies. The cortical voxels with the maximal amplitudes in these spatial source distributions at the peak latencies were defined as estimated source locations. Fig. 5.5B plots the event-related waveforms (solid lines) at the estimated source locations in comparison with the real source waveforms (cross lines). The spatial patterns, as well as the temporal morphology of the real sources, were well retained in the estimation. These results suggest high spatial specificity and high temporal precision of the proposed approach in imaging the event-related source activity.

To further evaluate the proposed approach in various conditions, we assigned a variety of other waveforms to the three simulated dipoles, as used in Liu and He (2008). Event-related waveforms were reconstructed at estimated source locations for temporally overlapped sources (Fig. 5.5C), transient neural activity (Fig. 5.5D), rhythmic oscillations (Fig. 5.5E-F), and waveforms gained from real human data (Fig. 5.6G). For all these source configurations, the results indicate tight correlations between the estimated temporal dynamics and the real source waveforms.

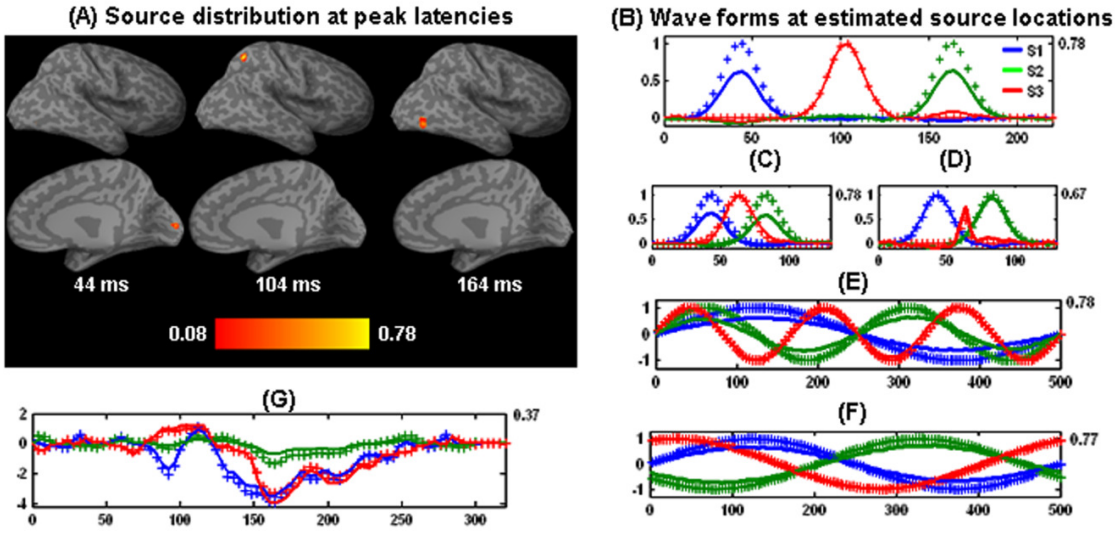

Fig 5.5 Event-related spatiotemporal source estimates. We first assigned temporally uncorrelated waveforms to the simulated dipoles and derived (A) cortical current distributions at three peak latencies. (B) Estimated event-related waveforms at three estimated source locations (solid lines) in comparison with the real source wave forms (cross lines). We then tested various complex source configurations, and showed the estimated event-related waveforms for (C) temporally overlapped sources, (D) transient neural response, (E) rhythmic activity with the same phase but different frequencies, (F) rhythmic activity with same frequency but different phase (G) waveforms extracted from real human data. The labels on the left of the graphs are the amplitude of the simulated source waveforms while the labels on the right are the amplitude of the estimated waveforms.

5.3.3 Experimental results

As shown in Fig. 5.6A, six ICs drawn from EEG data showed alpha spectral power modulated by the eyes-open-eyes-closed experimental paradigm. These selected ICs and the simultaneously recorded fMRI data were used to image the spatiotemporal pattern of the modulated alpha activity. In order to display the alpha spectral power distribution, we calculated FFT of the estimated time course of each voxel, and plotted the resultant alpha band spectral power on the inflated cortical surface (Fig. 5.6B). The alpha activity was mainly originated from the occipital visual area, the parieto-occipital sulcus and in part from the precentral gyrus of the right hemisphere. The estimated cortical location of the alpha modulation is consistent with previously reported fMRI and EEG/MEG studies (Feige et al., 2005; Goldman et al., 2002; Gross et al., 2001; Laufs et al., 2003). Detailed 3.5-minute temporal information can be drawn from different cortical regions. For instance, spectrograms were plotted for two ROIs (Fig. 5.6B, green circled) located on the left hemisphere (Fig. 5.6C) and right hemisphere (Fig. 5.6D). Both of the highlighted ROIs show alpha activity increased in eyes-closed conditions versus eyes-open conditions. The time-frequency phase relation (Fig. 5.6E) and the 8-12 Hz PSV curves (Fig. 5.6F) show increased phase-synchronization in the alpha-band in the eyes-closed conditions versus eyes-open conditions. The increased synchronization was also observed between other imaged regions, but was not shown here.

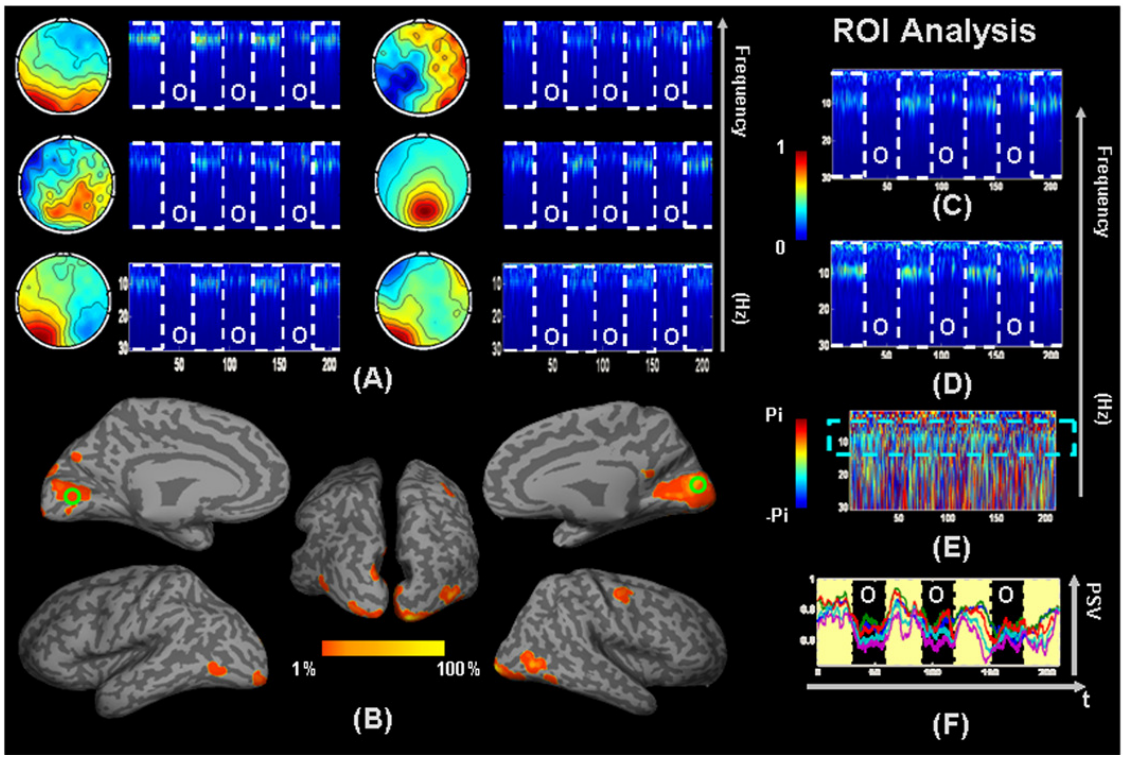

Fig 5.6 Experimental results in a human subject. Six ICs (A) show correlated alpha band activity with the eyes-open-eyes-closed paradigm. The box marked with "O" denotes the eyes-open conditions. Based on the EEG-fMRI reciprocal imaging results, (B) alpha spectral power distribution was plotted on the inflated cortical surface. Time courses were extracted from two ROIs (green circled) and spectrograms were calculated for the left hemisphere ROI (C) and right hemisphere ROI (D). Phase differences (E) and the 8-12 Hz PSV curve (F) between the two ROIs were calculated. Both suggest increased synchronization in eyes-closed conditions versus eyes-open conditions.

5.4 Discussion

In this chapter, we describe the EEG-fMRI reciprocal neuroimaging approach. The "reciprocal" here indicates the sequential use of EEG-informed fMRI imaging and fMRI-constrained EEG source imaging to integrate EEG and fMRI signals. Our simulation and experimental results have demonstrated that the method is well suited for the spatiotemporal imaging of neural activity. The high resolution in time and space will allow us to further investigate continuous neural activities and large-scale neural interactions in different brain conditions.

The basis of EEG-fMRI integration is the neurovascular coupling between the electrophysiological signals – EEG and the hemodynamic signals – fMRI. Recent studies have conducted parallel (or simultaneous) measurements of invasive EEG and BOLD fMRI in animal models or patients with intracranial EEG. Studies have revealed tight correlation between BOLD signal and local field potential (LFP) measured from the same location (Arthurs et al., 2000; Logothetis et al., 2001; Mukamel et al., 2005). In a human study, Mukamel et al (2005) found correlation between a spatially localized BOLD increase (or decrease) with the regional modulation of oscillatory activities measured in LFP. Scalp EEG, although measures signals by electrodes sitting outside of the skull, are believed to share the common electrophysiological origins with LFP signals. In line with these studies, simultaneous EEG-fMRI studies have demonstrated correlated relationship between EEG and fMRI signals in various EEG-informed fMRI or fMRI-weighted EEG imaging studies (Debener et al., 2006; Goldman et al., 2002; Liu et al., 1998). In this chapter, we developed this EEG-fMRI imaging approach based on the assumptions that

the neural electrophysiological change measured by EEG and the hemodynamic change measured by BOLD fMRI are coupled in time and overlapped in space.

Source separation and space-time separation

ICA has been considered as a data-driven tool to divide neural activity into groups, with temporal behaviors coherent within each group but independent across groups (Makeig et al., 2002). Importantly, it also serves to decompose spatio-temporal signals into representations in a time-by-space format, which allows for a separation of the temporal and spatial aspects of neural activity. Previous studies have demonstrated that the linear neurovascular coupling assumption can be applied to interpret the temporal relationship between the IC time courses and BOLD fMRI responses (Calhoun et al., 2006; Debener et al., 2006; Eichele et al., 2009; Feige et al., 2005). Spatial correspondence has also been reported between the IC scalp maps and fMRI maps (Debener et al., 2005). Taking advantages of ICA, we can target a single group of sources at a time. A time-space-separated strategy can be utilized, through which EEG and fMRI signals are integrated in the time domain and the spatial domain in two sequential steps.

The interpretation of components derived from ICA analysis remains an important question in many ICA related studies. ICA has been used to identify artifactual components (Jung et al., 2000; Iriarte et al., 2003; Urrestarazu, et al., 2004), and more importantly, physiologically plausible components, such as the modulation of rhythmic activities (Feige et al., 2005; Nam et al., 2002) and single-trial neural activities (Makeig et al., 2002; Debener et al., 2005, 2006). Here, we selected components according to their

spatial and time-frequency features. Components showing time-frequency features of interest (e.g. modulation of alpha rhythmic discharges associated with behavioral changes) were selected, which allows the imaging of continuous rhythmic activity as well as its modulation patterns. The selection criterion in the EEG-fMRI reciprocal imaging framework can be changed according to different experimental designs and different temporal or spectral features of interest.

EEG-informed fMRI analysis

The EEG-informed fMRI analysis has been used extensively in order to find hemodynamic signals related to certain electrophysiological features. Although an assumption of linear neurovascular coupling using canonical HRF has been most commonly made, studies have also explored many linear or non-linear mathematical models to explain the neurovascular coupling between EEG and fMRI signals. Differences between locations, frequencies, normal and pathological brains can change the correlation between the electrophysiological signals and hemodynamic signals (Bai et al., 2010; Büchel et al., 1998; De Munck et al., 2007; Kilner et al., 2005). Although we used a linear neurovascular coupling assumption in the simulation and experimental studies, the EEG-fMRI reciprocal imaging framework discussed in this chapter is not limited to a single neurovascular coupling assumption. It can be generalized to any linear or non-linear relationships by deriving fMRI regressors from various mathematical models (Büchel et al., 1998, Kilner et al., 2005; De Munck et al., 2007; Bai et al., 2010).

By using the EEG-informed fMRI analysis, we are able to study continuous rhythmic activity in task-free conditions, such as the spontaneous neural activity and its modulation (Laufs et al., 2003; Mantini et al., 2007). However, EEG-informed fMRI analysis alone may impose insufficient spatial constraints on physically plausible source locations (He and Liu, 2008). This can be caused by the inherent difference in the temporal resolutions between EEG and fMRI. As our results suggest, fMRI maps lack the temporal specificity to differentiate brain regions, of which the temporal patterns are similar in hemodynamics but different in electrophysiology.

fMRI-weighted EEG source imaging

Therefore, we used the spatial information from EEG to achieve better spatial specificity through a sequential step of fMRI-weighted source imaging. Our results show that brain regions indistinguishable through EEG-informed fMRI analysis can be differentiated through the subsequent step of the fMRI-weighted source imaging.

The co-localization between EEG and fMRI signals have been found in various animal and human models (Arthurs et al., 2000; Debener et al., 2005; Logothetis et al., 2001; Mukamel et al., 2005). However, EEG and fMRI measure different aspects of the neural activity. EEG sources can be invisible in fMRI and fMRI sources can be invisible in EEG (He and Liu, 2008; Liu and He, 2008). To enhance robustness of the source imaging against EEG-fMRI mismatch, recent studies have developed fMRI-weighted source imaging algorithms using partial fMRI weighting (Liu et al., 1998), or EEG-fMRI-combined weighting (Liu and He, 2008). In the framework of the EEG-fMRI

reciprocal imaging approach, the issue of the EEG-fMRI mismatch can be considered by changing the way that fMRI constraints are applied in the step of fMRI-weighted source imaging.

Continuous spatiotemporal imaging

The EEG-fMRI reciprocal imaging framework provides a way to image the continuous change of rhythmic activity. The reconstructed source imaging has high temporal resolution from EEG and high spatial resolution from fMRI. Such a high-resolution spatiotemporal imaging can be further applied to different neuroscience studies, such as the study of functional networks or single-trial activity. More significantly, it allows us to focus the source imaging on certain time-frequency features of interest, or in order words, certain modulation patterns of oscillatory activity (Gross et al., 2001; Lin et al., 2004). External stimulations, cognitive tasks, or spontaneous behavioral changes can modulate different frequency components of the neural electrophysiological signals. The capability of imaging these modulated activities would help us to better understand the correspondence between different behavioral states and the underlying neural mechanisms.

In a simple example in this chapter, we estimated the alpha-band modulation in correlation with the behavioral changes (eye open vs. eye close). The spatial distribution of the alpha modulation in the parieto-occipital cortex agrees with previous EEG-fMRI (Feige et al., 2005; Goldman et al., 2002) and EEG/MEG studies (Gross et al., 2001; Hari et al., 1997). The alpha amplitude and phase-synchronization increased in the eyes-closed

conditions and decreased in the eyes-open conditions. Previous studies have suggested that visual attention network communicates by neural phase-synchronization (Gross et al., 2004; Womelsdorf et al., 2007). Accompanying the variation of visual attention, alpha modulation has been consistently observed in parieto-occipital brain (Foxe et al., 1998; Worden et al., 2000). In line with these studies, the modulation of the alpha activity and its phase-synchronization described in this chapter may suggest a significant change of visual attention demands in the parieto-occipital network. The eyes-closed resting state requires minimum demand of visual attention, and the parieto-occipital network is characterized by high synchronization. Such synchronization in the visual attention network may be suppressed with eyes open, as neurons responsible to different visual fields may compete for attentional resources even in the absence of visual stimuli (Smith et al., 2000). This hypothesis, although being speculative, does provide a plausible interpretation on our data that alpha amplitudes and phase-synchronization were larger during eye-closed periods than during eye-open periods.

In summary, in this chapter we described an EEG-fMRI "reciprocal" integrated imaging method, which utilizes the EEG-informed fMRI analysis, and fMRI-weighted source imaging. The approach offers a model-based framework to integrate fMRI and EEG, and provides high resolution in both time and space. A unique contribution of the approach lies in its capability of imaging continuously rhythmic activities and their modulation patterns. Such high-resolution spatiotemporal neuroimaging approach would be a useful tool for various neuroscience studies to understand the spontaneous neural

oscillations, correspondence between neural rhythmic activity and behavioral changes, and the connection between various cortical areas and networks. In pathological conditions, such as epilepsy, most of the brain activity is spontaneous (e.g., interictal spikes, seizures). Using a continuous EEG-fMRI imaging technique would significantly improve our ability to image the brain networks involved in the diseases, which would benefit the treatment of individual patient or improve our knowledge about the mechanisms of the diseases. However, before the method can be applied in pathological models, the neurovascular coupling in different pathological models need to be systematically investigated.

Chapter 6 Conclusions and perspectives

6.1 Conclusions

Non-invasive functional neuroimaging techniques have been actively investigated in human subjects since the discovery of EEG in the late 1920s (Berger, 1929). Tremendous efforts have been made in order to improve the temporal and spatial resolutions of non-invasive approaches. Along this line, EEG and MEG source imaging (Baillet et al., 2001; Hamalainen and Sarvas, 1989; Michel et al., 2004), fMRI (Bandettini et al., 1992; Kwong et al., 1992; Ogawa et al., 1992), and multimodal EEG-fMRI imaging (Dale and Halgren, 2001; He and Liu, 2008; Liu et al., 1998) have improved our capability of noninvasive imaging to a resolution with a millimeter scale in space and a millisecond scale in time. While neuroimaging techniques have been extensively used in neuroscience research, it is, to a lesser extent, applied to clinical diagnoses and treatments. An important application of functional neuroimaging techniques in the diseased brain is the pre-surgical evaluation of epilepsy. Collectively, information from multiple independent modalities, such as semiology, neuroimaging, and neurological tests, provides clues to delineate a surgical plan. The current pre-surgical imaging procedure has noninvasive components including the imaging of anatomy (MRI), imaging of hemodynamic and metabolic responses (SPECT, fMRI, PET), and scalp mapping of electrophysiological signals (Engel et al., 2008; Rosenow and Luders, 2001). A potential trend in the clinical investigations is to include the localization of interictal activity from EEG or MEG as an imaging tool. However, with the many established neuroimaging protocols, there still lacks an established non-invasive

component that can image electrophysiological signals during seizures. The development of such a component can be extraordinarily important, because the seizure is the most clinically important event in epilepsy patients, the cure of which is the ultimate goal of any epilepsy treatment.

In the present dissertation research, we developed a non-invasive seizure imaging protocol, which combines high-resolution EEG recording and spatiotemporal source imaging. By testing the new protocol in epilepsy patients, we demonstrated the feasibility of the high resolution EEG recording protocol for clinical long-term monitoring. The extended recording time is crucial for capturing spontaneous and infrequent seizure events. We then evaluated the capability of the spatiotemporal EEG seizure imaging approach by information obtained through the most invasive procedures: resective surgery and chronic invasive recording of iEEG. The concordance with the invasive results suggests the clinical feasibility of such a noninvasive electrophysiological seizure imaging protocol. It is widely applicable to every patient because of its noninvasiveness. As a potential pre-surgical evaluation tool, it can be used as priori information to assist the implant of iEEG electrodes. If it is consistent with other non-invasive neuroimaging or neurological tests, the proportion of patients that must undergo invasive iEEG monitoring can be reduced. By adding this seizure imaging component, the non-invasive neuroimaging aspect of the pre-surgical evaluation in epilepsy can be significantly enhanced.

Epileptic seizures impact widespread brain networks beyond the extent of the epileptogenic zone. As a result, patients can experience a variety of manifestations in

behaviors. One common phenomenon is the loss or decrease of consciousness and responsiveness to the external world (Arthuis et al., 2009; Englot et al., 2010; Guye et al., 2006; Lee et al., 2002; Lux et al., 2002). In the analysis of abnormal slow-wave rhythms following epileptic seizures, we found changes of cortical electrophysiology corresponding to the different levels of cognitive deficits in epileptic patients. In line with previous neuroimaging and intracranial EEG studies (Lux, et al., 2002; Lee et al., 2002; Englot et al., 2010; Arthuis et al., 2009; Guye et al., 2006), yet providing more cortical coverage, our results suggest that widespread neocortical regions are affected by seizures. The spectral shifts to lower-frequency and the spatial shifts to neocortical regions (most prominently to frontal regions) outside of the epileptogenic zone may be an electrophysiological representation of the impact of epileptic seizures on the brain. These changes in slow rhythms may also be related to the altered cognitive functions in epilepsy patients.

Although continuous spatiotemporal imaging can be achieved noninvasively by EEG source imaging techniques, by adding multimodal information from other modalities, the spatial and temporal resolutions can be significantly improved. In the dissertation research, we also developed an EEG-fMRI integrated imaging approach, which combines the temporal resolution of EEG and spatial resolution of fMRI. We have shown in our computer simulations and experimental study in normal healthy subjects that we are able to reconstruct the continuous rhythmic activities, as well as their modulation that corresponds to the behavioral changes. Such a high-resolution spatiotemporal imaging technique can be important for neuroscience research. Potential

applications also include the localization of the epileptic networks in epilepsy patients (Grouiller et al., 2011; Laufs et al., 2007; Tyvaert et al., 2008).

In summary, the present dissertation research developed and evaluated the spatiotemporal source imaging approaches for the non-invasive localization of dynamic neural activity in the diseased and normal brains. An evaluation has been conducted in patient groups in order to test the clinical applicability of such a pre-surgical noninvasive seizure imaging tool. An investigation has been conducted to study the widespread impact of epileptic seizures on the brain and, as a result, on the behaviors and cognitions of epilepsy patients. The spatial resolution has been further improved by adding the component of fMRI through an EEG-fMRI integrated imaging framework. All of the results that were obtained suggest the importance of noninvasive spatiotemporal neuroimaging approaches for solving clinical problems and for investigating neuroscience questions. Furthermore, an improved understanding of neurological diseases and their mechanisms would help us to develop and deliver curative treatments of neurological diseases.

6.2. Perspectives

In addition to the development and progress obtained in the present dissertation research, there are remaining challenges, which also represent opportunities for future improvement of techniques and clinical applications.

Prospective clinical studies

We have demonstrated the feasibility and accuracy of the noninvasive, spatiotemporal seizure imaging approach through comparison against invasive procedures in a retrospective study. However, before applying a new neuroimaging method to clinical routines, prospective studies of large groups of patients are crucial in order to design a protocol that is most suitable for clinical applications. It is important, in these prospective studies, to include the noninvasive seizure imaging protocol into the routine evaluation of epilepsy patients. The results of noninvasive seizure imaging need to be presented in the pre-surgical conference, during which neurologists and neurosurgeons determine surgical plans based on the information obtained through various pre-surgical diagnostic resources. Surgical plans, including both the plan to implant intracranial electrodes as well as the plan to resect brain tissues, shall be determined twice. The first plan is determined based on conventional procedures without EEG seizure imaging results. The second plan is determined with the EEG seizure imaging results. Possible outcomes of the two plans can be the same, which indicates that EEG source imaging is consistent with conventional procedures. The outcomes can also be the determination of more or less iEEG coverage or resection, which indicates that EEG source imaging provides additional information to the conventional procedures. In optimal cases, when EEG source imaging confirms with anatomical MRI and other noninvasive neurological tests, patients can go to resection without the need of another surgery to implant iEEG. The difference between the outcomes of the two plans will show the extent to which such a noninvasive seizure imaging protocol can change the

conventional clinical practice of the surgical treatment of epilepsy. The yield and accuracy of the resultant iEEG recording and the success rate of surgery will be important measures to determine the significance and the added value of such a new protocol to the routine pre-surgical evaluation.

Behavioral testing systems in epilepsy

The study of the slow waves and consciousness in the current dissertation research is also limited by the retrospective nature of the study. The current practice to determine the consciousness of patients during partial seizures is very limited with classification to only two categories: simple partial seizures and complex partial seizures (Commission of ILAE 1981). Such a classification cannot distinguish the cause of the cognitive dysfunctions (e.g., consciousness vs. memory, languages, and motor functions) or different levels of impairment of consciousness. These behavioral measures, however, are extremely important for a quantitative evaluation of their correlation with electrophysiology. A fine-scale score and a time-varying system to evaluate the behavioral and cognitive changes of patients would improve the current practice and management of patients. Because seizures are one of the very few pathological models to study consciousness, a well-established behavioral testing system would also significantly improve our ability to investigate and understand the consciousness process in humans.

Neurovascular coupling in pathological models

The EEG-fMRI integrated imaging methods have been widely used in the investigation of normal and diseased brains. In the dissertation research, we proposed a framework to integrate EEG and fMRI information, and demonstrated the approach using a linear neurovascular coupling model. However, the neurovascular coupling between EEG and fMRI signals is not well understood, especially in pathological conditions. The EEG-informed fMRI analysis in epilepsy patients identified the epileptogenic zone, as well as activation or deactivation in more fundamental brain networks (Blumenfeld et al., 2009; Gotman et al., 2005; Grouiller et al., 2011; Laufs et al., 2007). The hemodynamic response function in epilepsy patients can be different than that of normal healthy subjects, and can also change from location to location (Bai et al., 2010). Therefore, before the implementation and interpretation of the EEG-fMRI integrated imaging in epilepsy patients, systematic studies are necessary in order to investigate how the EEG and fMRI signals correlate in time and overlap in space. The EEG-fMRI imaging framework we proposed was designed to incorporate various neurovascular coupling models, and therefore can be suited to study different activities if the relationship between EEG and fMRI signals is well understood.

References

Commission on classification and terminology of the international league against epilepsy. Proposal for revised clinical and electroencephalographic classification of epileptic seizures. Epilepsia 1981; 22: 489-501.

Ajmone-Marsan C, Van Buren JM. Epileptiform activity in cortical and subcortical structures in the temporal lobe of man. Temporal lobe epilepsy 1958; 89: 79-108.

Alkire MT, Hudetz AG, Tononi G. Consciousness and anesthesia. Science 2008; 322: 876.

Arthuis M, Valton L, Régis J, Chauvel P, Wendling F, Naccache L, et al. Impaired consciousness during temporal lobe seizures is related to increased long-distance cortical–subcortical synchronization. Brain 2009; 132: 2091.

Arthurs O, Williams E, Carpenter T, Pickard J, Boniface S. Linear coupling between functional magnetic resonance imaging and evoked potential amplitude in human somatosensory cortex. Neuroscience 2000; 101: 803-6.

Assaf BA, Ebersole JS. Continuous source imaging of scalp ictal rhythms in temporal lobe epilepsy. Epilepsia 1997; 38: 1114-23.

Assaf BA, Karkar KM, Laxer KD, Garcia PA, Austin EJ, Barbaro NM, et al. Ictal magnetoencephalography in temporal and extratemporal lobe epilepsy. Epilepsia 2003; 44: 1320-7.

Bai X, Vestal M, Berman R, Negishi M, Spann M, Vega C, et al. Dynamic time course of typical childhood absence seizures: EEG, behavior, and functional magnetic resonance imaging. Journal of Neuroscience 2010; 30: 5884-93.

Baillet S, Mosher JC, Leahy RM. Electromagnetic brain mapping. Signal Processing Magazine, IEEE 2001; 18: 14-30.

Bandettini PA, Wong EC, Hinks RS, Tikofsky RS, Hyde JS. Time course EPI of human brain function during task activation. Magnetic Resonance in Medicine 1992; 25: 390-7.

Baumgartner C, Pataraia E. Revisiting the role of magnetoencephalography in epilepsy. Curr Opin Neurol 2006; 19: 181-6.

Berger H. Über das elektrenkephalogramm des menschen. Eur Arch Psychiatry Clin Neurosci 1933; 98: 231-54.

Berger H. Über das elektrenkephalogramm des menschen. Eur Arch Psychiatry Clin Neurosci 1929; 87: 527-70.

Bickford RG, Butt HR. Hepatic coma: The electroencephalographic pattern. J Clin Invest 1955; 34: 790.

Blair RDG. Temporal lobe epilepsy semiology. Epilepsy Research and Treatment 2012; 2012.

Blanco JA, Stead M, Krieger A, Stacey W, Maus D, Marsh E, et al. Data mining neocortical high-frequency oscillations in epilepsy and controls. Brain 2011; 134: 2948-59.

Blumenfeld H, Rivera M, McNally KA, Davis K, Spencer DD, Spencer SS. Ictal neocortical slowing in temporal lobe epilepsy. Neurology 2004; 63: 1015.

Blumenfeld H, Varghese G, Purcaro M, Motelow J, Enev M, McNally K, et al. Cortical and subcortical networks in human secondarily generalized tonic-clonic seizures. Brain 2009; 132: 999.

Blumenfeld H, McNally KA, Vanderhill SD, Paige ALB, Chung R, Davis K, et al. Positive and negative network correlations in temporal lobe epilepsy. Cerebral Cortex 2004; 14: 892.

Boon P, D'Havé M, Vanrumste B, Van Hoey G, Vonck K, Van Walleghem P, et al. Ictal source localization in presurgical patients with refractory epilepsy. Journal of clinical neurophysiology 2002; 19: 461.

Brodbeck V, Spinelli L, Lascano A, Wissmeier M, Vargas M, Vulliemoz S, et al. Electroencephalographic source imaging: A prospective study of 152 operated epileptic patients.. Brain 2011; 134: 2887-97.

Broyd SJ, Demanuele C, Debener S, Helps SK, James CJ, Sonuga-Barke EJS. Default-mode brain dysfunction in mental disorders: A systematic review. Neuroscience & Biobehavioral Reviews 2009; 33: 279-96.

Büchel C, Holmes A, Rees G, Friston K. Characterizing stimulus-response functions using nonlinear regressors in parametric fMRI experiments. Neuroimage 1998; 8: 140-8.

Calhoun VD, Adali T, Pearlson G, Kiehl K. Neuronal chronometry of target detection: Fusion of hemodynamic and event-related potential data. Neuroimage 2006; 30: 544-53.

Collins DL, Zijdenbos AP, Kollokian V, Sled JG, Kabani N, Holmes CJ, et al. Design and construction of a realistic digital brain phantom. Medical Imaging, IEEE Transactions on 1998; 17: 463-8.

Cuffin BN. A method for localizing EEG sources in realistic head models. Biomedical Engineering, IEEE Transactions on 1995; 42: 68-71.

Dale AM, Halgren E. Spatiotemporal mapping of brain activity by integration of multiple imaging modalities. Curr Opin Neurobiol 2001; 11: 202-8.

Dale AM, Sereno MI. Improved localizadon of cortical activity by combining eeg and meg with mri cortical surface reconstruction: A linear approach. J Cogn Neurosci 1993; 5: 162-76.

Dang-Vu TT, Schabus M, Desseilles M, Albouy G, Boly M, Darsaud A, et al. Spontaneous neural activity during human slow wave sleep. Proceedings of the National Academy of Sciences 2008; 105: 15160.

De Munck J, Goncalves S, Huijboom L, Kuijer J, Pouwels P, Heethaar R, et al. The hemodynamic response of the alpha rhythm: An EEG/fMRI study. Neuroimage 2007; 35: 1142-51.

Debener S, Ullsperger M, Siegel M, Engel AK. Single-trial EEG-fMRI reveals the dynamics of cognitive function. Trends Cogn Sci (Regul Ed) 2006; 10: 558-63.

Debener S, Ullsperger M, Siegel M, Fiehler K, Von Cramon DY, Engel AK. Trial-by-trial coupling of concurrent electroencephalogram and functional magnetic resonance imaging identifies the dynamics of performance monitoring. The Journal of Neuroscience 2005; 25: 11730-7.

Delorme A, Makeig S. EEGLAB: An open source toolbox for analysis of single-trial EEG dynamics including independent component analysis. J Neurosci Methods 2004; 134: 9-21.

Ding L, Worrell GA, Lagerlund TD, He B. Ictal source analysis: Localization and imaging of causal interactions in humans. Neuroimage 2007; 34: 575-86.

Eadie MJ, Bladin PF. A disease once sacred: A history of the medical understanding of epilepsy. : John Libbey & Company; 2001.

Eichele T, Calhoun VD, Debener S. Mining EEG-fMRI using independent component analysis. International Journal of Psychophysiology 2009; 73: 53-61.

Engel J. Seizures and epilepsy. : FA Davis Co.; 1989.

Engel J, Pedley TA, Aicardi J. Epilepsy: A comprehensive textbook. : Lippincott Williams & Wilkins; 2008.

Englot DJ, Yang L, Hamid H, Danielson N, Bai X, Marfeo A, et al. Impaired consciousness in temporal lobe seizures: Role of cortical slow activity. Brain 2010; 133: 3764.

Feige B, Scheffler K, Esposito F, Di Salle F, Hennig J, Seifritz E. Cortical and subcortical correlates of electroencephalographic alpha rhythm modulation. J Neurophysiol 2005; 93: 2864-72.

Fisher RS, Schachter SC. The postictal state: A neglected entity in the management of epilepsy. Epilepsy & Behavior 2000; 1: 52-9.

Fox MD, Snyder AZ, Vincent JL, Corbetta M, Van Essen DC, Raichle ME. The human brain is intrinsically organized into dynamic, anticorrelated functional networks. Proc Natl Acad Sci U S A 2005; 102: 9673.

Foxe JJ, Simpson GV, Ahlfors SP. Parieto-occipital~ 1 0Hz activity reflects anticipatory state of visual attention mechanisms. Neuroreport 1998; 9: 3929.

Foyaca-Sibat H, editor. Novel aspects on epilepsy. : InTech; 2011.

Friston KJ, Holmes AP, Worsley KJ, Poline JP, Frith CD, Frackowiak RSJ. Statistical parametric maps in functional imaging: A general linear approach. Hum Brain Mapp 1994; 2: 189-210.

Friston K, Fletcher P, Josephs O, Holmes A, Rugg M, Turner R. Event-related fMRI: Characterizing differential responses. Neuroimage 1998; 7: 30-40.

Fuchs M, Drenckhahn R, Wischmann H, Wagner M. An improved boundary element method for realistic volume-conductor modeling. IEEE Transactions on Biomedical Engineering 1998; 45: 980-97.

Gevins A. High resolution EEG. Brain Topogr 1993; 5: 321-5.

Gibbs FA, Lennox WG, Gibbs EL. The electro-encephalogram in diagnosis and in localization of epileptic seizures. Archives of Neurology & Psychiatry 1936; 36: 1225.

Goldensohn E. Simultaneous recording of EEG and clinical seizures using kinescope. Electroencephalogr Clin Neurophysiol 1966; 21: 623.

Goldman RI, Stern JM, Engel Jr J, Cohen MS. Simultaneous EEG and fMRI of the alpha rhythm. Neuroreport 2002; 13: 2487.

Gorodnitsky IF, Rao BD. Sparse signal reconstruction from limited data using FOCUSS: A re-weighted minimum norm algorithm. Signal Processing, IEEE Transactions on 1997; 45: 600-16.

Gotman J, Grova C, Bagshaw A, Kobayashi E, Aghakhani Y, Dubeau F. Generalized epileptic discharges show thalamocortical activation and suspension of the default state of the brain. Proc Natl Acad Sci U S A 2005; 102: 15236.

Gross J, Kujala J, Hämäläinen M, Timmermann L, Schnitzler A, Salmelin R. Dynamic imaging of coherent sources: Studying neural interactions in the human brain. Proceedings of the National Academy of Sciences 2001; 98: 694.

Gross J, Schmitz F, Schnitzler I, Kessler K, Shapiro K, Hommel B, et al. Modulation of long-range neural synchrony reflects temporal limitations of visual attention in humans. Proc Natl Acad Sci U S A 2004; 101: 13050.

Grouiller F, Thornton RC, Groening K, Spinelli L, Duncan JS, Schaller K, et al. With or without spikes: localization of focal epileptic activity by simultaneous electroencephalography and functional magnetic resonance imaging.. Brain 2011; 134: 2867-86.

Guye M, Régis J, Tamura M, Wendling F, Gonigal AM, Chauvel P, et al. The role of corticothalamic coupling in human temporal lobe epilepsy. Brain 2006; 129: 1917.

Hämäläinen M, Hari R, Ilmoniemi RJ, Knuutila J, Lounasmaa OV. Magnetoencephalography—theory, instrumentation, and applications to noninvasive studies of the working human brain. Reviews of modern Physics 1993; 65: 413-97.

Hamalainen M, Sarvas J. Realistic conductivity geometry model of the human head for interpretation of neuromagnetic data. IEEE Transactions on Biomedical Engineering 1989; 36: 165-71.

Hammers A, Asselin MC, Hinz R, Kitchen I, Brooks DJ, Duncan JS, et al. Upregulation of opioid receptor binding following spontaneous epileptic seizures. Brain 2007; 130: 1009.

Hari R, Salmelin R, Makela J, Salenius S, Helle M. Magnetoencephalographic cortical rhythms. International journal of psychophysiology 1997; 26: 51-62.

He B, Liu Z. Multimodal functional neuroimaging: Integrating functional MRI and EEG/MEG. Biomedical Engineering, IEEE Reviews in 2008; 1: 23-40.

He B, Lian J. High-resolution spatio-temporal functional neuroimaging of brain activity. Crit Rev Biomed Eng 2002; 30: 283.

He B, Yang L, Wilke C, Yuan H. Electrophysiological imaging of brain activity and connectivity - challenges and opportunities. IEEE Transactions on Biomedical Engineering 2011; 58: 1918-31.

He B, Musha T, Okamoto Y, Homma S, Nakajima Y, Sato T. Electric dipole tracing in the brain by means of the boundary element method and its accuracy. IEEE Transactions on Biomedical Engineering 1987: 406-14.

Henry TR, Chupin M, Lehéricy S, Strupp JP, Sikora MA, Zhiyi YS, et al. Hippocampal sclerosis in temporal lobe epilepsy: Findings at 7 T. Radiology 2011; 261: 199-209.

Hofle N, Paus T, Reutens D, Fiset P, Gotman J, Evans AC, et al. Regional cerebral blood flow changes as a function of delta and spindle activity during slow wave sleep in humans. The Journal of neuroscience 1997; 17: 4800.

Holmes MD, Tucker DM, Quiring JM, Hakimian S, Miller JW, Ojemann JG. Comparing noninvasive dense array and intracranial electroencephalography for localization of seizures. Neurosurgery 2010; 66: 354-62.

Hudetz AG. Suppressing consciousness: Mechanisms of general anesthesia. 2006; 25: 196-204.

Hudetz AG, Imas OA. Burst activation of the cerebral cortex by flash stimuli during isoflurane anesthesia in rats. Anesthesiology 2007; 107: 983.

Hufnagel A, Poersch M, Elger CE, Zentner J, Wolf HK, Schramm J. The clinical and prognostic relevance of the postictal slow focus in the electrocorticogram. Electroencephalogr Clin Neurophysiol 1995; 94: 12-8.

Hunter J, Jasper HH. A method of analysis of seizure pattern and electroencephalogram; a cinematographic technique. Electroencephalogr Clin Neurophysiol 1949; 1: 113.

Iriarte J, Urrestarazu E, Valencia M, Alegre M, Malanda A, Viteri C, et al. Independent component analysis as a tool to eliminate artifacts in EEG: A quantitative study. Journal of clinical neurophysiology 2003; 20: 249.

Jackson JH. On the anatomical, physiological, and pathological investigation of epilepsies. : Spottiswoode and Company; 1873.

Jackson JH, Taylor J, Holmes SG, Walshe FMR. Selected writings of john hughlings jackson. 1931.

Jan M, Sadler M, Rahey SR. Lateralized postictal EEG delta predicts the side of seizure surgery in temporal lobe epilepsy. Epilepsia 2001; 42: 402-5.

Jung KY, Kang JK, Kim JH, Im CH, Kim KH, Jung HK. Spatiotemporospectral characteristics of scalp ictal EEG in mesial temporal lobe epilepsy with hippocampal sclerosis. Brain Res 2009; 1287: 206-19.

Jung TP, Makeig S, Westerfield M, Townsend J, Courchesne E, Sejnowski TJ. Removal of eye activity artifacts from visual event-related potentials in normal and clinical subjects. Clinical Neurophysiology 2000; 111: 1745-58.

Kavanagk RN, Darcey TM, Lehmann D, Fender DH. Evaluation of methods for three-dimensional localization of electrical sources in the human brain. Biomedical Engineering, IEEE Transactions on 1978: 421-9.

Kelley WM, Miezin FM, McDermott KB, Buckner RL, Raichle ME, Cohen NJ, et al. Hemispheric specialization in human dorsal frontal cortex and medial temporal lobe for verbal and nonverbal memory encoding. Neuron 1998; 20: 927-36.

Kilner J, Mattout J, Henson R, Friston K. Hemodynamic correlates of EEG: A heuristic. Neuroimage 2005; 28: 280-6.

Klimesch W. EEG alpha and theta oscillations reflect cognitive and memory performance: A review and analysis. Brain Res Rev 1999; 29: 169-95.

Knowlton RC, Razdan SN, Limdi N, Elgavish RA, Killen J, Blount J, et al. Effect of epilepsy magnetic source imaging on intracranial electrode placement. Ann Neurol 2009; 65: 716-23.

Knowlton RC, Elgavish RA, Al Bartolucci BO, Limdi N, Blount J, Burneo JG, et al. Functional imaging: II. prediction of epilepsy surgery outcome. Ann Neurol 2008; 64: 35-41.

Koessler L, Benar C, Maillard L, Badier JM, Vignal JP, Bartolomei F, et al. Source localization of ictal epileptic activity investigated by high resolution EEG and validated by SEEG. Neuroimage 2010; 51: 642-53.

Kwong KK, Belliveau JW, Chesler DA, Goldberg IE, Weisskoff RM, Poncelet BP, et al. Dynamic magnetic resonance imaging of human brain activity during primary sensory stimulation. Proceedings of the National Academy of Sciences 1992; 89: 5675.

Lachaux JP, Rodriguez E, Martinerie J, Varela FJ. Measuring phase synchrony in brain signals. Hum Brain Mapp 1999; 8: 194-208.

Lachaux JP, Rodriguez E, Le Van Quyen M, Lutz A, Martinerie J, Varela FJ. Studying single-trials of phase synchronous activity in the brain. International Journal of Bifurcation and Chaos in Applied Sciences and Engineering 2000; 10: 2429-40.

Lai Y, Van Drongelen W, Ding L, Hecox K, Towle V, Frim D, et al. Estimation of in vivo human brain-to-skull conductivity ratio from simultaneous extra-and intra-cranial electrical potential recordings. Clinical neurophysiology 2005; 116: 456-65.

Lantz G, Grave de Peralta R, Spinelli L, Seeck M, Michel C. Epileptic source localization with high density EEG: How many electrodes are needed? Clinical Neurophysiology 2003; 114: 63-9.

Lantz G, Michel C, Seeck M, Blanke O, Spinelli L, Thut G, et al. Space-oriented segmentation and 3-dimensional source reconstruction of ictal EEG patterns. Clinical Neurophysiology 2001; 112: 688-97.

Laufs H, Lengler U, Hamandi K, Kleinschmidt A, Krakow K. Linking generalized Spike-and-Wave discharges and resting state brain activity by using EEG/fMRI in a patient with absence seizures. Epilepsia 2006; 47: 444-8.

Laufs H, Hamandi K, Salek-Haddadi A, Kleinschmidt AK, Duncan JS, Lemieux L. Temporal lobe interictal epileptic discharges affect cerebral activity in "default mode" brain regions. Hum Brain Mapp 2007; 28: 1023-32.

Laufs H, Krakow K, Sterzer P, Eger E, Beyerle A, Salek-Haddadi A, et al. Electroencephalographic signatures of attentional and cognitive default modes in spontaneous brain activity fluctuations at rest. Proc Natl Acad Sci U S A 2003; 100: 11053.

Lee K, Meador K, Park Y, King D, Murro A, Pillai J, et al. Pathophysiology of altered consciousness during seizures. Neurology 2002; 59: 841.

Leonardi M, Ustun TB. The global burden of epilepsy. Epilepsia 2002; 43: 21-5.

Lin FH, Witzel T, Hämäläinen MS, Dale AM, Belliveau JW, Stufflebeam SM. Spectral spatiotemporal imaging of cortical oscillations and interactions in the human brain. Neuroimage 2004; 23: 582-95.

Littre É. Hippocrates: Oeuvres completes D'hippocrate. Hippocrates: Oeuvres Completes D'Hippocrate 1849; 6.

Liu AK, Belliveau JW, Dale AM. Spatiotemporal imaging of human brain activity using functional MRI constrained magnetoencephalography data: Monte carlo simulations. Proceedings of the National Academy of Sciences 1998; 95: 8945.

Liu X, Zhu XH, Zhang Y, Chen W. Neural origin of spontaneous hemodynamic fluctuations in rats under Burst–Suppression anesthesia condition. Cerebral Cortex 2011; 21: 374.

Liu Z, He B. fMRI-EEG integrated cortical source imaging by use of time-variant spatial constraints. Neuroimage 2008; 39: 1198-214.

Liu Z, Rios C, Zhang N, Yang L, Chen W, He B. Linear and nonlinear relationships between visual stimuli, EEG and BOLD fMRI signals. Neuroimage 2010; 50: 1054-66.

Logothetis NK, Pauls J, Augath M, Trinath T, Oeltermann A. Neurophysiological investigation of the basis of the fMRI signal. Nature 2001; 412: 150-7.

Lux S, Kurthen M, Helmstaedter C, Hartje W, Reuber M, Elger CE. The localizing value of ictal consciousness and its constituent functions. Brain 2002; 125: 2691.

Makeig S, Westerfield M, Jung TP, Enghoff S, Townsend J, Courchesne E, et al. Dynamic brain sources of visual evoked responses. Science 2002; 295: 690-4.

Mantini D, Perrucci MG, Del Gratta C, Romani GL, Corbetta M. Electrophysiological signatures of resting state networks in the human brain. Proceedings of the National Academy of Sciences 2007; 104: 13170.

Marsh ED, Peltzer B, Brown III MW, Wusthoff C, Storm Jr PB, Litt B, et al. Interictal EEG spikes identify the region of electrographic seizure onset in some, but not all, pediatric epilepsy patients. Epilepsia 2010; 51: 592-601.

Massimini M, Ferrarelli F, Huber R, Esser SK, Singh H, Tononi G. Breakdown of cortical effective connectivity during sleep. Science 2005; 309: 2228.

Matsuura K, Okabe Y. Selective minimum-norm solution of the biomagnetic inverse problem. Biomedical Engineering, IEEE Transactions on 1995; 42: 608-15.

Menendez RGP, Andino SG, Lantz G, Michel CM, Landis T. Noninvasive localization of electromagnetic epileptic activity. I. method descriptions and simulations. Brain Topogr 2001; 14: 131-7.

Michel CM, Murray MM, Lantz G, Gonzalez S, Spinelli L, Grave de Peralta R. EEG source imaging. Clinical neurophysiology 2004; 115: 2195-222.

Mosher JC, Leahy RM. Source localization using recursively applied and projected (RAP) MUSIC. Signal Processing, IEEE Transactions on 1999; 47: 332-40.

Mosher JC, Lewis PS, Leahy RM. Multiple dipole modeling and localization from spatio-temporal MEG data. Biomedical Engineering, IEEE Transactions on 1992; 39: 541-57.

Mukamel R, Gelbard H, Arieli A, Hasson U, Fried I, Malach R. Coupling between neuronal firing, field potentials, and FMRI in human auditory cortex. Science 2005; 309: 951.

Nam H, Yim TG, Han SK, Oh JB, Lee SK. Independent component analysis of ictal EEG in medial temporal lobe epilepsy. Epilepsia 2002; 43: 160-4.

Oakes TR, Pizzagalli DA, Hendrick AM, Horras KA, Larson CL, Abercrombie HC, et al. Functional coupling of simultaneous electrical and metabolic activity in the human brain. Hum Brain Mapp 2004; 21: 257-70.

Ogawa S, Tank DW, Menon R, Ellermann JM, Kim SG, Merkle H, et al. Intrinsic signal changes accompanying sensory stimulation: Functional brain mapping with magnetic resonance imaging. Proceedings of the National Academy of Sciences 1992; 89: 5951.

Ou W, Hämäläinen MS, Golland P. A distributed spatio-temporal EEG/MEG inverse solver. Neuroimage 2009; 44: 932-46.

Palus M, Hoyer D. Detecting nonlinearity and phase synchronization with surrogate data. IEEE Engineering in Medicine and Biology Magazine 1998; 17: 40-5.

Panet-Raymond D, Gotman J. Asymmetry in delta activity in patients with focal epilepsy. Electroencephalogr Clin Neurophysiol 1990; 75: 474-81.

Pascual-Marqui R. Standardized low-resolution brain electromagnetic tomography (sLORETA): Technical details. Methods Find Exp Clin Pharmacol 2002; 24: 5-12.

Pascual-Marqui R, Michel C, Lehmann D. Low resolution electromagnetic tomography: A new method for localizing electrical activity in the brain. International Journal of Psychophysiology 1994; 18: 49-65.

Patel A, Alotaibi F, Blume WT, Mirsattari SM. Independent component analysis of subdurally recorded occipital seizures. Clinical Neurophysiology 2008; 119: 2437-46.

Plummer C, Harvey AS, Cook M. EEG source localization in focal epilepsy: Where are we now? Epilepsia 2008; 49: 201-18.

Raichle ME, MacLeod AM, Snyder AZ, Powers WJ, GusnardDA SGL. Adefaultmodeof brain function. PNAS USA 2001; 98: 676-82.

Rodriguez E, George N, Lachaux JP, Martinerie J, Renault B, Varela FJ. Perception's shadow: Long-distance synchronization of human brain activity. Nature 1999; 397: 430-3.

Rosenow F, Luders H. Presurgical evaluation of epilepsy. Brain 2001; 124: 1683-700.

Scherg M, Von Cramon D. Two bilateral sources of the late AEP as identified by a spatio-temporal dipole model. Electroencephalography and Clinical Neurophysiology/Evoked Potentials Section 1985; 62: 32-44.

Seber GAF. Multivariate observations. New York: John Wiley & Sons Inc; 1984.

Sekihara K, Nagarajan SS, Poeppel D, Marantz A, Miyashita Y. Reconstructing spatio-temporal activities of neural sources using an MEG vector beamformer technique. Biomedical Engineering, IEEE Transactions on 2001; 48: 760-71.

Siniatchkin M, Groening K, Moehring J, Moeller F, Boor R, Brodbeck V, et al. Neuronal networks in children with continuous spikes and waves during slow sleep. Brain 2010; 133: 2798-813.

Smith AT, Singh KD, Greenlee MW. Attentional suppression of activity in the human visual cortex. Neuroreport 2000; 11: 271.

Spath H. The cluster dissection and analysis theory FORTRAN programs examples. New York: Halsted Press; 1985.

Spencer SS. The relative contributions of MRI, SPECT, and PET imaging in epilepsy. Epilepsia 1994; 35: S72-89.

Spitzer AR, Cohen LG, Fabrikant J, Hallett M. A method for determining optimal interelectrode spacing for cerebral topographic mapping. Electroencephalogr Clin Neurophysiol 1989; 72: 355-61.

Srinivasan R, Nunez PL, Tucker DM, Silberstein RB, Cadusch PJ. Spatial sampling and filtering of EEG with spline laplacians to estimate cortical potentials. Brain Topogr 1996; 8: 355-66.

Stefan H, Hummel C, Scheler G, Genow A, Druschky K, Tilz C, et al. Magnetic brain source imaging of focal epileptic activity: A synopsis of 455 cases. Brain 2003; 126: 2396-405.

Szentagothai J. Local neuron circuits of the neocortex. The neurosciences 4th study program 1979: 399-415.

Tao JX, Chen XJ, Baldwin M, Yung I, Rose S, Frim D, et al. Interictal regional delta slowing is an EEG marker of epileptic network in temporal lobe epilepsy. Epilepsia 2011.

Theiler J, Eubank S, Longtin A, Galdrikian B, Doyne Farmer J. Testing for nonlinearity in time series: The method of surrogate data. Physica D 1992; 58: 77-94.

Tyvaert L, Hawco C, Kobayashi E, LeVan P, Dubeau F, Gotman J. Different structures involved during ictal and interictal epileptic activity in malformations of cortical development: An EEG-fMRI study. Brain 2008; 131: 2042-60.

Urrestarazu E, Iriarte J, Alegre M, Valencia M, Viteri C, Artieda J. Independent component analysis removing artifacts in ictal recordings. Epilepsia 2004; 45: 1071-8.

Van Veen BD, Van Drongelen W, Yuchtman M, Suzuki A. Localization of brain electrical activity via linearly constrained minimum variance spatial filtering. Biomedical Engineering, IEEE Transactions on 1997; 44: 867-80.

Vitikainen AM, Lioumis P, Paetau R, Salli E, Komssi S, Metsahonkala L, et al. Combined use of non-invasive techniques for improved functional localization for a selected group of epilepsy surgery candidates. Neuroimage 2009; 45: 342-8.

Vulliemoz S, Carmichael DW, Rosenkranz K, Diehl B, Rodionov R, Walker MC, et al. Simultaneous intracranial EEG and fMRI of interictal epileptic discharges in humans. Neuroimage 2010.

Wagner M, Fuchs M, Kastner J. SWARM: SLORETA-weighted accurate minimum norm inverse solutions. 2007; 1300: 185-8.

Wang JZ, Williamson SJ, Kaufman L. Magnetic source images determined by a lead-field analysis: The unique minimum-norm least-squares estimation. Biomedical Engineering, IEEE Transactions on 1992; 39: 665-75.

Wilke C, Worrell G, He B. Graph analysis of epileptogenic networks in human partial epilepsy. Epilepsia 2011; 52: 84-93.

Wolters CH, Anwander A, Tricoche X, Weinstein D, Koch MA, MacLeod R. Influence of tissue conductivity anisotropy on EEG/MEG field and return current computation in a realistic head model: A simulation and visualization study using high-resolution finite element modeling. Neuroimage 2006; 30: 813-26.

Womelsdorf T, Schoffelen JM, Oostenveld R, Singer W, Desimone R, Engel AK, et al. Modulation of neuronal interactions through neuronal synchronization. Science 2007; 316: 1609-12.

Worden MS, Foxe JJ, Wang N, Simpson GV. Anticipatory biasing of visuospatial attention indexed by retinotopically specific-band electroencephalography increases over occipital cortex. J Neurosci 2000; 20: 1-6.

Worrell GA, Lagerlund TD, Sharbrough FW, Brinkmann BH, Busacker NE, Cicora KM, et al. Localization of the epileptic focus by low-resolution electromagnetic tomography in patients with a lesion demonstrated by MRI. Brain Topogr 2000; 12: 273-82.

Yan Y, Nunez P, Hart R. Finite-element model of the human head: Scalp potentials due to dipole sources. Medical and Biological Engineering and Computing 1991; 29: 475-81.

Yang L, Liu Z, He B. EEG-fMRI reciprocal functional neuroimaging. Clinical Neurophysiology 2010; 121: 1240-50.

Yang L, Wilke C, Brinkmann B, Worrell G, He B. Dynamic imaging of ictal oscillations using non-invasive high-resolution EEG. NeuroImage 2011; 56: 1908-17.

Yuan H, Doud A, Gururajan A, He B. Cortical imaging of event-related (de) synchronization during online control of brain-computer interface using minimum-norm estimates in frequency domain. Neural Systems and Rehabilitation Engineering, IEEE Transactions on 2008; 16: 425-31.

Yuan H, Liu T, Szarkowski R, Rios C, Ashe J, He B. Negative covariation between task-related responses in alpha/beta-band activity and BOLD in human sensorimotor cortex: An EEG and fMRI study of motor imagery and movements. Neuroimage 2010; 49: 2596-606.

Zhang Y, van Drongelen W, He B. Estimation of in vivo human brain-to-skull conductivity ratio with the aid of intracranial electrical simulation. Appl Phys Lett 2006; 89.

Zijlmans M, Jiruska P, Zelmann R, Leijten FSS, Jefferys JGR, Gotman J. High-frequency oscillations as a new biomarker in epilepsy. Ann Neurol 2012; 71: 169-78.